2013

Interactions between arenavirus proteins and small molecule inhibitors of infection

Emily L. Messina

INTERACTIONS BETWEEN ARENAVIRUS PROTEINS AND SMALL MOLECULE INHIBITORS OF INFECTION

By

EMILY LYNN MESSINA

B.S. Biology Virginia Tech, Blacksburg, VA, 2004

Dissertation

presented in partial fulfillment of the requirements
for the degree of

PhD Integrative Microbiology and Biochemistry Degree

The University of Montana
Missoula, MT

December 2013

Approved by:

Sandy Ross, Dean of The Graduate School
Graduate School

Committee:

Jack Nunberg, Chair
Montana Biotechnology Center

Steve Lodmell
Division of Biological Sciences

Scott Wetzel
Division of Biological Sciences

Brent Ryckman
Division of Biological Sciences

Keith Parker
Department of Biomedical and Pharmaceutical Sciences

ProQuest LLC.
789 East Eisenhower Parkway
P.O. Box 1346
Ann Arbor, MI 48106 - 1346

Messina, Emily, PhD, Fall 2013 Integrative Microbiology and Biochemistry

Interactions between Arenavirus Proteins and Small Molecule Inhibitors of Infection

Chairperson: Jack Nunberg

Arenaviruses are globally distributed, negative-sense, single-stranded RNA viruses which persist in specific rodent host species. Of the 32 known arenaviruses, 10 have been associated with human disease. Of these, Lassa, Junín, Machupo, Guanarito, and Sabia viruses cause severe hemorrhagic fevers. The only current option for the treatment of arenavirus infection is the off-label use of ribavirin. However, ribavirin is associated with severe side effects. Clearly, there exists a need for the study of arenavirus biology and of novel drugs for the treatment of arenaviral infection. My work focused on two attractive targets for inhibition of infection: the arenaviral RNA-dependent RNA polymerase, to block replication of the viral genome, and the arenaviral envelope glycoprotein (GPC), to prevent delivery of the viral genome to the cytosol. We showed that the novel purine analogue, T-705, is effective at inhibiting the replication of highly pathogenic arenaviruses *in vitro*. Further, we showed that T-705 specifically blocks viral transcription without significantly reducing cellular transcription activity. We also explored the interactions between the SSP and G2 subunits within GPC. We demonstrated that the first transmembrane region of SSP is a functional subdomain and that the interactions between this region and the transmembrane region of G2 are essential to fusion activity. Further, we demonstrated that residues in this subdomain are key to drug sensitivity. We also worked to characterize the arrangement between the transmembrane regions using cysteine-scanning mutagenesis and we engineered a construct linking the first transmembrane region of SSP to the transmembrane region of G2 to serve as a potential model for studying the interactions between these two regions.

Acknowledgments

I would like to take the opportunity to thank those that supported me and during my time at the University of Montana. Obviously, I need to thank Jack Nunberg, for his time and work as my advisor. I also need to express my appreciation for the other members of my laboratory who assisted me on countless occasions: Jo York, Nick Baird, Sundaresh Shankar, Celestine Thomas, Hedi Casquilo-Gray, and Donna Twedt. I am grateful to my committee members, Steve Lodmell, Scott Wetzel, Brent Ryckman, and Keith Parker, for all of their time and efforts throughout my studies. In particular, I am especially indebted to Steve and Scott for always be available to listen and address my concerns despite their busy schedules.

I want to express my gratitude to my husband, Paul, and to my friends Sundaresh Shankar, Indu Warrier, Melissa and Greg Hargreaves, Wes Samson, Tammy Ravas, and my former boss Dawn Bowles. I think there are many ups and downs for any graduate student, but without their kindness and emotional support, my road would have been a lot bumpier.

Table of Contents **Page**

List of Abbreviations Used

BS^3 - bis(sulfosuccinimidyl)suberate
CC_{50} – concentration of drug that yields 50% cytotoxicity
CHAPS - 3-[(3-cholamidopropyl)dimethylammonio]-1-propanesulfonate
CMV – cytomegalovirus
CuP – copper(II)-(1,10 phenanthroline)$_3$
DAPI - 4',6-diamidino-2-phenylindole
DDM - Lauryl-β-D-maltoside
DPC - n-dodecylphosphocholine,
EC_{50} – concentration of drug that yields 50% effectiveness
EPR – electron paramagnetic resonance
FITC - Fluorescein isothiocyanate
fLuc – firefly luciferase
GPC – arenaviral envelope glycoprotein
GnHCl - guanidine hydrochloride
GTOV – Guanarito virus
GTP – guanosine triphosphate
G1 – receptor binding subunit of GPC
G2 – fusion subunit of GPC
HF - hemorrhagic fever
IMPDH – inosine monophosphate dehydrogenase
IP - immunoprecipitations
IMP – inosine monophosphate
JGPC- Junín GPC
JCD4A – JGPC construct in which SSP is replaced by the signal peptide from human cluster of differentiation 4
JUNV – Junín virus
L – arenaviral RNA-dependent RNA-polymerase
LASV – Lassa virus
LCMV – Lymphocytic choriomeningitis virus
MACV – Machupo virus
MG – minigenome cassette
MoMuLV - Moloney murine leukemia virus
NP – arenaviral nucleoprotein
PAGE – polyacrylamide gel electrophoresis
OW – old world
PBS – phosphate buffered saline
PFA - Paraformaldehyde
POPC- palmitoyloleoyl phosphatidylcholine
POPE- palmitoyloleoyl phosphatidylethanolamine
POPG- palmitoyloleoyl phosphatidylglycerol
NW – new world
RdRp - RNA-dependent RNA-polymerase
rLuc – Renilla luciferase
RT – room temperature

SEC – size exclusion chromatography
SDS – Sodium dodecyl sulfate
Spep – S-peptide
SSP – stable signal peptide, subunit of GPC
TM – transmembrane
TM1 – N-terminal transmembrane region in SSP
TM2 - C-terminal transmembrane region in SSP
TMCON – transmembrane construct
Tris – trisaminomethane
TX-100 - Triton X-100 (Polyethylene glycol *tert*-octylphenyl ether)
T-705 – favipiravir
T-705RTP - T-705 ribofuranosyl triphosphate
wt- wild type
XMP – xanthosine monophosphate
VHF – viral hemorrhagic fever
Z – arenaviral matrix protein
ZBD – zinc binding domain

List of Figures and Tables **Page**

Chapter 1: Introduction

1a. The Arenavirus Family

The *Arenaviridae* family of viruses comprises one genus, *Arenavirus*, which can be divided phylogenetically into two serocomplexes: the Old World (OW), or the Lassa-Lymphocytic choriomeningitis group, and New World (NW) group. Viruses from each serocomplex have been identified as causative agents of viral hemorrhagic fevers (VHF) (McLay et al., 2013). The NW viruses can be further divided into three clades (A, B, C) with all of the NW viruses capable of causing VHF clustered within clade B (Emonet et al., 2009). These include the Junín (JUNV), Guanarito (GTOV) and Machupo (MACV) viruses (Buchmeier et al., 2007). Arenaviruses are each harbored primarily within one major reservoir from the rodent family *Muridae,* with the possible exception of the NW Tacaribe virus that been found in bats (Charrel et al., 2011; Salazar-Bravo et al., 2002). The association of virus and host limits the geographic distribution of each virus to the range of its host. The prototypic OW Lymphocytic choriomeningitis virus (LCMV), which persists in the common house mouse, *Mus musculus,* is the only arenavirus found globally (figure 1). Of the arenaviruses, LCMV, Lassa virus (LASV) and JUNV are of particular significance to my research. LCMV, first isolated 1933, is the prototypic arenavirus and it has been extensively used as a model of arenaviral biology and infection. It is reported that about 5% of humans are seropositive for LCMV (Emonet et al., 2009; Peters, 2006). Generally not considered a public health threat as most acquired infections are asymptomatic, LCMV does cause serious infection in immunocompromised individuals and is an overlooked fetal teratogen (Barton et al., 2002; McLay et al., 2013).

LASV is the causative agent of Lassa fever, first described in Nigeria in 1969. LASV is estimated to cause between 300,000–500,000 infections and 5000-6000 deaths annually throughout West Africa. The highest incidence of disease has been reported in Mano River Union countries of Sierra Leone, Liberia, and Guinea. (Khan et al., 2008; Russier et al., 2012). Significantly, LASV has also been exported to North America and Europe several times by travelers (Ftika and Maltezou, 2013; Macher and Wolfe, 2006; Safronetz et al., 2010). The natural reservoir of LASV is the ubiquitous rodent,

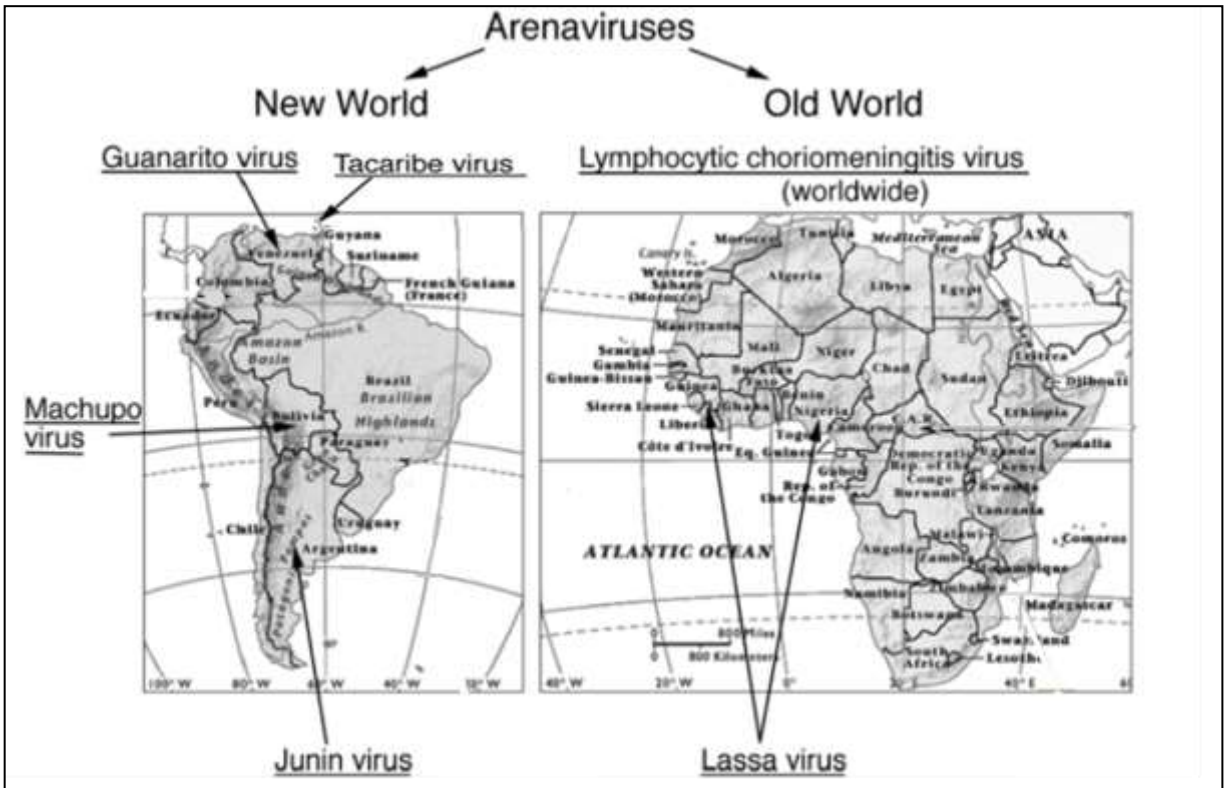

Figure 1: The Global Distribution of Arenaviruses. Adapted from Stephan Gunther and Oliver Lenz. Critical Reviews in Clinical Laboratory Sciences. 41(4):339-390 (2004)

Mastomys natalensis, which is found throughout sub-Saharan Africa (Ogbu et al., 2007). People most often become infected with LASV through either direct contact with infected rodents or inhalation of rodent excreta. Those living in rural communities or areas with poor sanitation are most at risk. Infection may then be passed between humans through

direct contact with bodily fluids or fomites. The outcome of LASV infection varies from asymptomatic or mildly acute cases to severe disease and death. The overall mortality rate for LASV infection is low, around 1%. Of those hospitalized for LASV infection, the mortality rate is 15%-20%. Further, a significant number of Lassa fever survivors experience long-term neurological side effects such as deafness (30%) (Cummins D et al., 1990). It is still unclear why some patients appear to recover from LASV and others develop VHF (Ogbu et al., 2007; Russier et al., 2012).

JUNV, the causative agent of Argentine hemorrhagic fever, was first discovered and characterized in the 1950s (Parodi et al., 1958). As with LASV, humans generally become infected through direct or indirect contact with the rodent reservoir, *Calomys musculinus,* though nosocomial spread is also possible. The persons at highest risk are agricultural workers who have increased contact with *C. musculinus.* (Colebunders et al., 2002; Enria et al., 2008; Radoshitzky et al., 2012). It is estimated that most (80%) infections of JUNV result in disease. Of these, the mortality rate is between 15% and 30%. Before the development and use of the JUNV vaccine strain Candid-1 in Argentina in the 1990s, JUNV caused between 300 and 1000 cases of VHF per year. Since then, the rate has dropped to between 30 and 50 infections every year (Ambrosio et al., 2011; Enria et al., 2008; Harrison et al., 1999). Saliently, the region of endemic infection has been increased by 150,000km^2 and there are now an estimated 5 million people at risk for infection (Ambrosio et al., 2011; Radoshitzky et al., 2012).

VHFs caused by LASV and JUNV display similar symptoms. Reported incubation periods for LASV range from 3-21 days and 6-14 days for JUNV. Generally,

illness begins with non-specific signs: malaise, headache, fever, and muscle aches. Disease then progresses to petechial hemorrhage, edema, respiratory distress, shock, decreased platelets and white blood cells, and mucosal bleeding. Liver dysfunction is more common in severe cases of Lassa fever than in VHF caused by NW viruses. Neurologic symptoms such as irritability, confusion, and tremors are much more common in JUNV infections. Hemorrhage in LASV infections occurs in roughly 20% of patients, and is frequently localized to the gums. In the case of JUNV infection, hemorrhage is more common, widespread, and severe. (Cummins, 1991; Enria et al., 2008; Khan et al., 2008; McLay et al., 2013; Ogbu et al., 2007).

Treatment options for arenaviral infections are limited. The Candid-1 attenuated vaccine is not FDA-licensed and there are no vaccines available for LASV or any other pathogenic arenavirus. Treatment of JUNV patients with donor serum from survivors has been successful in treating JUNV infection when administered within 8 days of onset of symptoms, (Enria et al., 2008; Harrison et al., 1999) but this has not been the case with LASV infection (Cummins, 1991). The only currently available drug for the treatment of arenaviral infection is the off-label use of ribavirin. This drug has been used to treat LASV and JUNV infections with success, if administered early in the course of infection. However, its use is associated with some severe side-effects, such as anemia (Cummins, 1991; Damonte and Coto, 2002; Enria et al., 2008).

Arenaviruses continue to be a significant public health threat. The increase of human activity (agricultural or recreational) within the natural habitats of rodent reservoirs, in combination with ecological changes, has been linked to the spread of

known arenaviruses and the emergence of new arenaviral species in people (Ambrosio et al., 2011; Charrel et al., 2011). Novel pathogenic arenaviruses are reported to emerge on average every 2-3 years (Pasquato et al., 2011). Further, the repeated exportation of LASV to the western world demonstrates that these viruses are not just a threat to their endemic regions, but to the global community. Additionally, the fact that the natural mode of infection is inhalation of rodent excreta raises the concern that these viruses maybe intentionally aerosolized for use as weapons. These factors, combined with high mortality rates and the lack of treatment options, have led to the classification of Lassa, Junín, Machupo, and Guanarito viruses as Category A priority pathogens by the U.S. (NIAID,2011). There is a clear need to study arenaviral biology to further our understanding of how these viruses cause infection and how we may develop antiviral drugs to interfere with the viral life cycle.

1b. Viral Life Cycle Overview

Arenaviruses are pleomorphic enveloped viruses which contain a bi-segmented ambisense RNA genome. The large genome segment encodes the RNA-dependent RNA polymerase (L) and the matrix protein (Z). The small segment encodes the envelope glycoprotein (GPC) and the nucleoprotein (NP) (figure 2) (Emonet et al., 2009; Meyer et al., 2002). GPC is expressed as a trimer on the viral envelope. It forms a spike that is composed of three non-covalently associated subunits, G1, G2, and a stable signal peptide (SSP). The G1 subunit is the 'head' on the spike and provides the receptor-binding function for the virus (Kunz et al., 2003). OW viruses and clade C NW viruses use α-dystroglycan to bind to the cell surface while NW clade B viruses utilize transferrin receptor-1 (Cao et al., 1998; Kunz, 2009; Radoshitzky et al., 2007; Rojek et al., 2008).

G2 forms the 'stalk' and is responsible for membrane fusion. SSP is a 58 amino acid peptide that spans the membrane twice, with both termini residing on the cytosolic face of the membrane (Agnihothram et al., 2007). Its importance in the structure and function of GPC will be discussed at length below. The non-lytic viral life-cycle is initiated when virus binds to the surface of the cell. The virion is then endocytosed. Unlike NW clade B arenaviruses, which are endocytosed in a clathrin-dependent fashion (Vela et al., 2007), OW arenaviruses undergo an unusual endocytotic pathway independent of clathrin, caveolin, dynamin, and actin (Pasqual et al., 2011). Although the pathways are distinct, delivery into the low-pH late-endosome is essential for entry by both NW and OW arenaviruses (Rojek et al., 2008). As the endosome is acidified, a series of dramatic conformational changes in G2 takes place which leads to fusion of the viral envelope with the endosomal membrane. This allows entry of the viral genome into the host cytosol, where viral replication occurs. NP and L are necessary and sufficient for replication of the genome (Emonet et al., 2009). As the host does not have an RdRp, the viral polymerase is an attractive target for antiviral strategies and has been shown to be sensitive to drugs such as the purine analogs ribavirin and T-705, which we have investigated in chapter 2. Preventing access of the virus to the cytosol by blocking membrane fusion is another very attractive target in the viral life cycle. Elucidating the precise structure of GPC and how it mediates membrane fusion will help us to better understand the biology of arenaviruses and potentially aid in the development of fusion inhibitors. This is the focus of chapters 3-5.

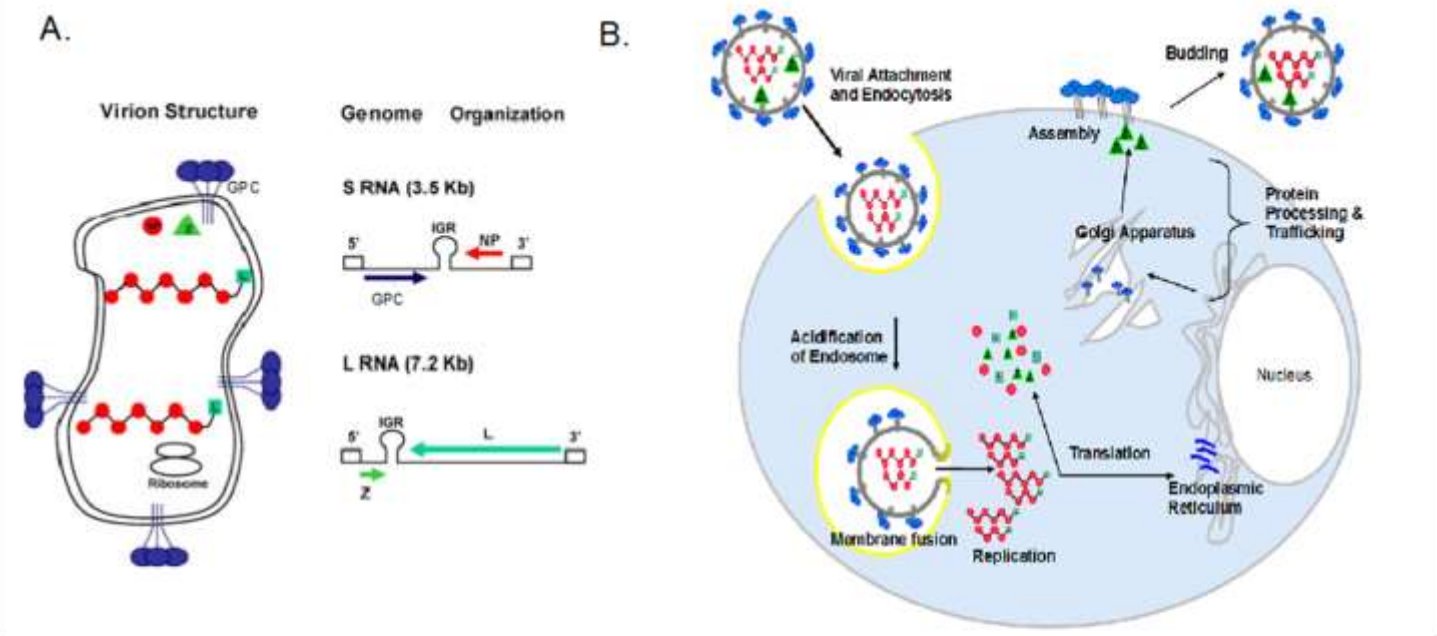

Figure 2: Arenavirus Structure and Life Cycle. (A) Pleomorphic virions range in size from 50-300nm in diameter. Each virion contains two ssRNA segments, a large (L) and small (S), which are coated in nucleoprotein (NP) and display a "string of beads" structure. Both segments use an ambisense coding strategy to direct the expression of two proteins in opposite directions. Open reading frames are separated by a non-coding intergenic region (IGR). The glycoprotein (GPC), shown in blue, forms trimeric "spikes" on the viral envelope. GPC is made of three subunits: G1, G2, and SSP (not shown here, see figure 6). The "head" of the spike is composed of the receptor-binding subunit G1, and the "stalk" of the spike is formed by the G2 subunit. (B) Viral Life Cycle. The virus attaches to the cell through G1 binding and is subsequently endocytosed. As the endosome is acidified, GPC undergoes a series of dramatic conformational changes which drive membrane fusion. This step is targeted by small molecule inhibitors such as ST-294 and ST-161. Membrane fusion allows the viral genome to enter the cytosol, where replication occurs. T-705 and ribavirin target this step. Adapted from Emonet et al. Infection, Genetics, and Evolution. 9(4):417-429 (2009).

1c. Inhibiting Replication

The arenavirus RdRp transcribes and replicates the viral genome. During transcription, the RdRp produces subgenomic mRNAs which terminate at the IGR (figure 2A) (Conzelmann, 1996). In replicating the genome, the RdRp reads through the IGR and synthesizes uncapped, full-length genomic and anti-genomic viral RNAs. NP associates with the viral RNA to form the nucleocapsid, the template for the RdRp (Fuller-Pace and Southern, 1988). The 3' terminus of both the L and S segments contains a conserved sequence of 19 nucleotides which base-pairs with an almost complementary sequence in

the 5' terminus to form a panhandle. This structure, and its sequence, are essential for forming a functional promoter for transcription and replication (Perez and de la Torre, 2003). Together, the nucleocapsid and the RdRp make up the viral ribonucleoprotein complex, the minimum requirement for genome replication (Lee et al., 2000). We have taken advantage of this fact by using a minigenome system to study the activity of the RdRp. This system, developed by collaborators in the de la Torre laboratory (Lee et al., 2000), involves the use of an LCMV minigenome cassette (MG) co-transfected with plasmids coding for the viral polymerase and the NP. The MG plasmid contains the firefly luciferase gene in the antisense orientation flanked by the necessary noncoding segments from the LCMV S RNA (5' UTR, IGR and the 3' UTR) and is dependent upon the viral polymerase for expression of luciferase.

To date, the only treatment available for arenaviral infections is the off-label use of ribavirin (1-beta-D-ribofuranosyl-1,2, 4-triazole-3-carboxamide), which is phosphorylated in the cell to its active form (figure 3A). Ribavirin has been used to treat other viral infections such as chronic hepatitis C (Maag et al., 2001) and it has been used to treat Lassa victims with mixed results (Khan et al., 2008). The mechanism of action of ribavirin is unclear and it may vary among different viruses. Ribavirin is known to act as an inhibitor of RNA-capping in vaccinia infections and to antagonize RdRp activity by competing with GTP during influenza replication (Graci and Cameron, 2006).

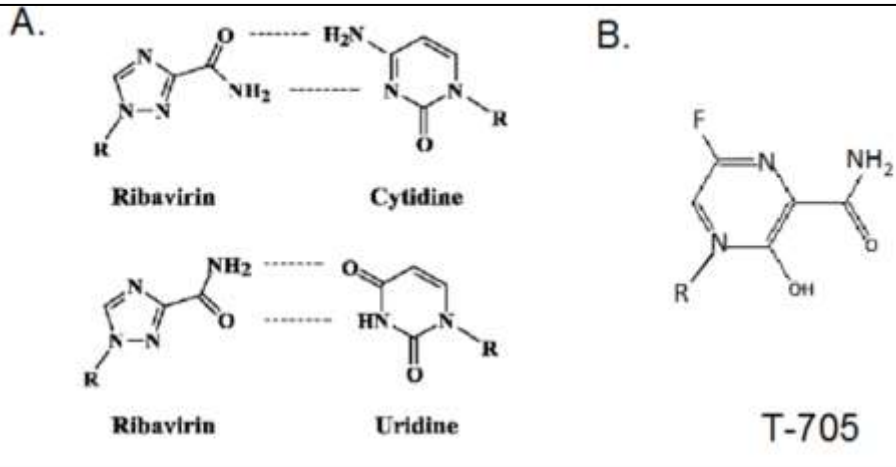

Figure 3: Structures of the active form of ribavirin and T-705. (A) Ribavirin can base pair equally with both cytidine or uridine. R denotes ribofuranosyl mono- or triphosphate. Adapted from Maag *et al.* The Journal of Biological Chemistry, 276:46094-46098 (2007). **(B)** Structure of T-705. Adapted from Erik De Clercq. Nature Reviews Drug Discovery 5, 1015-1025 (Dec 2006). Both molecules are converted to triphosphorylated nucleosides inside the cell.

Ribavirin can base pair to both cytidine and uridine (figure 3A), and therefore has the potential to lead a virus to lethal mutagenesis, as demonstrated in its inhibition of poliovirus (Crotty et al., 2000), LCMV (Moreno et al., 2011) and hepatitis C (Maag et al., 2001). Ribavirin is also known to inhibit the enzyme inosine monophosphate dehydrogenase (IMPDH). This enzyme catalyzes the synthesis of xanthosine-5'-monophosphate, the precursor to guanosine-5'-monophosphate. Therefore, inhibition of IMPDH disrupts guanosine triphosphate (GTP) pools (figure 4). This reduction in available GTP has been implicated in the inhibition of flaviviruses, paramyxoviruses, nidoviruses, and LCMV (Kim and Lee, 2013; Leyssen et al., 2005; Moreno et al., 2011). It is likely that the strong inhibitory effect of ribavirin on arenaviral infection is due to the combined effects of simultaneously increasing the rate of mutagenesis in the viral genome and by reducing available GTP (Moreno et al., 2011). Importantly, the inhibition of IMPDH is not only inhibitory to viral replication, but also affects cellular transcription

(Damonte and Coto, 2002).

There is a need for a safer alternative to ribavirin. One novel candidate is the base analog T-705 (6-fluoro-3-hydroxy-2-pyrazinecarboxamide), also known as favipiravir. T-705 has been used to inhibit several positive- and negative-sense RNA viruses, but not DNA viruses (Clercq, 2012). Like ribavirin, T-705 is converted in the cell to a nucleoside triphosphate, T-705RTP (figure 3B). It has been shown to inhibit influenza replication by antagonizing the RdRp in a dose-dependent fashion and this effect could be reversed by the addition of GTP. However, T-705RTP did not inhibit IMPDH (Furuta et al., 2005).

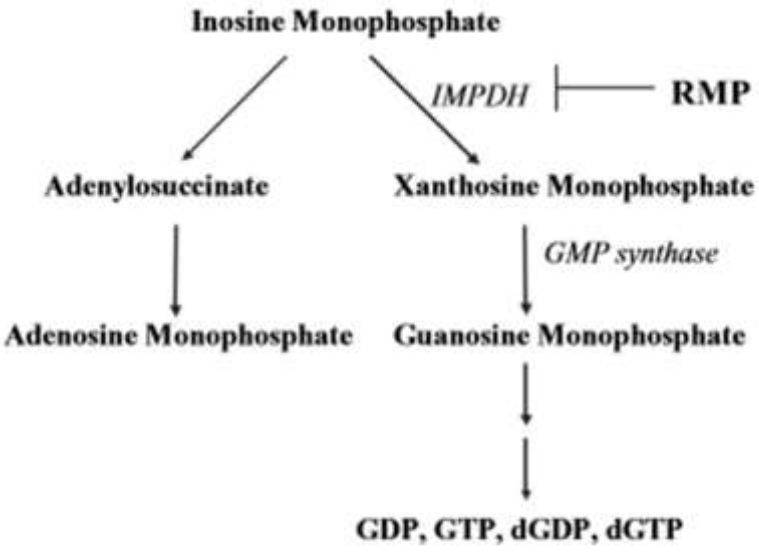

Figure 4: Ribavirin disrupts GTP pools.
Ribavirin is converted to its active form in the cell, ribavirin monophosphate (RMP). RMP inhibits IMPDH, which catalyzes the synthesis of xanthosine-5'-monophosphate, the precursor to guanosine-5'-monophosphate. Therefore, inhibition of IMPDH reduces the levels of available guanosine triphosphate (GTP). From Jason D. Graci and Craig E. Cameron. Rev. Med. Virol. 2006; 16: 37–48

These results indicate T-705 may be a more specific inhibitor of viral replication with fewer off-target effects than ribavirin. T-705 has been shown to effectively inhibit nonpathogenic arenaviral infection in tissue culture and rodent models (Gowen et al., 2007). However, T-705 has not been evaluated against highly pathogenic arenaviruses and its mechanism of action against arenaviruses remains undetermined. In chapter 2, we determine the activity of T-705 against Junín, Machupo, and Guanarito viruses and we explore the mechanism of action of T-705 using the LCMV minigenome system..

1d. The unique Arenaviral GPC and Inhibition of Fusion

Entry is a promising step in the viral life-cycle for inhibiting the virus before it can usurp the host's machinery and a better understanding of entry mechanisms will likely inform the search for antivirals (Rojek and Kunz, 2008). Newly available small-molecule inhibitors of membrane fusion may be the most promising new therapies to combat arenaviral infection (Bolken et al., 2006; Charrel and de Lamballerie, 2010; Larson et al., 2008). Further, use of these fusion inhibitors may aid in probing the structure and function of GPC. There are three main classes of viral fusion glycoproteins with varied organization, structures, and triggers. However, they mediate a common function, membrane fusion, and they do so in a remarkably conserved manner. In general, the fusion protein expressed on the viral envelope waits in a pre-fusion or a 'native' state for an appropriate trigger. This could be low pH and/or interaction with a host receptor. Once triggered, the protein undergoes a series of conformational changes that result in the viral and cellular membranes fusing. In class-I fusion, the fusion subunit extends and the receptor binding subunit is released, allowing the fusion peptide to be

inserted into the host membrane. Now in a pre-hairpin intermediate form, this extended structure folds back on itself to form a trimer of hairpins. This energetically favorable conformational change drives the merging of the two membranes (figure 5) (Kim et al., 2011; Schibli and Weissenhorn, 2004; White et al., 2008).

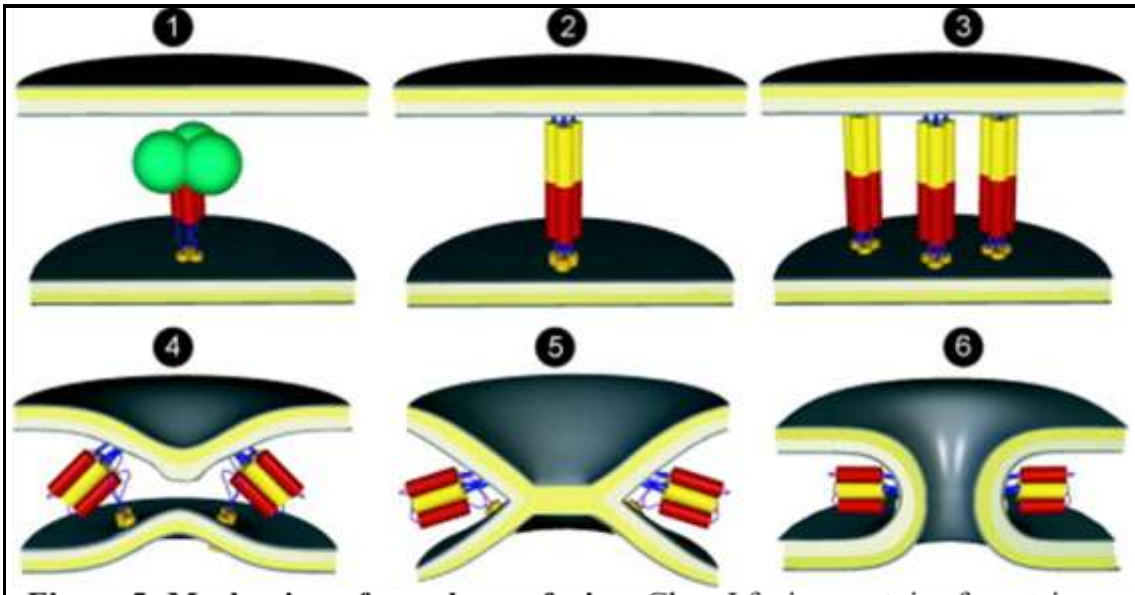

Figure 5: Mechanism of membrane fusion. Class I fusion proteins form trimers on the surface of the viral envelope, with fusion peptides buried within the trimer interface **(1)**. Upon triggering the envelope proteins undergo conformational changes leading to exposure of fusion peptides, which then insert into the target membrane **(2)**. Multiple fusion proteins may cluster to form a fusion site **(3)**. Additional conformational changes lead to the formation of a six-helix bundle **(4)**, resulting in hemifusion, and mixing of the outer leaflets of the viral and cellular membranes **(5)**. A fusion pore then forms **(6)**, and enlarges. From Rodrigo A. Villanueva, Yves Rouillé, Jean Dubuisson. Interactions Between Virus Proteins and Host Cell Membranes During the Viral Life CycleInternational Review of Cytology, Volume 245, 2005, Pages 171–244

The arenaviral GPC is a class-I fusion protein (Gallaher et al., 2001). Class-I fusion proteins exist as trimers in both the pre- and post- fusion state. They are exemplified by their post-fusion adoption of a six-helix bundle. This structure consists of a central N-terminal trimeric α-helical coiled-coil which is surrounded by 3 C-terminal helices (White et al., 2008). Previous work in our laboratory has shown that the N- and

C- terminal heptad repeats in G2 (figure 6) are critical to fusion and can form a canonical six-helix bundle (York et al., 2005).

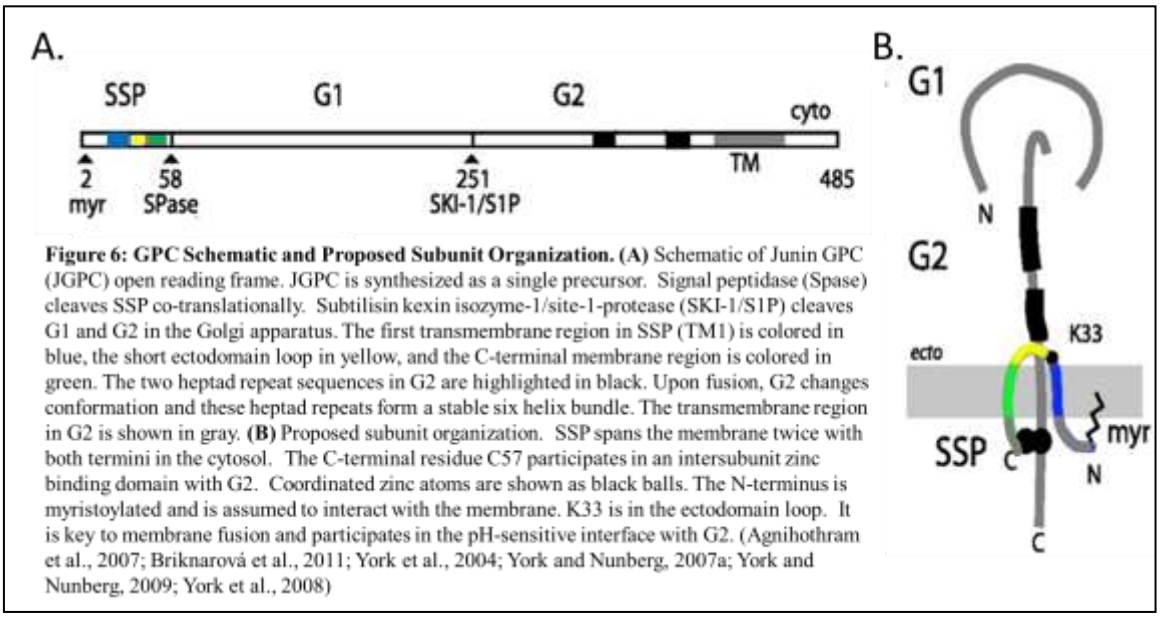

Figure 6: GPC Schematic and Proposed Subunit Organization. (A) Schematic of Junin GPC (JGPC) open reading frame. JGPC is synthesized as a single precursor. Signal peptidase (Spase) cleaves SSP co-translationally. Subtilisin kexin isozyme-1/site-1-protease (SKI-1/S1P) cleaves G1 and G2 in the Golgi apparatus. The first transmembrane region in SSP (TM1) is colored in blue, the short ectodomain loop in yellow, and the C-terminal membrane region is colored in green. The two heptad repeat sequences in G2 are highlighted in black. Upon fusion, G2 changes conformation and these heptad repeats form a stable six helix bundle. The transmembrane region in G2 is shown in gray. **(B)** Proposed subunit organization. SSP spans the membrane twice with both termini in the cytosol. The C-terminal residue C57 participates in an intersubunit zinc binding domain with G2. Coordinated zinc atoms are shown as black balls. The N-terminus is myristoylated and is assumed to interact with the membrane. K33 is in the ectodomain loop. It is key to membrane fusion and participates in the pH-sensitive interface with G2. (Agnihothram et al., 2007; Briknarová et al., 2011; York et al., 2004; York and Nunberg, 2007a; York and Nunberg, 2009; York et al., 2008)

GPC is synthesized as a single precursor protein that must be cleaved twice. The first cleavage event is performed co-translationally by signal peptidase, which cleaves SSP. The second proteolytic maturation step is performed by subtilisin kexin isozyme-1/site-1-protease (SKI-1/S1P), which cleaves G1 and G2, and occurs in the Golgi apparatus. Mature cleaved GPC is transported to the plasma membrane where virion budding occurs, mediated by Z (Emonet et al., 2009) (figure 2). Importantly, all three GPC subunits remain non-covalently associated with each other throughout the viral life cycle (figure 6). This is unique to the arenaviral GPC.

SSP is associated with G2 through its penultimate cysteine (C57), which participates in an intersubunit zinc binding domain (ZBD) (Briknarová et al., 2011; York and Nunberg, 2007a). As SSP remains associated with the mature glycoprotein complex, each trimeric GPC on the viral envelope contains nine TM domains. Interestingly, SSP can be expressed in *trans* with a G1/G2 construct bearing the human CD4 signal peptide,

and these subunits will associate functionally to yield a mature GPC (York et al., 2004).

Previous work has shown that SSP masks ER retention/retrieval signals in G2 and ergo, is essential to the proper trafficking, cleavage, and cell surface expression of GPC (Agnihothram et al., 2006). SSP has also been shown to be essential for membrane fusion. In Junín GPC (JGPC), lysine-33 (K33), in the short ectodomain loop of SSP, has been demonstrated to be critical in determining the pH at which fusion occurs. Substitution of K33 with the uncharged residue glutamine appears to stabilize the complex from pH-induced conformational change. Compared to wild-type (wt) JGPC, which optimally fuses at pH5, K33Q requires a lower pH (4.5) to trigger membrane fusion. Genetic studies have shown that compensating secondary mutations in the membrane-proximal region of G2 (D400A, E410A, R414A, K417A) are able to reverse the shift of pH-triggered fusion caused by the K33Q mutation (York and Nunberg, 2009). Together, the short ectodomain loop of SSP and the membrane-proximal region of G2 form a pH-sensitive interface that is key to proper membrane fusion.

Much study has been dedicated to this pH-sensitive, membrane-proximal interface between SSP and G2 and notably, it is can be targeted by small-molecule inhibitors to prevent membrane fusion (York et al., 2008). These inhibitors block pH-induced activation by stabilizing the pre-fusion form of GPC and they can be classified based on their specificity to OW viruses, NW viruses, or both. Studies have shown that mutations within this membrane-proximal region can alter the sensitivity of GPC to these inhibitors. For example, mutations in the NW JGPC (T418N, L420T, A435I, I347A, D400A, K33H, K33R) reduce the sensitivity of JGPC to the NW specific fusion inhibitor ST-294. However, the mutation K33H confers sensitivity to the OW specific fusion inhibitor ST-

161 (York et al., 2008).

Interestingly, mutations within the transmembrane region of G2 have also been shown to be important to fusion (F427A, A435I, F438I, W428A) and drug sensitivity (F427A). G2 mutations at residues F427, W428, and F438 also compensate for the K33Q fusion-deficient mutant. (York and Nunberg, 2009; York et al., 2008).

The TM regions within GPC are not uniformly hydrophobic. Both the TM domain in G2 and the first TM region in SSP are predicted to form amphipathic helices while the second TM region of SSP has been shown to be resilient to alanine mutations and uniformly hydrophobic (Agnihothram et al., 2007). My work in chapters 3-5 focuses on furthering our understanding of the interactions between TM regions of SSP and G2.

1e. Hypotheses and Significance

Without a licensed vaccine or treatment, arenaviruses continue to remain a significant threat to public health warranting further investigation into the biology of arenaviruses and treatment of arenaviral infections. During my research I have focused on studying two aspects of arenavirus biology: the inhibition of viral replication by T-705 and understanding the interactions between subunits within GPC.

T-705 is a promising new antiviral for the inhibition of RNA viruses and may be an alternative to the currently used ribavirin. However, its ability to inhibit pathogenic arenaviral infections remained untested and it is important to learn more about its mechanism of action in arenaviral inhibition. In chapter 2, we hypothesized that T-705 would specifically inhibit the viral RdRp with less cytotoxicity than ribavirin. Consistent with this hypothesis, we demonstrated that three VHF viruses Junín, Machupo, and

Guanarito were inhibited by T-705 at similar concentrations to those used to inhibit the vaccine Candid-1 viral strain in tissue culture. Importantly, time of addition studies demonstrated that T-705 is only effective during the middle of the viral life cycle, after entry and before budding, which is when viral replication occurs. Using the LCMV MG system, I showed that T-705 inhibits viral polymerase activity at much lower concentrations than those required to interfere with cellular transcription, in contrast to ribavirin. Using a panel of competing nucleosides and bases, I also demonstrated that T-705 seems to be acting by a different mechanism than ribavirin. These data are consistent with results others have observed using T-705 to inhibit influenza and serve as an important step in the development of T-705 as a treatment for acute arenaviral infection (Mendenhall et al., 2011).

To further our goal of understanding the structure and function of GPC more precisely, we first sought in chapter 3 to identify the region(s) within SSP essential to fusion activity. Because we know that the pH-sensitive, membrane-proximal interface is essential to membrane fusion, we hypothesized that the ectodomain loop of SSP would prove to be the most essential region. However, we were surprised when our data indicated that a homotypic match between G2 and the first TM region of SSP was actually necessary and sufficient for fusogenicity. Further, while it was previously accepted that the first TM region nominally began with E17 (Eichler et al, 2004), our studies suggest that this TM region actually begins at P12. We discovered that residues P12 to K33 form a functional sub-domain within SSP and that sequence specificity within this domain is important to membrane fusion and drug sensitivity (Messina et al, 2012).

This novel information prompted us to probe deeper into the potential interactions between SSP and G2. Based on these new findings and previous data that indicate the TM region of G2 may be important to membrane fusion and drug sensitivity, we hypothesized that the first TM region of SSP interacts with the TM region of G2. We explored two avenues to address this hypothesis. I created a truncated GPC construct, termed TMCON, to serve as a potential model to study the interactions between the G2 TM and the first TM of SSP. The generation and preliminary characterization of this construct is discussed in chapter 4. The other approach we used to pursue this hypothesis was to use cysteine-scanning mutagenesis and crosslinking experiments to study the orientation of the TM helices to each other within the trimeric GPC. This approach and results are reviewed in chapter 5.

The work I present here has furthered the understanding of T-705 in the treatment of arenaviral infection. I developed a new biosafe fusion assay that does not rely on vaccinia virus as the current fusion assay used by the laboratory does (York et al., 2004). I used this novel assay to advance our understanding of how SSP interacts with G2 to mediate function. I have also generated a model construct for use in future studies for examining potential interactions between the first TM region of SSP and the TM region of G2. Finally, I have attempted to map the arrangement of the transmembrane domains within GPC by creating a library of cysteine mutations and performing an exhaustive search for appropriate crosslinking conditions.

Chapter 2: T-705 (Favipiravir) Inhibition of Arenavirus Replication in Cell Culture

Michelle Mendenhall, Andrew Russell, Terry Juelich, Emily L. Messina, Donald F. Smee, Alexander N. Freiberg, Michael R. Holbrook, Yousuke Furuta, Juan-Carlos de la Torre, Jack H. Nunberg, and Brian B. Gowen. Antimicrobial Agents and Chemotherapy. 2011 February; 55(2): 782–787.

This study was done in collaboration with Brian Gowen's laboratory where the experiments using intact viruses were performed. I contributed the experiments involving the replicon system.

Abstract

A number of New World arenaviruses (Junín [JUNV], Machupo [MACV], and Guanarito [GTOV] viruses) can cause human disease ranging from mild febrile illness to a severe and often fatal hemorrhagic fever syndrome. These highly pathogenic viruses and the Old World Lassa fever virus pose a significant threat to public health and national security. The only licensed antiviral agent with activity against these viruses, ribavirin, has had mixed success in treating severe arenaviral disease and is associated with significant toxicities. A novel pyrazine derivative currently in clinical trials for the treatment of influenza virus infections, T-705 (favipiravir), has demonstrated broad-spectrum activity against a number of RNA viruses, including arenaviruses. T-705 has also been shown to be effective against Pichinde arenavirus infection in a hamster model. Here, we demonstrate the robust antiviral activity of T-705 against authentic highly pathogenic arenaviruses in cell culture. We show that T-705 disrupts an early or intermediate stage in viral replication, distinct from absorption or release, and that its antiviral activity in cell culture is reversed by the addition of purine bases and nucleosides, but not with pyrimidines. Specific inhibition of viral replication/transcription by T-705 was demonstrated using a lymphocytic choriomeningitis arenavirus replicon

system. Our findings indicate that T-705 acts to inhibit arenavirus replication/transcription and may directly target the viral RNA-dependent RNA polymerase.

A. Introduction

Several New World arenaviruses, including Junín (JUNV), Machupo (MACV), and Guanarito (GTOV) viruses, as well as the related Old World Lassa virus, are among a phylogenetically diverse group of negative-sense RNA viruses that cause severe viral hemorrhagic fevers (VHFs) in regions of the world where they are endemic (Geisbert and Jahrling, 2004). The National Institutes of Health has classified these viruses as category A agents because of the threat they pose to the U.S. population (NAID, 2002). Despite the biodefense and public health risks associated with these highly pathogenic viruses, there are no FDA-licensed arenavirus vaccines and current antiarenaviral therapy is limited to an off-label use of ribavirin (1-β-d-ribofuranosyl-1,2,4-triazole-3-carboxamide), which has had only mixed success in the treatment of severe infections and is associated with significant toxicity in humans (Enria et al., 2008; Khan et al., 2008; Snell, 2001). Therefore, it is important to develop novel and effective antiviral drugs to combat arenaviral hemorrhagic fevers.

T-705 (favipiravir; 6-fluoro-3-hydroxy-2-pyrazinecarboxamide) is a pyrazine derivative with broad antiviral activity against RNA viruses, including influenza viruses (Furuta et al., 2002; Kiso et al., 2010; Sidwell et al., 2007; Sleeman et al., 2010), flaviviruses (Julander et al., 2009; Morrey et al., 2008), bunyaviruses, and several

nonpathogenic arenaviruses (Gowen et al., 2007, 2008, 2010). Moreover, studies employing the hamster Pichinde virus (PICV) infection model of acute arenaviral disease have demonstrated that T-705 can be used effectively to treat advanced infections in animals (Gowen et al., 2008). However, T-705 has not yet been tested against highly pathogenic human arenaviruses.

Evidence indicates that T-705 is ribosylated and phosphorylated to the active T-705-4-ribofuranosyl-5′-triphosphate form (T-705RTP) that inhibits influenza virus infection by interfering with viral RNA replication and transcription through inhibition of the virus RNA-dependent RNA polymerase (RdRp) (Furuta et al., 2005). The broad activity of T-705 against a number of RNA viruses suggests that this inhibitor may target a conserved functional element in the viral polymerase. The ability of T-705 to specifically target the viral replication machinery may minimize the possibility of *in vivo* toxicity. In contrast, ribavirin also inhibits cellular IMP dehydrogenase (IMPDH), a key enzyme in guanosine biosynthesis, and thereby perturbs cellular nucleotide pools. In the present study, we explored the mechanism of action of T-705 in cell culture and assessed the *in vitro* activity of T-705 against three highly pathogenic arenaviruses.

B. Materials and Methods

Viruses. JUNV, Candid 1 strain (JUNV-C), and GTOV, strain S-26764, were provided by Robert Tesh at the World Reference Center for Emerging Viruses and Arboviruses (WRCEVA; University of Texas Medical Branch [UTMB], Galveston, TX). JUNV, Romero strain (JUNV-R), and MACV, strain Carvallo, were kindly provided by Tom Ksiazek (Special Pathogens Branch, Centers for Disease Control and Prevention, Atlanta,

GA). Virus stocks of JUNV-R, MACV, and GTOV were grown in Vero (African green monkey kidney) cells. All work with JUNV-R, MACV, and GTOV was performed under biosafety level 4 (BSL4) containment at the Robert E. Shope Laboratory at UTMB.

Tacaribe virus (TCRV), strain TRVL 11573 (ATCC, Manassas, VA), was passaged once in baby hamster kidney (BHK) cells and three times in Vero cells. The attenuated JUNV-C was passaged once in BSC-1 cells and once in Vero cells. Purified stocks were prepared for both TCRV and JUNV-C by sucrose cushion ultracentrifugation. Infected Vero cells culture lysates were clarified by low-speed centrifugation (4,500 × *g*), and the supernatants were overlaid onto a 20% (wt/vol) sucrose solution (TN buffer; 0.05 M Tris-HCl, pH 7.4, and 0.1 M NaCl) and centrifuged at 100,000 × *g* for 1 h in an SW28 rotor (Beckman Coulter, Brea, CA). The virus pellets were resuspended in phosphate-buffered saline (PBS), aliquoted, and stored at −80°C until use.

Antiviral compounds, nucleotides, and nucleosides. T-705 was provided by the Toyama Chemical Company, Ltd. (Toyama, Japan). Ribavirin was from MP Biomedical (Santa Ana, CA). Adenine, adenosine, guanine, guanosine, 2-deoxyguanosine, inosine, hypoxanthine, xanthine, cytosine, cytidine, thymine, thymidine, uracil, uridine, and uric acid were from Sigma (St. Louis, MO), and 2-deoxyadenosine, 2-deoxycytidine, and xanthosine were from ICN Nutritional Biochemicals (Cleveland, OH).

Virus yield reduction assays. For experiments evaluating drug inhibition of JUNV-R, MACV, or GTOV replication, Vero E6 (African green monkey kidney) cell cultures were

infected with a multiplicity of infection (MOI) of 0.1 in duplicates in the presence of serially 2-fold diluted (1,000 to 4 uM) T-705 or ribavirin. Supernatants from infected cells were harvested at 4 days postinfection (d p.i.) for MACV, 6 d p.i. for JUNV-R, or 10 d p.i. for GTOV.

Viral titers for drug-treated JUNV-R infections were determined by plaque assay. Vero E6 cells were infected with serial 10-fold dilutions of virus for 1 h at 37°C. Cell monolayers were then overlaid with 0.5% SeaKem ME agarose (Cambrex, East Rutherford, NJ) in minimal essential medium (MEM) supplemented with 2% fetal bovine serum (FBS) and 1% penicillin and streptomycin (P/S). Infected cells were cultured for 6 days, at which time a second overlay containing 1% neutral red was added. PFU were counted 18 to 24 h after addition of the second overlay, and the 90% and 50% effective concentrations (EC_{90} and EC_{50}, respectively) were calculated by regression analysis.

GTOV titers were also measured by plaque assay. Vero cell monolayers were infected with serial 10-fold dilutions of GTOV for 1 h at 37°C. After infection, cells were overlaid with 0.5% methyl cellulose in MEM supplemented with 2% FBS and 1% P/S. After a 10-day culture period, the overlay was removed, and cells were fixed with 10% buffered formalin for 20 min and stained with 1% crystal violet (Sigma). PFU were counted, and the EC_{90} and EC_{50} were calculated by regression analysis.

MACV titers were measured by a focus-forming unit (FFU) assay. Vero E6 monolayers were infected with serial 10-fold dilutions of virus for 1 h at 37°C. Following infection, cells were overlaid with 0.8% tragacanth (Sigma) in MEM supplemented with 2% FBS and 1% P/S. After infected cells were cultured for 4 days, the overlay was

removed, and cells were fixed with 10% buffered formalin for 30 min and then refrigerated overnight. Fixed cells were permeabilized in 70% ethanol for 20 min and washed with PBS. Primary antibodies were diluted in PBS with 5% milk and 1% Tween 20. MACV-infected cells were incubated with primary antibody, JUNV-C antisera (kindly provided by R. Tesh, WRCEVA, UTMB), and incubated overnight at room temperature. The primary antibody was removed, and the plates were washed once with PBS. The secondary antibody, goat anti-mouse IgG labeled with horseradish peroxidase (HRP; Southern Biotech, Birmingham, AL), was diluted in PBS with 1% bovine growth serum and added to plates for 1 to 5 h at room temperature, and then the plates were washed with PBS. AEC substrate chromogen (DakoCytomation, Carpinteria, CA) was added for 15 min at room temperature. The reaction was stopped with distilled water, and fluid was removed from the wells. FFU were counted, and the EC_{90} and EC_{50} were calculated as described above.

Time-of-addition and reversal of antiviral activity assays. In time-of-addition and reversal of antiviral activity assays, Vero monolayers (70% confluent) were first inoculated with TCRV or JUNV-C. Cells and virus were incubated at 37°C for 1 h to allow virus adsorption. The inoculum was removed, monolayers were washed twice, and test medium (MEM containing 2% FBS and 50 μg/ml gentamicin) was added to the wells.

Two time-of-addition methods were employed. In method 1, monolayers were infected with TCRV or JUNV-C at an MOI of 0.2 (time zero), and T-705 was added at 1, 2, 4, 6, 8, 10, 12, or 15 h p.i. to give a final concentration of 200 μM. Cells were

incubated at 37°C, and culture supernatants were collected at 24 h p.i. for virus yield determination by cell culture infectious dose assay (Gowen et al., 2007). Briefly, each sample was serially diluted in 10-fold increments and plated on Vero cells in 96-well microplates. Plates were incubated for 7 days, and viral cytopathic effect (CPE) was determined for calculation of 50% endpoints (50% cell culture infectious dose [$CCID_{50}$]) as previously described (Reed and Muench, 1938).

In the second method, cell monolayers in triplicate wells were infected with an MOI of 0.05, and cells were treated by adding T-705 to a final concentration of 400 μM for the indicated periods (−2 to 0, 0 to 3, 3 to 6, 6 to 9, 9 to 12, 12 to 15, and 15 to 18 h p.i.). Test medium was replaced, and incubation was continued. Cells were incubated at 37°C, supernatants were collected 24 h p.i., and virus yields were determined.

Reversal of antiarenaviral T-705 activity by the addition of a molar excess of purine and pyrimidine bases and nucleosides was investigated with Vero cells infected with an MOI of 0.2 of TCRV or JUNV-C. T-705 was added to a final concentration of 200 μM; each competitive agent was added to triplicate wells to a final concentration of 400 μM. Cells were incubated at 37°C until 48 h p.i., at which time supernatants were collected and virus yields determined.

LCMV MG rescue assay. The lymphocytic choriomeningitis arenavirus (LCMV) minigenome (MG) rescue assay was used as previously described (Lee et al., 2000, 2002). Briefly, BHK-21 cells were transfected with one plasmid that directs synthesis of an LCMV MG RNA expressing the firefly luciferase (fLuc) reporter gene in an antisense orientation together with two polymerase II expression plasmids encoding the L

polymerase (pC-L) and nucleoprotein (pC-NP), required for MG replication and expression. The plasmid mixture was transfected at a 1:2:1 ratio of MG-fLuc-pC-L-pC-NP using Lipofectamine 2000 (Invitrogen, Carlsbad, CA). To assess potential cytotoxic effects of T-705 and ribavirin, the cells were also cotransfected with the pRL-CMV plasmid (Promega, Madison, WI) expressing the *Renilla* luciferase (RLuc) reporter gene under the control of cellular, rather than viral, transcription machinery. Four hours later, cells were reseeded into 96-well microculture dishes and incubated for 44 h with replicate serial dilutions of T-705 or ribavirin. Cells were then lysed, and fLuc and RLuc activities were detected using a dual reporter assay kit (Promega) and SpectraMax L luminometer (Molecular Devices, Sunnyvale, CA).

Reversal of T-705 and ribavirin activity in the LCMV replicon system by the addition of purine or pyrimidine bases and nucleosides was also investigated with BHK cells using the LCMV replicon system. T-705 or ribavirin was added to cells at a final concentration of 200 or 100 μM, respectively, and each base/nucleoside was added to a final concentration of 400 μM. Cells were lysed 48 h posttransfection and assayed for bioluminescence.

C. Results

T-705 activity against hemorrhagic fever-causing arenaviruses. T-705 has been shown to inhibit the replication of several nonpathogenic arenaviruses but has not to date been tested for activity against the highly pathogenic viruses known to cause VHFs. Therefore, we evaluated the inhibitory activity of T-705 in JUNV-R, MACV, and GTOV infection. As shown in Table 1, T-705 was effective against GTOV, JUNV-R, and

MACV at inhibitory concentrations similar to those reported for JUNV-C and other nonpathogenic arenaviruses (Gowen et al., 2007). Ribavirin was also effective against the three viruses, but to a lesser degree, as reflected by higher inhibitory concentrations (Table 1) and right-shifted dose-response curves (figure 7) relative to T-705. Evidence of cytotoxicity by either compound was not observed at the tested concentrations.

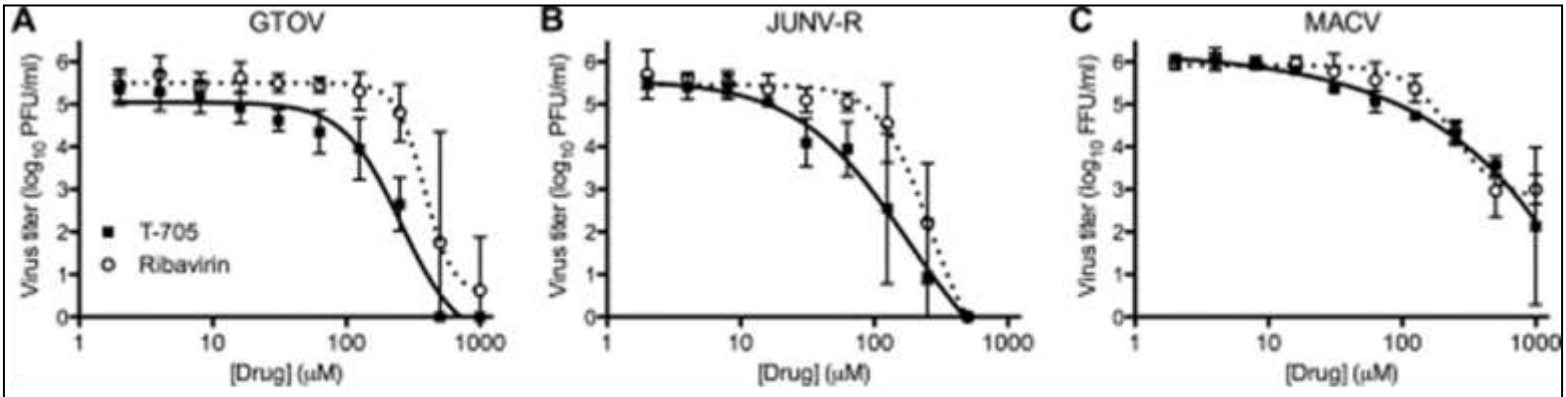

Figure 7: T-705 inhibition of highly pathogenic arenaviruses in Vero E6 cells. The dose-response curves shown reflect the effects of T-705 (solid line) and ribavirin (hashed line) on GTOV **(A)**, JUNV-R **(B)**, and MACV **(C)** replication.

TABLE 1. *In vitro* inhibitory effects of T-705 and ribavirin against VHF arenaviruses[a]

Virus	Virus yield determination assay	T-705		Ribavirin	
		EC_{90} ± SD	EC_{50} ± SD	EC_{90} ± SD	EC_{50} ± SD
GTOV	Plaque	43 ± 20	15 ± 12	303 ± 228	239 ± 213
JUNV-R	Plaque	21 ± 19	12 ± 11	71 ± 81	49 ± 71
MACV	Focus-forming unit	53 ± 11	14 ± 5	122 ± 13	68 ± 21

[a]Data are the means and standard deviations from 3 or 4 separate experiments using VeroE6 cells. Values for 90% and 50% effective concentrations (EC_{90} and EC_{50}, respectively) are expressed in μM

T-705 time-of-addition effect on arenavirus multiplication in cultured cells. Time-of-addition studies were conducted to assess the stage of arenaviral replication at which T-705 imparts its antiviral activity. Inhibitor was added at various times p.i., and the reduction in virus production relative to the untreated culture was assessed at 24 h p.i. In untreated cultures, infectious TCRV and JUNV-C particles could be detected in the supernatant by 14 h (not shown), suggesting an eclipse period of approximately 14 h. TCRV replication was inhibited when drug was added up to 6 h p.i. and left on throughout the 24-h incubation period (figure 8, left). With JUNV-C, inhibition was seen when T-705 was withheld until as late as 8 h p.i. (figure 8, right). Robust inhibition was

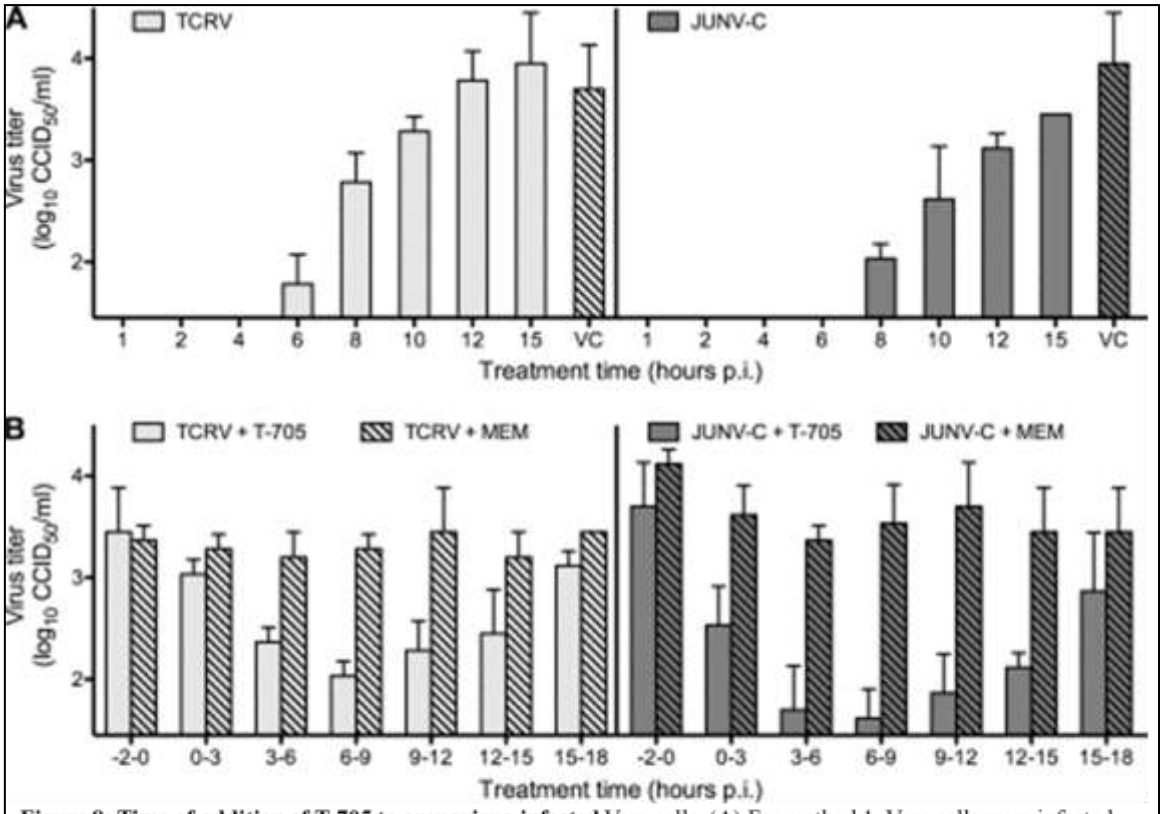

Figure 8: Time of addition of T-705 to arenavirus-infected Vero cells. (A) For method 1, Vero cells were infected with TCRV or JUNV-C and at indicated times (*x* axis) T-705 was added to infected cells at a final concentration of 200 µM. Infected cells exposed to MEM lacking T-705 (virus control [VC]) were included for comparison. Supernatants were collected 24 h p.i., and virus yields were determined. (B) For method 2, Vero cells were infected with TCRV or JUNV-C, and at indicated time intervals (*x* axis) T-705 or MEM vehicle was added to infected cells at a final concentration of 400 µM. Supernatants were collected and virus yields determined as described above. Data shown are representative of three or four independent experiments per method for each virus, and error bars represent standard deviations for triplicate samples.

observed generally in cultures treated within 6 to 8 h of infection. As T-705 is likely metabolized by the cell to form T-705RTP (Smee et al., 2009), these times represent minimal estimates for T-705 sensitivity. Nonetheless, the data suggest that T-705 acts at early or middle stages of the virus life cycle.

To investigate the timing of inhibition by T-705 in more detail, we conducted experiments wherein cells were exposed to the drug for short periods within the 24-h time frame of the experiment. The most robust inhibition of TCRV and JUNV-C replication was observed upon T-705 treatment during postinfection periods of 3 to 6 h, 6 to 9 h, 9 to 12 h, and 12 to 15 h (figure 8B). Little or no inhibition was seen when T-705 was added from −2 to 0 h, 0 to 3 h, or 15 to 18 h p.i. Taken together, these studies suggest a window for T-705 inhibition within the early and intermediate stages of virus replication, following virus entry and prior to virus assembly and budding.

Effects of purines at molar excess concentration on T-705-mediated anti-TCRV and -JUNV-C activity. Based on a previous study demonstrating that the antiviral action of T-705 in influenza virus-infected cells could be reversed by the addition of purines or purine nucleosides, but not by pyrimidines (Furuta et al., 2005), we investigated the requirements for the reversal of T-705 activity in arenavirus infection. As seen in figure 9, TCRV and JUNV-C production could be rescued from T-705 action by the addition of a molar excess of purines, including adenine, adenosine, 2-deoxyadenosine, guanine, guanosine, 2-deoxyguanosine, inosine, and hypoxanthine. In contrast, compounds generated in purine catabolism (xanthine and uric acid) and xanthosine did not reverse the action of T-705. Likewise, the pyrimidine nucleobases (cytosine, thymine, and uracil)

and nucleosides (cytidine, 2-deoxycytidine, thymidine, and uridine) had little or no impact on T-705 anti-arenavirus activity.

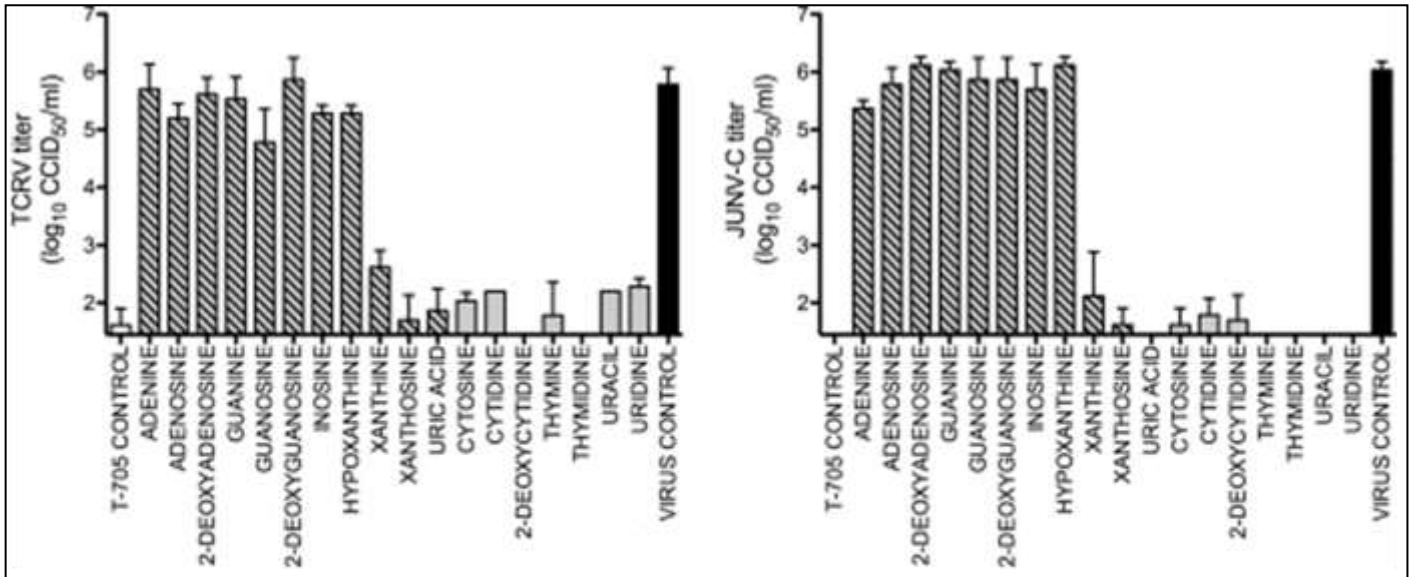

Figure 9: Reversal of T-705 antiarenavirus activity in Vero cells infected with TCRV (left) or JUNV-C (right). Vero cells were infected with TCRV or JUNV-C, and medium containing 200 μM T-705 and 400 μM of the indicated compound (*x* axis) was added to infected cells. Supernatants were collected 48 h p.i., and virus yields determined. Patterned gray bars indicate purines, and unpatterned gray bars indicate pyrimidines or their respective nucleosides or derivatives. Black bars indicate virus controls. Results shown are representative of two independent experiments for each virus, and error bars represent standard deviations for triplicate samples.

Effect of T-705 on the activity of an LCMV MG. Previous studies have shown that arenavirus replication can be modeled using a recombinant plasmid replicon system comprising the viral RdRp (L), the nucleoprotein (N), and an RNA MG (Flatz et al., 2006; Lee et al., 2000, 2002; Rusnak et al., 2009). To specifically investigate the effects of T-705 on viral replication and transcription, we made use of the LCMV replicon system. In this assay, RdRp-dependent replication of the antigenomic viral RNA is evidenced by expression of a firefly luciferase (fLuc) reporter gene in the MG RNA. Inhibition of fLuc expression in cells transfected with the three-plasmid replicon would be consistent with a disruption of RdRp function. As shown in figure 10A, transcription from the LCMV replicon system was inhibited by T-705 (EC_{50} of 29 μM). Cell-driven

expression of a cotransfected *Renilla* luciferase (RLuc) plasmid, which provides a measure of the effects on cellular transcription, was minimally affected at the highest concentrations of T-705 tested (figure 10B). This result demonstrates the specificity and apparent absence of general cytotoxicity by T-705. Ribavirin was also shown to inhibit fLuc expression by the LCMV replicon (EC_{50} of 13 μM), but considerable cytotoxicity (50% cytotoxic concentration [CC_{50}] of ~100 μM) was also observed (figure 10B). This cytotoxic effect likely contributes to the unusually steep dose-response curve observed for ribavirin (figure 10A) and artifactually reduces its EC_{50}.

Consistent with our antiviral studies, the inhibitory action of T-705 was also reversed by

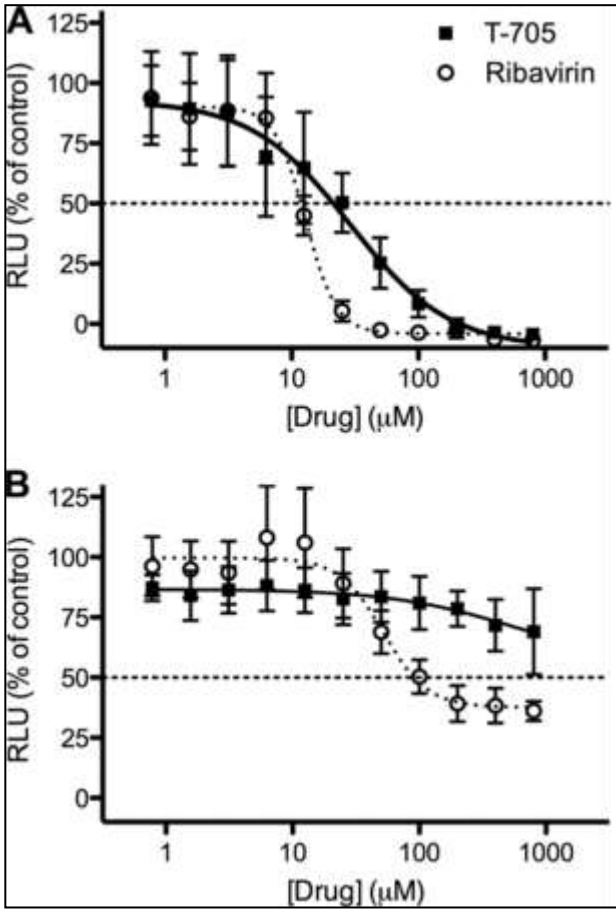

Figure 10: T-705 inhibition of LCMV replicon system. BHK cells transfected with the LCMV replicon system (fLuc) and control (RLuc) plasmids were exposed to serial dilutions of T-705 or ribavirin. After 44 h in culture, the cells were lysed, and fLuc and RLuc luminescence was detected by dual luciferase reporter assay. fLuc expression reflects L- and N-dependent replication and transcription from the LCMV MG (A), and RLuc reporter activity is representative of cellular transcription and is a measure of cell viability (B). Results are compiled from three independent experiments and are presented as percentages of untreated controls. Error bars represent standard deviations. RLU, relative light units.

purines and purine nucleosides when assessed using the LCMV replicon system. Significant rescue from inhibition was provided by adenine, adenosine, 2-deoxyadenosine, 2-deoxyguanosine, inosine, and hypoxanthine (figure 11). Guanine and guanosine also reversed the effect of T-705, albeit to a lesser extent. The pyrimidines, as well as xanthine, xanthosine, and uric acid, were again inactive in this assay. Inhibition by ribavirin was also partly reversed by guanine and guanosine. In contrast to T-705, however, the addition of adenine or adenosine did not prevent inhibition by ribavirin. This is consistent with the known inhibitory effect of ribavirin on the cellular IMPDH, which is not involved in adenosine biosynthesis. This observation suggests that the target for inhibition by T-705 is distinct from that of ribavirin, which appears to act predominantly to inhibit IMPDH and the synthesis of GMP.

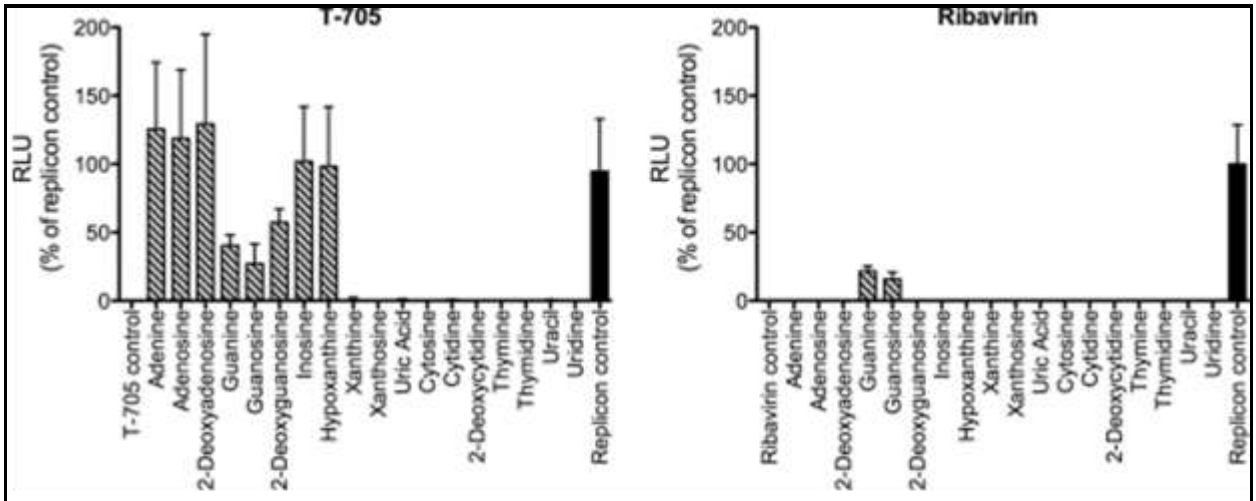

Figure 11. Reversal of T-705 LCMV replicon inhibition. Following transfection as described in the legend to Figure 10, 400 μM of the indicated compounds (*x* axis) was added to the cells with 200 μM T-705 (A) or 100 μM ribavirin (B). Cells were lysed after a 44-h culture period. Patterned gray bars indicate purines and their respective nucleosides or derivatives, and unpatterned gray bars indicate pyrimidines. Data are presented as percentages of untreated replicon controls (black bars). Results shown are representative of two independent experiments, and error bars represent standard deviations calculated from a minimum of 4 replicates. RLU, relative light units.

D. Discussion

T-705 has demonstrated remarkably broad *in vitro* activity against a range of RNA viruses. For many of these viruses, treatment options are severely limited, and in the case of influenza virus, oseltamivir resistance remains a concern (Bloom et al., 2010). In particular, therapeutic options for treating severe arenaviral hemorrhagic fever cases are restricted to the use of ribavirin (Borio et al., 2002) or, in the case of Argentine hemorrhagic fever, to transfusion of immune plasma. Safer and more effective countermeasures are clearly needed (Enria et al., 2008; Khan et al., 2008). T-705 is currently being evaluated in clinical trials in Japan and the United States for use in the treatment of influenza virus infections (Furuta et al., 2009). FDA approval for the safe use of T-705 for influenza virus infection would facilitate its development for other RNA virus treatment indications. Here, we have demonstrated for the first time that T-705 is active against the highly pathogenic human arenaviruses JUNV-R, MACV, and GTOV and provided evidence that suggests that T-705 may act as a purine nucleoside analog specifically targeting arenaviral RdRp.

A recent study exploring the mechanism of action of T-705 against influenza virus infection suggests that the viral polymerase is the principal target of the active T-705 metabolite T-705RTP (Furuta et al., 2005). We hypothesize that T-705 is also able to inhibit arenavirus multiplication by targeting the virus polymerase complex. It has been shown that influenza virus replication is inhibited by T-705 at an early or middle stage of infection and that purines but not pyrimidines are able to competitively reverse anti-

influenza virus activity (Furuta et al., 2005). In the present study, we observed analogous results in arenavirus infection.

In our studies of the reversal of T-705 inhibition, nearly all purine-based compounds showed a significant effect on T-705 activity. The notable exceptions were uric acid, xanthine, and xanthosine. Uric acid is the end product of purine degradation and would thus not be expected to affect inhibition by T-705. The biological consequences of xanthine and xanthosine metabolism are poorly defined. Indeed, all biosynthetic and catabolic purine pathways in the cell are highly interconnected and tightly regulated, making it difficult to ascribe a specific mechanism for the reversal of T-705 inhibition. However, in *in vitro* assays of influenza virus RdRp activity, GTP has been shown to be competitive with T-705RTP (Furuta et al., 2005). Further biochemical studies are needed to test the leading hypothesis that T-705 acts as a nucleoside analog to inhibit the arenaviral RdRp. Additional information from the analysis of T-705 resistance will also be helpful in identifying the precise viral target.

Inhibition of the LCMV MG system indicates that T-705 interferes with virus transcription and/or replication. The molecular mechanism for inhibition, however, is not known and may include effects on L, NP, or MG. Cellular transcription, as measured by the RLuc reporter, was unaffected. In contrast, ribavirin demonstrated significant inhibition of cellular processes at concentrations only slightly greater than those that inhibit the LCMV replicon. This is consistent with its known inhibition of IMPDH (Furuta et al., 2005; Streeter et al., 1973) and its recognized *in vivo* toxicity(Chapman et al., 1999; Rusnak et al., 2009). The ability of hypoxanthine to reverse inhibition by T-

705, but not by ribavirin, provides additional evidence that T-705 does not inhibit cellular IMPDH (Weber et al., 1992). The specific inhibitory activity of T-705 against South American VHF viruses and its apparent lack of cellular toxicity bode well for further development of T-705 in the treatment of severe arenaviral hemorrhagic fevers.

Acknowledgements

J.H.N. is grateful to Ana Sanchez (The Scripps Research Institute) and Sudhakar Agnihothram (The University of Montana) for facilitating implementation of the minigenome rescue assay.

This work was funded by subawards to B.B.G. and J.H.N. as part of National Institutes of Health (NIH) grant U54 AI-065357 (Rocky Mountain RCE; J. Belisle, principal investigator [PI]) and supported in part by NIH contract N01 AI-30048 (D.F.S., PI). J.-C.D.L.T. was supported by NIH grant R01 AI-075298.

Y.F. is an employee of the Toyama Chemical Co., Ltd., the manufacturer of T-705. All other authors declare no conflict of interest.

Chapter 3: Dissection of the Role of the Stable Signal Peptide of the Arenavirus Envelope Glycoprotein in Membrane Fusion

Emily L Messina, Joanne York, Jack H Nunberg. The Journal of Virology. 2012 June; 86(11): 6138–6145.

This study was performed in our laboratory. Joanne York contributed the experiments performed using vaccinia virus.

Abstract

The arenavirus envelope glycoprotein (GPC) retains a stable signal peptide (SSP) as an essential subunit in the mature complex. The 58-amino-acid residue SSP comprises two membrane-spanning hydrophobic regions separated by a short ectodomain loop that interacts with the G2 fusion subunit to promote pH-dependent membrane fusion. Small-molecule compounds that target this unique SSP-G2 interaction prevent arenavirus entry and infection. The interaction between SSP and G2 is sensitive to the phylogenetic distance between New World (Junín) and Old World (Lassa) arenaviruses. For example, heterotypic GPC complexes are unable to support virion entry. In this report, we demonstrate that the hybrid GPC complexes are properly assembled, proteolytically cleaved, and transported to the cell surface but are specifically defective in their membrane fusion activity. Chimeric SSP constructs reveal that this incompatibility is localized to the first transmembrane segment of SSP (TM1). Genetic changes in TM1 also affect sensitivity to small-molecule fusion inhibitors, generating resistance in some cases and inhibitor dependence in others. Our studies suggest that interactions of SSP

TM1 with the transmembrane domain of G2 may be important for GPC-mediated membrane fusion and its inhibition.

A. Introduction

Arenaviruses comprise a diverse family of enveloped negative-strand RNA viruses that are endemic to rodent populations worldwide. Infection can be transmitted to humans to cause severe acute hemorrhagic fevers with high morbidity and mortality. Lassa fever virus (LASV) is prevalent in western Africa, infecting a half-million persons annually (McCormick et al., 1987). Five species of New World (NW) hemorrhagic fever viruses are distributed throughout South America, including the Junín virus (JUNV) in Argentina. New arenavirus species frequently emerge from rodent reservoirs (Briese et al., 2009; Centers for Disease Control and Prevention (CDC), 2000; Eichler et al., 2003). In the absence of effective vaccines or therapies, the hemorrhagic fever arenaviruses are recognized to pose significant threats to public health and biodefense. Accordingly, these viruses are classified as Category A priority pathogens, and JUNV has additionally been determined by the Department of Homeland Security to pose a Material Threat to the U.S. population.

Arenavirus entry into the host cell is mediated by the virus envelope glycoprotein (GPC) (figure 12). Upon binding to a cell surface receptor (reviewed in references (Choe et al., 2011; Rojek and Kunz, 2008), the virion is endocytosed, and GPC-mediated fusion of the viral and endosomal membranes is activated upon acidification in the maturing endosome. GPC is synthesized as a precursor glycoprotein and cleaved by the cellular SKI-1/S1P protease in the Golgi (Kunz et al., 2003; Lenz et al., 2001) to generate the

receptor-binding (G1) and transmembrane fusion (G2) subunits. The mature GPC complex is metastable and thus primed to mediate membrane fusion in response to acidic pH. Upon activation, GPC undergoes a series of conformational changes leading to formation of a trimer-of-hairpins structure (Eschli et al., 2006; Igonet et al., 2011; York et al., 2010) and fusion of the viral and cellular membranes (reviewed in references(Harrison, 2008; White et al., 2008)). The arenavirus GPC is unique among

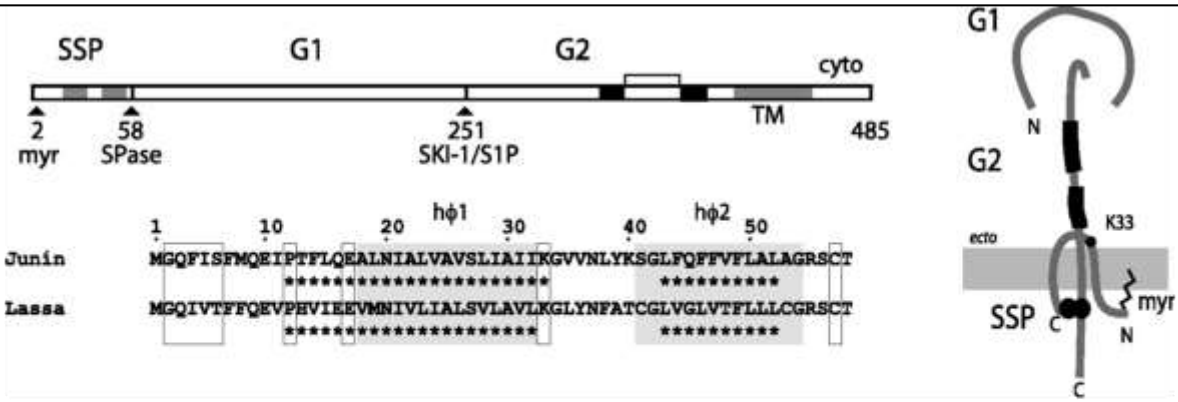

Figure 12: GPC open reading frame and subunit organization, and comparison of JUNV and LASV SSP amino acid sequences. (Top left) Amino acid residues are numbered according to the sequences of JUNV GPC. The mature subunits (SSP, G1, and G2) are labeled, as are the signal peptidase (SPase) and SKI-1/S1P cleavage sites. The myristoylation site at glycine-2 is labeled, and the transmembrane regions in SSP and G2 are shaded. The two heptad-repeat sequences in G2, and the hinge-region disulfide-bonded loop, are drawn in black. (Bottom left) The amino acid sequences of JUNV and LASV SSP are compared. The two hydrophobic membrane-spanning regions (hϕ1 and hϕ2) are shaded, and conserved residues referred to in the text are boxed (myristoylation motif, P12, E17, K33, and C57). Asterisks below the sequences indicate helical folds predicted by the PROFsec algorithm as implemented by PredictProtein (reliability score, ≥7). (Right) Schematic model for the subunit organization of the tripartite GPC complex. SSP is shown spanning the membrane twice; the myristoylated N terminus is presumed to be associated with the cytoplasmic face of the membrane, and the penultimate C-terminal C57 residue participates in a binuclear zinc-finger motif in G2. The K33 position in the ectodomain of SSP modulates pH-dependent membrane fusion and sensitivity to small-molecule fusion inhibitors. The two heptad-repeat regions in the G2 ectodomain are shown in black. The relative placement of the three transmembrane regions is arbitrary and the drawing is not to scale. (Agnihothram et al., 2007; Briknarová et al., 2011; York et al., 2004; York and Nunberg, 2007a; York and Nunberg, 2009; York et al., 2008)

class I envelope glycoproteins in that it retains its cleaved signal peptide as a third subunit (Eichler et al., 2003; Froeschke et al., 2003; York et al., 2004).

The 58-amino-acid stable signal peptide (SSP) of GPC contains two hydrophobic segments that span the membrane and are joined by a short ectodomain loop figure 12 (Agnihothram et al., 2007). The cytoplasmic N terminus of SSP is myristoylated, while the penultimate C-terminal cysteine (C57) coordinates with a zinc-binding domain in the cytoplasmic tail of G2 to form an intersubunit structure that anchors SSP in the GPC complex (Briknarová et al., 2011; York and Nunberg, 2007a). SSP association masks endogenous endoplasmic reticulum (ER) retention/retrieval signals in the cytoplasmic domain of G2 to facilitate GPC transport through the Golgi (Agnihothram et al., 2006), whereupon the precursor is proteolytically cleaved and transported to the cell surface for virion assembly.

Our studies suggest that pH-induced activation of the mature GPC complex is controlled by a unique interaction between the short ectodomain loop of SSP and the G2 fusion subunit. Side chain substitutions that reduce positive polarity at SSP K33 depress the pH required to trigger membrane fusion (York and Nunberg, 2006) , and this phenotype can be rescued by secondary mutations in G2 (York and Nunberg, 2009). Importantly, this SSP-G2 interaction provides a molecular target for small-molecule compounds that stabilize the prefusion GPC complex, thereby preventing pH-induced activation in the endosome (Bolken et al., 2006; Larson et al., 2008; Lee et al., 2008; York et al., 2008). The different classes of fusion inhibitors demonstrate distinct patterns of specificity against New World (NW) and Old World (OW) arenaviruses yet share a

binding site on GPC (Bolken et al., 2006; Larson et al., 2008; Thomas et al., 2011; York et al., 2008). Sequence variation at the nominal SSP-G2 interface likely accounts for the differences in species specificity (Thomas et al., 2011; York et al., 2008). Several of these fusion inhibitors have recently been shown to protect against lethal arenavirus disease in animal models (Bolken et al., 2006; Cashman et al., 2011).

Sequence variation between OW and NW arenavirus species may also affect the ability of one SSP to function in the context of a heterotypic GPC complex. For instance, recombinant JUNV virions in which SSP and the G1G2 precursor are heterotypic are not viable (Albariño et al., 2011). We have exploited this interspecies incompatibility between LASV and JUNV GPCs to identify determinants in SSP required for membrane fusion activity. We found that SSP association, proteolytic maturation, and transport to the cell surface are promiscuous in interspecific hybrid GPCs and that heterotypic SSPs support these functions in the context of either JUNV or LASV G1G2 precursors. Preservation of pH-dependent membrane fusion, however, requires a specific homotypic match in the first transmembrane domain (TM1) of SSP. We propose that this amphipathic helical region of SSP interacts with the transmembrane domain of G2 and thus contributes to the pH-dependent membrane fusion activity of arenavirus GPC.

B. Materials and Methods

Plasmids. GPC from the pathogenic MC2 isolate of JUNV (Ghiringhelli et al., 1991) and from the Josiah isolate of LASV (Larson et al., 2008) was expressed using the minimal T7 promoter sequence in pcDNA 3.1-based vectors (Life Technologies). In order to obviate concerns regarding signal peptidase cleavage of SSP in the chimeric GPC

constructs, SSP and G1G2 open reading frames were expressed from separate plasmids, taking advantage of the ability of the two polypeptides to associate in *trans* to reconstitute the functional GPC complex (Eichler et al., 2003; York and Nunberg, 2007b). The G1G2 precursor was directed to the membrane using the conventional signal peptide of human CD4, as previously described (York and Nunberg, 2007b). An innocuous FLAG affinity tag was appended to the C terminus of LASV G1G2 to facilitate detection (York et al., 2004). SSP chimeras were constructed using conventional PCR procedures, and mutations were introduced using QuikChange methodology (Stratagene).

Antibodies and small-molecule entry inhibitors .JUNV G1-specific monoclonal antibodies (MABs) BF11 and BE08 (Sanchez et al., 1989) were obtained through the NIAID Biodefense and Emerging Infections Research Resources Program (BEIResources) and the FLAG peptide-specific MAB (M2) was purchased from Sigma. The LASV G1-specific MAB L52 134-23 (Ruo et al., 1991) was kindly provided by Connie Schmaljohn (USAMRIID). The small-molecule fusion inhibitors ST-294, ST-193, ST-161, and ST-761 have been previously described (Bolken et al., 2006; Larson et al., 2008; Thomas et al., 2011; York et al., 2008) and were kindly provided by SIGA Technologies (Corvallis, OR).

Analysis of GPC expression. GPC was expressed by transient transfection in Vero cells infected with the vTF-7 vaccinia virus expressing T7 polymerase (Fuerst et al., 1986) or in engineered BHK-21 cells expressing T7 polymerase (BSR T7/5) (Buchholz et al., 1999), kindly provided by Klaus Conzelmann (Ludwig-Maximilians-University Munich). Proteins were metabolically labeled using ^{35}S-labeled amino acids (Perkin Elmer) and

immunoprecipitated with the appropriate MAB as previously described (York and Nunberg, 2007b). Flow cytometric detection of cell surface GPC was hindered by low levels of expression using our pcDNA-based vectors in BSR T7/5 cells, especially for LASV GPC (see Results and Discussion). Therefore, for these studies GPC was expressed in Vero cells using a pCAGGS-MCS vector (Niwa et al., 1991) provided by Juan Carlos de la Torre (Scripps Research Institute) (Urata et al., 2011). Cell surface expression was determined using the JUNV G1-specific MAB BE08 (Sanchez et al., 1989)or the LASV G1-specific MAB L52 134-23 (Ruo et al., 1991), and a secondary fluorescein isothiocyanate (FITC)-labeled anti-mouse immunoglobulin antibody. The cell populations were stained with propidium iodine to exclude dead cells, fixed with 2% formaldehyde, and analyzed using a FACSCalibur flow cytometer (BD Biosciences).

Analysis of GPC-dependent membrane fusion .The recombinant vaccinia virus-based assay for GPC-mediated cell-cell fusion was performed as previously described (York and Nunberg, 2006). Briefly, Vero cells infected by vTF-7 and expressing GPC are cocultured with cells infected with a recombinant vaccinia virus vCB21R-lacZ bearing the β-galactosidase gene under the control of the T7 promoter (Nussbaum et al., 1994). Cell-cell fusion is triggered by exposure to medium adjusted to pH 5.0 and detected through β-galactosidase expression in the newly formed syncytia. Fusion is quantitated by chemiluminescence using the GalactoLite Plus substrate (Life Technologies). Fusion inhibition by small-molecule SIGA compounds was determined as previously described (York et al., 2008) and GraphPad Prism software was used for nonlinear regression calculations using a single-slope dose-response model constrained to 100% fusion in the absence of inhibitor.

In order to circumvent biosafety concerns associated with the use of vaccinia viruses, we developed an alternative fusion reporter assay based on expression of T7 polymerase in BSR T7/5 cells. In this format, GPC-expressing BSR T7/5 cells were cocultured with human 293T cells transfected with the internal ribosome entry site (IRES)-containing pT7EMC-luc reporter plasmid expressing luciferase under the control of the T7 promoter (Satoh et al., 2008), which was kindly provided by Yoshiharu Matsuura (Osaka University). Following a 5-min exposure to medium adjusted to pH 5.0, the coculture was continued at neutral pH for 12 h to allow for luciferase expression. Cell-cell fusion was detected using the luciferase assay kit substrate (Promega). Consistency of GPC expression was monitored by immunohistochemical staining. Results from this novel fusion reporter assay were validated in parallel experiments using the well-established vaccinia virus-based assay.

C. Results and Discussion

Divergence between JUNV and LASV SSPs. A comparison of the amino acid sequences of JUNV and LASV SSPs reveals a high degree of sequence divergence, as well as an overall conservation of sequence motifs (figure 12). The two hydrophobic domains (hϕ1 and hϕ2) in each are separated by a short region containing the conserved K33 residue (York and Nunberg, 2006). A myristoylation motif and zinc-coordinating cysteine (C57) are present in both N- and C-terminal cytoplasmic domains, respectively (Agnihothram et al., 2007). Both SSPs are also predicted to possess similar secondary structure features, with two helical regions interspersed by an unstructured ectodomain

loop. Despite these similarities, fewer than 40% of the amino acids are identically conserved.

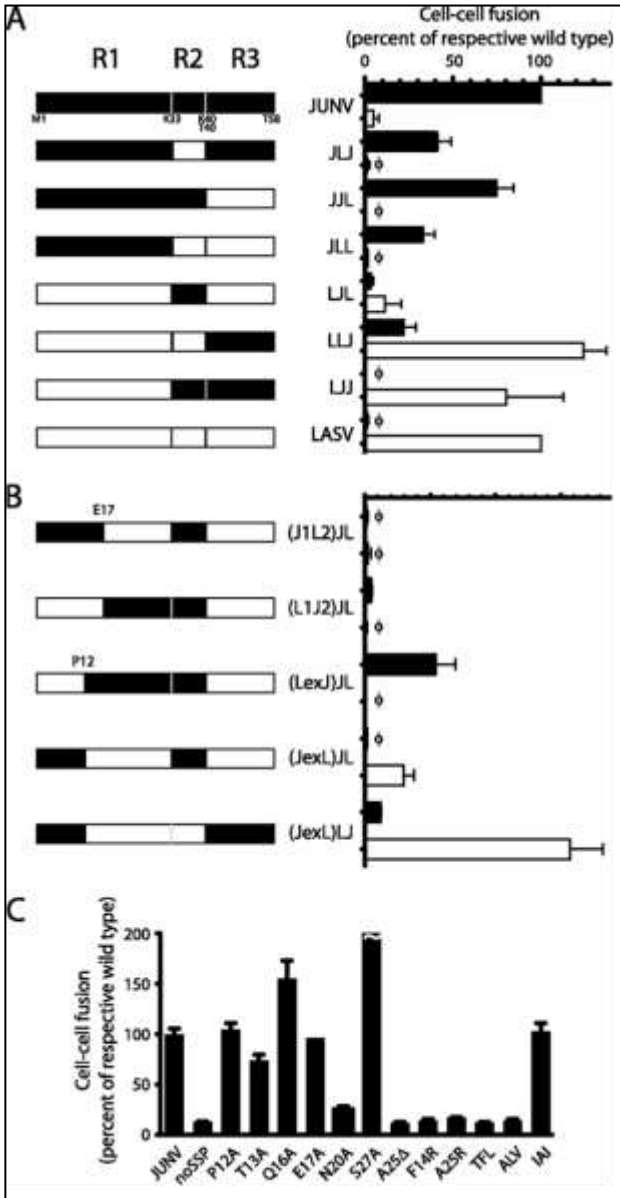

Figure 13: Membrane fusion activity of JUNV and LASV hybrids and TM1 mutants. Schematic drawings of chimeric SSP constructs are shown to the right of A and B. Regions 1, 2, and 3 (R1, R2, and R3, respectively) are boxed, and JUNV or LASV sequences are indicated by black or white fills, respectively. The regions are drawn to scale, and junction amino acid residues are labeled. Cell-cell fusion by hybrid GPCs containing JUNV or LASV G1G2 and the SSP chimeras is indicated by paired black and white bars, respectively, to the right. Fusion activity was determined using BSR T7/5 cells as described in Materials and Methods and normalized as a percentage of the respective wild-type JUNV or LASV GPC. The symbol ϕ is used to indicate the absence of significant fusion. Error bars represent the standard error of the mean (SEM) of 2 to 6 independent assays. (C) Mutated JUNV SSPs were expressed with JUNV G1G2 and cell-cell fusion was normalized to the wild type. One complete assay representative of at least four experiments with complete or partial collections of the mutants is depicted. Each point is an average of 8 duplicate wells, and error bars (SEM) are shown. The bar denoting S27A cell-cell fusion (284% ± 14%) is truncated at 200% of wild type.

Hybrid GPC containing heterologous SSP and G1G2. Reverse-genetics studies have shown that hybrid GPC complexes are functional for arenavirus infection if and only if SSP is homotypic with the TM and C-terminal cytoplasmic domains of G2 (Albariño et al., 2011). To investigate the molecular basis for this finding, we characterized the assembly, transport, and function of hybrid GPCs. Taking advantage of the observation that SSP can associate in *trans* with the G1G2 precursor to reconstitute the functional GPC complex (Eichler et al., 2003; York et al., 2004), we coexpressed JUNV or LASV SSP with the reciprocal G1G2 precursors, which contained the conventional signal peptide of human CD4 (York and Nunberg, 2007b; York et al., 2004). Membrane fusion activity of the homologous and heterologous hybrid GPCs was determined using a biosafe modification of the well-characterized vaccinia virus-based cell-cell fusion assay (York et al., 2004). BSR T7/5 cells expressing the bacteriophage T7 polymerase (Buchholz et al., 1999) were cotransfected with pcDNA3.1-based plasmids expressing SSP and the G1G2 precursor under the control of the T7 promoter. These cells were then cocultured with 293T fusion reporter cells expressing luciferase in a T7 polymerase-dependent manner. Cell-cell fusion was initiated by exposing the coculture to medium adjusted to pH 5.0, and luciferase expression in the newly formed syncytia was determined following continued incubation at neutral pH. Using this assay, we verified that neither of the two heterotypic GPC hybrids (JUNV SSP with LASV G1G2 or LASV SSP with JUNV G1G2) was able to mediate membrane fusion (figure 13A). Concordant cell-cell fusion results were obtained using the vaccinia virus-based fusion reporter assay ((York et al., 2004) and data not shown).

Hybrid GPC assembles and is transported to the cell surface. To determine the molecular basis of heterotypic incompatibility, we first investigated the ability of SSP to associate with the G1G2 precursor. It is possible that the absence of membrane fusion

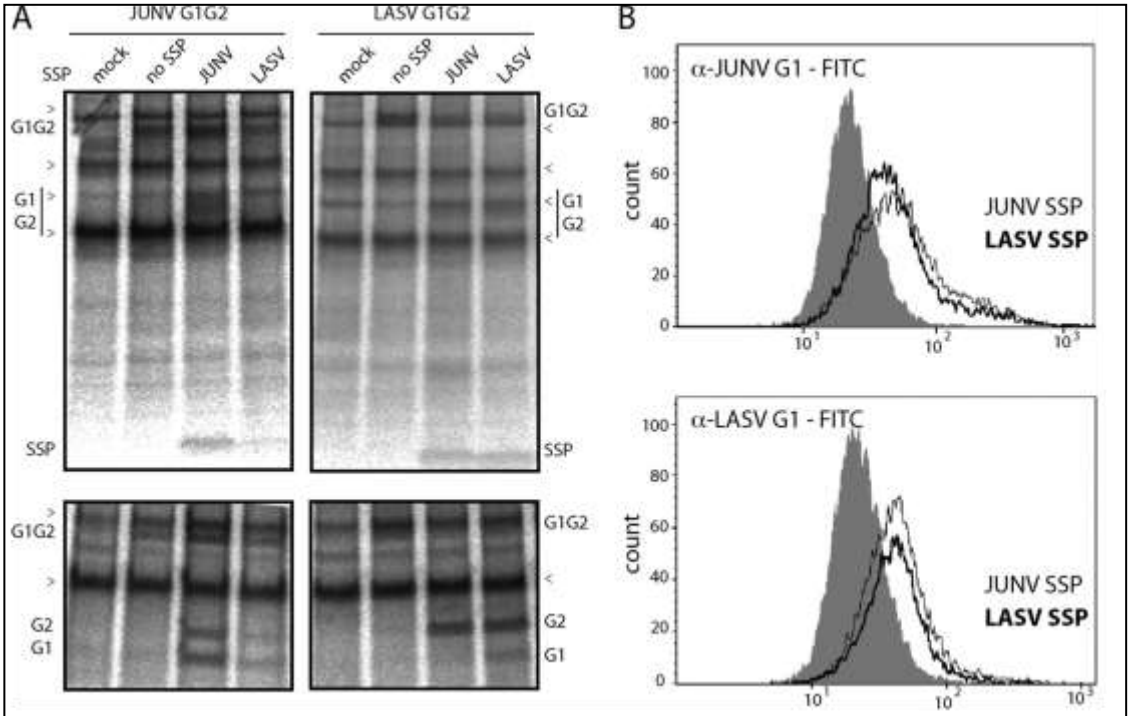

Figure 14: JUNV and LASV hybrid GPCs are properly assembled, proteolytically matured, and transported to the cell surface. Combinations of JUNV and LASV SSPs and G1G2 precursor proteins were coexpressed in BSR T7/5 cells, and the metabolically labeled GPCs were immunoprecipitated for SDS-PAGE analysis. GPCs containing JUNV G1G2 were precipitated using the G1-directed MAb BF11, and those containing LASV were collected using a FLAG tag appended to the C terminus of G1G2. (A) The immunoprecipitated proteins were resolved using a 4–12% NuPAGE Bis-Tris gel (Invitrogen). The JUNV and LASV G1G2 precursors and coprecipitated SSPs are indicated. The mature G1 and G2 glycoproteins are heterodisperse and are better resolved as polypeptides following deglycosylation using PNGaseF (New England BioLabs) (bottom). The unequal recovery of G1 and G2 subunits seen in some experiments using G1-directed (JUNV) or G2-directed FLAG (LASV) antibodies likely reflects partial dissociation of the complex during immunoprecipitation. While GPC expression in BSR T7/5 cells is adequate for membrane fusion activity, protein levels are low, and carets are used to distinguish background bands manifest in mock-transfected cells. (B) Cell surface accumulation of JUNV and LASV GPC hybrids expressed in Vero cells using a pCAGGS plasmid was determined by flow cytometry. GPC was detected using JUNV or LASV G1-specific MAbs (BE08 or L52 134-23, respectively) and a FITC-conjugated secondary antibody. Cells expressing JUNV SSP (thin line) or LASV SSP (thick line) are compared with those in which the cell surface transport of the respective G1G2 precursor is prevented by the absence of SSP (shaded histogram). (Agnihothram et al., 2006; Niwa et al., 1991; Ruo et al., 1991; Sanchez et al., 1989; Urata et al., 2011; York and Nunberg, 2006)

activity reflects an inability of SSP to bind the heterologous G1G2 precursor, thereby preventing GPC transport through the Golgi, proteolytic maturation, and cell surface expression. To assess GPC biogenesis, SSP and the G1G2 precursor were expressed in *trans*, and metabolically labeled GPC was immunoprecipitated (York and Nunberg, 2007b) using MABs directed to either JUNV G1 (Sanchez et al., 1989) or the C-terminal FLAG tag on LASV G2. We found that GPC protein synthesis was markedly reduced in BSR T7/5 cells relative to that typically seen in Vero cells infected with recombinant vaccinia viruses expressing T7 polymerase (Fuerst et al., 1986; York et al., 2004), presumably reflecting the absence of mRNA capping in the cytosol of transfected BSR T7/5 cells. Nevertheless, SDS-PAGE analysis showed that SSP association in the heterotypic GPCs was similar to that in the homotypic complex (figure 14A). Furthermore, this association was sufficient to promote a significant degree of proteolytic maturation of the heterologous G1G2 precursor (figure 14A). Flow cytometry was used to confirm trafficking of the heterotypic GPC hybrids to the cell surface. Due to the low level of expression of LASV GPC in BSR T7/5 cells (figure 14A), we used a well-characterized pCAGGS plasmid vector (Niwa et al., 1991) for these studies of GPC transport(Urata et al., 2011). Cell surface accumulation of heterologous GPC hybrid was found to be similar to that of the homotypic protein in both cases (figure 14B). As GPC transport does not require proteolytic cleavage (Agnihothram et al., 2006; Schibli and Weissenhorn, 2004), these findings assess an independent function of SSP association. Conversely, transit of GPC through the Golgi, as evidenced by proteolytic cleavage, is predictive of cell surface expression. Despite substantial sequence divergence, both heterologous SSPs were capable of promoting the assembly and maturation of the hybrid

GPC complex, as well as its transport to the plasma membrane. This result agrees with previous studies using a recombinant LASV GPC encoding JUNV SSP (Albariño et al., 2011). Because very low levels of mature GPC are sufficient to support membrane fusion activity (Agnihothram et al., 2007; York et al., 2005), we surmise that the partial reductions in SSP association and proteolytic cleavage in the heterotypic GPC hybrids are by themselves insufficient to explain the complete loss of fusogenicity. This conclusion is reinforced by the overall lack of correlation between variations in proteolytic cleavage and membrane fusion activity in studies using chimeric SSP molecules (see below).

Interchange of the ectodomain loop in SSP. We have previously shown that the short ectodomain loop of SSP is critical for pH-dependent membrane fusion and its inhibition by small-molecule inhibitors (York and Nunberg, 2006; York et al., 2008). This region of JUNV SSP is defined by charged residues at the ectodomain termini of TM1 and TM2 (K33 and K40, respectively) (figure 12). We therefore subdivided SSP into three regions for purposes of constructing chimeras: region 1 included the myristoylated N terminus of SSP and TM1 (residues M1 to K33), region 2 comprised the ectodomain loop (K33 to K40 in JUNV, T40 in LASV), and region 3 contained TM2 and the short cytoplasmic domain bearing C57 (to the C-terminal T58). All combinations of the three JUNV and LASV subdomains were constructed (figure 13A), and the chimeric SSPs were named according to the three regions. For instance, JJJ represents the wild-type JUNV SSP and JLJ signifies a chimera in which the ectodomain from LASV was fused to regions 1 and 3 of JUNV SSP. For clarity, we will refer to recombinant SSPs as chimeras and reserve the term hybrid for the reconstituted GPC complex.

As anticipated from the fully heterotypic GPC hybrids (figure 14A) , all of the chimeric SSPs associated with the JUNV G1G2 precursor and supported proteolytic cleavage in BSR T7/5 cells (figure 15). Parallel metabolic labeling studies using LASV GPC again showed poor expression but nonetheless allowed similar conclusions (not

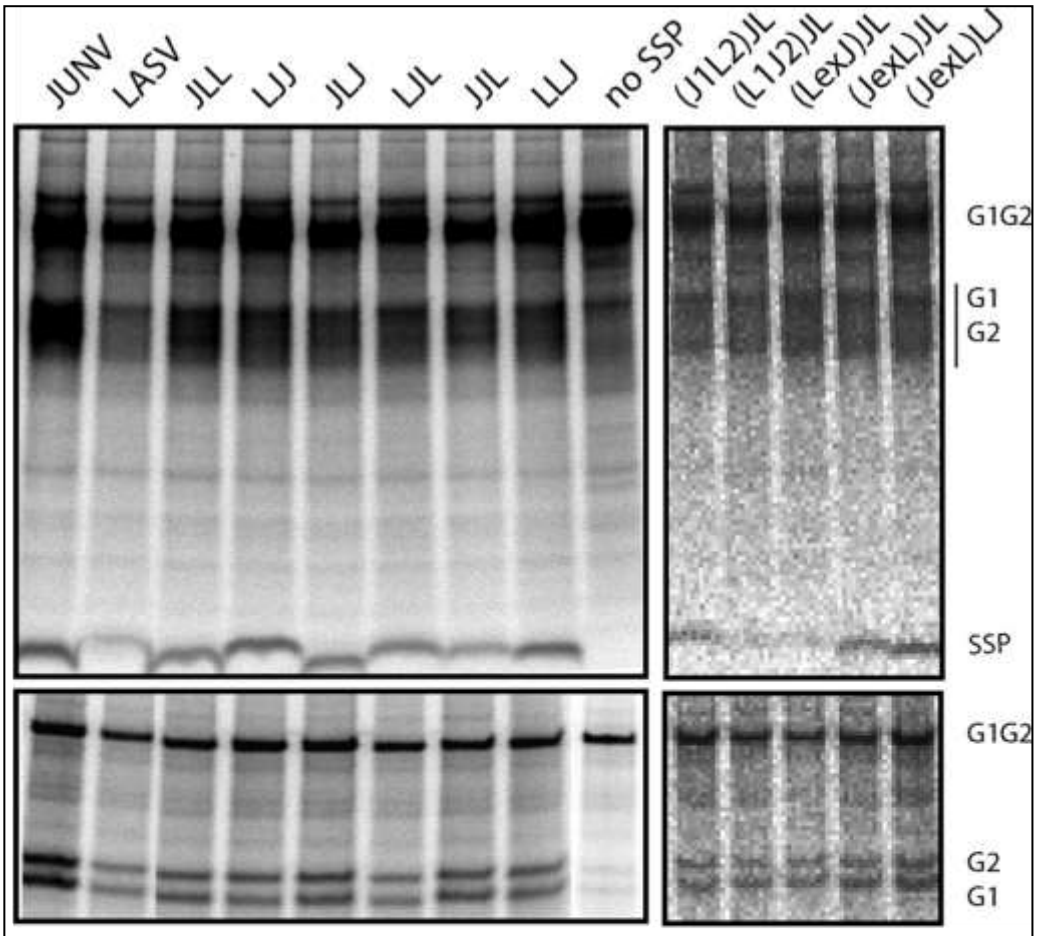

Figure 15: JUNV GPCs containing chimeric SSPs are properly assembled and proteolytically matured. JUNV G1G2 was coexpressed with the indicated chimeric SSPs in BSR T7/5 cells, and metabolically labeled GPC was immunoprecipitated for SDS-PAGE analysis as described in Fig. 14. The G1G2 precursors and coprecipitated SSPs are indicated (top). The mature G1 and G2 glycoproteins are heterodisperse and are better resolved as polypeptides following deglycosylation using PNGaseF (New England BioLabs) (bottom).

shown). These findings were further validated using recombinant vaccinia virus to drive GPC expression ((York et al., 2004) and data not shown). We conclude that the sequence requirements for SSP association and proteolytic maturation are relatively relaxed in interspecific GPC chimeras.

Despite its critical role in membrane fusion, interspecific exchange of the ectodomain loop had little effect on the fusion activity of hybrid GPCs (figure 13). LJL did not restore fusion activity to the JUNV G1G2 hybrid (~3% of wild-type JUNV GPC) and likewise the reciprocal JLJ SSP in the LASV G1G2 hybrid (<1% of wild-type LASV GPC). Conversely, replacement of the ectodomain in JUNV SSP with that of LASV (JLJ) had a relatively small effect on the fusion activity of the hybrid JUNV GPC (~40% of JUNV GPC). The reciprocal hybrid, LASV G1G2 bearing LJL SSP, retained a lower albeit significant level of activity (~10% of LASV GPC). We conclude that a homotypic ectodomain loop in SSP is neither sufficient nor absolutely necessary to support membrane fusion by the hybrid GPC complex.

Region 1 of SSP is essential for membrane fusion activity. Analysis of the remaining SSP chimeras did reveal an important role for the N-terminal region 1 in SSP function. Only LASV hybrids containing the homologous region 1 (LJL, LLJ, and LJJ) showed significant membrane fusion activity (figure 13A). Whereas the LJL hybrid supported ~10% of wild-type activity (above), the latter two SSP chimeras promoted cell-cell fusion at levels comparable to those of native LASV GPC. The reciprocal pattern was seen with the JUNV G1G2 precursor and the JLJ, JJL, and JLL chimeras. In JUNV GPC, SSP bearing a mismatch in regions 1 and 2 (LLJ) unexpectedly also exhibited fusion

activity (~20% of the wild type). By comparison, all hybrids displayed similar patterns of GPC expression (figure 15). Taken together, these results indicate that homotypic pairing in SSP region 1 is paramount for membrane fusion activity. Region 2 appears to contribute somewhat to activity when the homologous region 1 is present (JJL and LLJ), whereas homology in region 3 is relatively unimportant. The reciprocal relationship between JUNV and LASV hybrids validates the importance of region 1 as a determinant of GPC-mediated membrane fusion.

The apparent indifference to sequence variation in region 3 is consistent with previous results from mutational studies (Agnihothram et al., 2007). Triplet alanine replacements in TM2 of JUNV SSP (44FQF46 and 47FVF49 mutants) have no effect on fusogenicity. Similarly in the short C-terminal cytoplasmic tail of SSP, only the conserved C57 side chain is essential for membrane fusion activity (York and Nunberg, 2007b). Collectively, these observations suggest a lack of sequence specificity in the function of region 3. However, the presumed helical nature of TM2 appears to be important, as SSP association is completely abrogated by single amino acid deletions that are expected to alter the register of the helix (Agnihothram et al., 2007).

TM1 forms an extended helical domain. To further dissect the role of region 1 in fusogenicity, we bisected the N-terminal cytoplasmic and TM regions using the conserved E17 as the nominal cytosolic junction of TM1. Thus, the (J1L2) exchange in region 1 comprised JUNV residues M1 to E17 and LASV residues E17 to K33 (figure 13B). SSPs including the reciprocally exchanged sequences (J1L2 and L1J2) associated with and supported proteolytic maturation of both JUNV (figure 15) and LASV

precursors (not shown) but were entirely defective in promoting membrane fusion (figure 13B). In contrast, the parental SSP chimeras containing the intact region 1 (JJL and LJL) produced functional hybrids with their respective G1G2 precursors. The symmetric loss of fusogenicity at this junction is likely to reflect an internal sequence incompatibility within the SSP chimeras rather than between SSP and G2.

Secondary structure predictions suggested a possible explanation for this intramolecular incompatibility (figure 12). For both JUNV and LASV SSP, prediction algorithms (Rost and Sander, 1993) suggest that the helical structure of TM1 extends N terminally to the conserved proline at position 12. To test this notion, we generated additional region 1 exchanges in which TM1 was extended N terminally to P12. We found that an SSP chimera including the extreme N-terminal residues of LASV (residues M1 to P12) and the extended helical region of JUNV (residues P12 to K33), referred to as (LexJ)JL, supported cell-cell fusion comparably to the parental JJL chimera in the hybrid JUNV GPC (figure 13B). Likewise, SSPs containing the (JexL)LJ and (JexL)JL exchanges promoted detectable fusion activity in LASV G1G2 hybrids. In keeping with our previous finding that replacing E17 with alanine did not disrupt membrane fusion activity (York and Nunberg, 2006), we propose that TM1 spans P12 to K33 to form a functional transmembrane subdomain in SSP.

The above results also suggest that the extreme N terminus of SSP, comprising a myristoylation motif (GxxxS/T) and residues through I11, is interchangeable between JUNV and LASV. Indeed, alanine-scanning mutagenesis in this region of LCMV SSP showed only minimal effects on fusogenicity (Saunders et al., 2007). The amino acid

sequence of the cytoplasmic portion of region 1 appears relatively unimportant for membrane fusion activity. By contrast, the lack of myristoylation in SSP reduces fusogenicity by ~80% through an unknown mechanism (Saunders et al., 2007; York et al., 2004) .

Genetic analysis of the extended TM1. Site-directed mutagenesis was used to probe the extended TM1 helix in JUNV SSP. We reasoned that deletion of a single amino acid residue would alter the register of the helix without disrupting the overall helical fold (Agnihothram et al., 2007). A JUNV GPC mutant bearing a deletion at TM1 residue A25 was found to be devoid of membrane fusion activity (figure 13C), consistent with a requirement for specific interhelical interactions within the GPC complex. Replacing hydrophobic amino acids with arginines in a membrane-spanning region is expected to be highly destabilizing, and the F14R and A25R mutants were indeed defective in membrane fusion (figure 13C). The deficiency in F14R supports our previous suggestion that SSP enters the membrane at P12. Neither the deletion nor arginine replacement mutants associated with the G1G2 precursor (not shown). Taken together, these results point to the critical importance of the extended TM1 helix in GPC biology.

Owing to the helix-breaking property of proline, TM1 is unlikely to include residues N terminal to the conserved P12. To determine whether P12 itself is essential for GPC assembly and fusogenicity, we mutated this position in JUNV SSP to alanine. The P12A mutant was found to possess wild-type fusion activity (figure 13C). The identical mutant in LCMV SSP also showed significant fusion activity (~30% of the wild type) but did not promote entry by recombinant virus-like particles (Saunders et al., 2007) .

Thus, a proline-dependent articulation between the cytosolic N terminus and TM1 is not required for fusogenicity *per se*.

TM1 forms an amphipathic helix. A helical-wheel projection diagram reveals distinct hydrophobic and hydrophilic faces to the extended TM1 helices in JUNV and LASV SSPs (figure 16). By contrast, TM2 of SSP (K40/T40 to G54) is uniformly hydrophobic. As TM2 was found to be highly tolerant of triplet-alanine substitutions (Agnihothram et al., 2007), we employed a similar strategy to examine the requirement for side chain-specific interactions in TM1. We replaced three hydrophobic sequences in TM1 of JUNV SSP (13TFL15, 22ALV24, and 29IAI31) with triplet alanines, a small

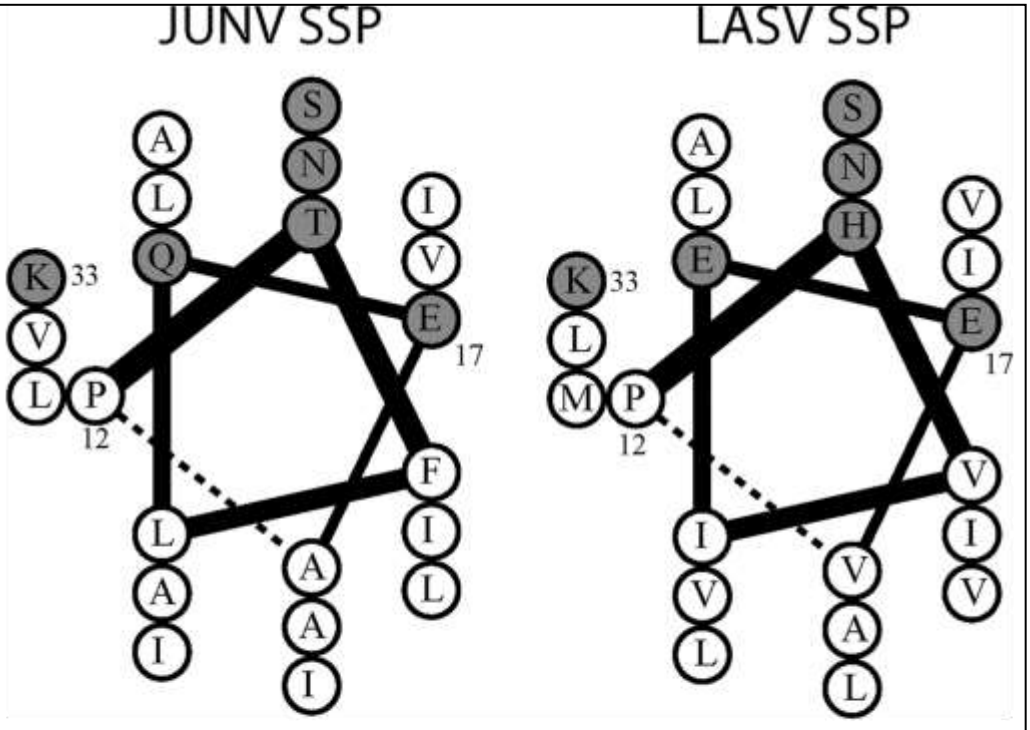

Figure 16: Helical-wheel projections of the amphipathic TM1 of JUNV and LASV SSP. The drawing was prepared using DrawCoil 1.0 . This view is from the N terminus of TM1 (P12) and extends through K33 in the SSP ectodomain. Polar residues are highlighted in gray. Grigoryan G. 2011. DrawCoil 1.0. arteni.cs.dartmouth.edu/drawcoil/

residue with high helical propensity. Alanine substitutions at 13TFL15 and 22ALV24 were found to disrupt membrane fusion activity (figure 13C). Fusogenicity was unaffected by alanine replacements at 29IAI31, probably due to its position in the helix and the conservative nature of the change. The defect in the 13TFL15 and 22ALV24 mutants strongly suggests that TM1 participates in side chain-specific interactions in the GPC complex, likely with the transmembrane helical domain of G2.

To probe the contributions of specific side chains in TM1 to these interactions, we individually replaced each polar residue on the hydrophilic face of TM1 with alanine (figure 13C) . T13A, Q16A, and S27A GPCs were essentially wild type in cell-cell fusion activity, as was E17A (Agnihothram et al., 2007). The N20A mutation, however, decreased membrane fusion activity to ~30% of the wild type (figure 13C) , as did the identical mutant in LCMV GPC (Saunders et al., 2007). Interestingly, structural predictions by the Robetta server (http://robetta.bakerlab.org) (Kim et al., 2004) consistently position N20 at a kink in the TM1 helix (not shown).

SSP chimeras differ in sensitivity to small-molecule fusion inhibitors. We have previously shown that both pH-dependent activation and its inhibition by small-molecule fusion inhibitors are mediated through interactions between SSP and the G2 fusion subunit (York and Nunberg, 2006, 2009; York et al., 2008)). We therefore examined the sensitivity of hybrid GPCs to inhibition by the four chemically distinct fusion inhibitors discovered by SIGA Technologies (Corvallis, OR) (Bolken et al., 2006; Larson et al., 2008; Thomas et al., 2011; York et al., 2008). These compounds share a binding site (Thomas et al., 2011) but differ in their specificity toward NW and OW arenaviruses: ST-

294 and ST-761 are active only against NW viruses, ST-161 is specific for LASV, and ST-193 is broadly inhibitory against both OW and NW arenaviruses (Bolken et al., 2006; Larson et al., 2008; Thomas et al., 2011; York et al., 2008).

As hybrid GPCs heterotypic in SSP region 1 are nonfunctional, we focused our attention on the ectodomain loop, a region previously shown to affect inhibition (York et al., 2008). Substitution of the JUNV ectodomain loop in LASV GPCs [LJJ and (JexL)JL] abrogated inhibition by the LASV-active compounds ST-161 and ST-193 (not shown). In contrast, replacement of the ectodomain loop in JUNV GPCs (JLL, JLJ) showed no significant effects on sensitivity; all were inhibited by ST-294, ST-761, and ST-193 and resistant to ST-161 (not shown). Structural differences at the hybrid inhibitor-binding site likely contribute to the differing contributions of the heterotypic SSP ectodomain in LASV and JUNV GPC. None of the hybrids displayed *de novo* sensitivity to inhibition.

We utilized the panel of alanine mutations in JUNV TM1 to further identify specific side chains that may influence sensitivity to inhibition. The triplet-alanine mutant (the 29IAI31 mutant), with substitutions adjacent to the SSP ectodomain and the critical K33 residue, was found to be unchanged in its sensitivity to ST-294 and ST-193 and resistance to ST-161 (figure 17 and table 2). Similarly, individual alanine mutations at Q16, E17, and S27 on the hydrophilic face of TM1 did not significantly alter the pattern of inhibition. By contrast, alanine substitutions toward the cytosolic terminus of TM1 (P12A and T13A) engendered resistance to ST-193 without qualitative or quantitative changes in the effects of ST-294, ST-761, or ST-161 (figure 17 and table 2). Furthermore, the N20A mutant was now strikingly dependent on ST-193 for wild-type

fusion activity. Fusion was enhanced by the addition of ST-193 in a dose-dependent manner. Maximal activity approaches that of the wild-type JUNV GPC at ~10 μM ST-193, at which point inhibitory and/or cytotoxic effects may intervene. Sensitivities to ST-294 and ST-161 remain unaffected. The diversity in the effects of these different amino acid substitutions highlights the multiplicity of determinants for fusion inhibition within the GPC complex (York and Nunberg, 2009; York et al., 2008).

We suggest that ST-193 binding to N20A compensates for structural changes induced by the mutation, thereby facilitating on-path conformational changes during pH-induced activation of membrane fusion. Mutations in G2 previously reported to increase the pH of activation in the K33Q mutant to wild type without themselves affecting pH sensitivity may act similarly (York and Nunberg, 2009). Among these compensatory G2 mutations, two (D400A and F427A) also engender resistance to ST-193 and ST-294 ((York et al., 2008) and unpublished data). Based on the dependence of the N20A mutant on the presence of inhibitor, we infer that resistance at the two G2 positions, as well as that in P12A and T13A SSP mutants, may reflect a balance of inhibitory and compensatory consequences of ST-193 binding rather than a simple loss in binding affinity.

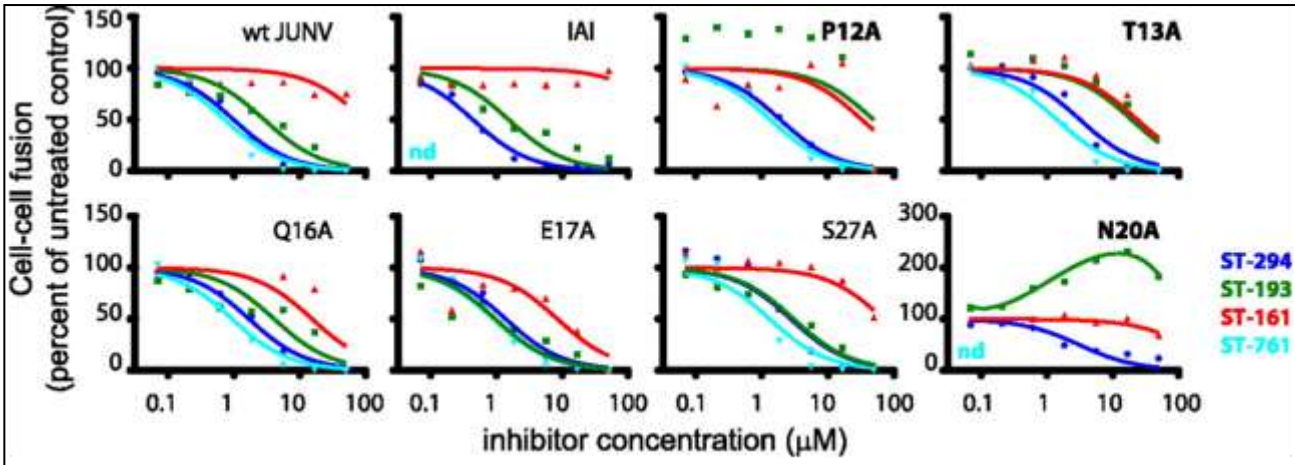

Figure 17: Mutations in SSP TM1 affect sensitivity to small-molecule fusion inhibitors. The highly sensitive recombinant vaccinia virus-based cell-cell fusion assay was used determine fusion inhibition by the chemically distinct small-molecule entry inhibitors ST-294 (blue), ST-193 (green), ST-161 (red), and ST-761 (cyan). The labels of mutants with altered sensitivity to ST-193 are in bold. Colored data points represent averages of triplicate 96-well microcultures using seven serial dilutions of inhibitor, and data are normalized as a percentage of the untreated control cultures. Lines are best-fit nonlinear regression curves for a dose-response model of inhibition constrained between 0 and 100% of the untreated control and using a single slope (−1) (GraphPad Prism). The line for ST-193 enhancement of fusion by N20A GPC is hand-drawn. nd, inhibition by ST-761 was not tested; wt, wild type. All conclusions reported were confirmed in at least two independent experiments. Inhibitor concentrations required to reduce membrane fusion by 50% (IC_{50}s) are listed in Table 2

Table 2: JGPC-mediated fusion IC_{50}s[a]

	IC_{50} (μM) (95% CI)			
SSP	ST-294	ST-761	ST-193	ST-161[b]
wt	1.0 (0.8–1.2)	0.7 (0.6–1.0)	2.9 (2.1–4.0)	96 (57–160)
IAI	0.4 (0.4–0.5)	nd	1.5 (1.1–2.2)	450 (67–3100)
P12A	1.9 (1.6–2.3)	1.4 (1.1–1.7)	**50** (9.5–250)	33 (9.4–120)
T13A	3.2 (2.4–4.3)	1.4 (1.1–1.9)	**19** (12–33)	24 (11–51)
Q16A	1.7 (1.5–1.9)	0.9 (0.8–1.2)	4.1 (2.4–7.0)	15 (4.4–54)
E17A	1.4 (1.1–1.8)	0.9 (0.7–1.2)	1.0 (0.6–1.6)	8.4 (4.1–17)
N20A	3.1 (2.0–4.7)	nd	Enhanced	140 (77–250)
S27A	2.8 (1.7–4.4)	1.3 (0.9–3.0)	3.0 (2.3–3.9)	71 (45–110)

[a] Best-fit nonlinear regression using dose-response model and data shown in Fig. 6. Significant changes in inhibitor concentrations required to reduce JUNV GPC-mediated fusion by 50% (IC_{50}s) are indicated in bold. Enhanced, dose-dependent enhancement of fusion activity. nd, inhibition by ST-761 was not tested; wt, wild type; CI, confidence interval.

[b] JUNV is nominally resistant ($IC_{50} \geq 10$ μM) to ST-161.

D. Conclusions

Our previous studies have shown that the short ectodomain loop of SSP and its interactions with G2 are important determinants for both pH-dependent membrane fusion and its inhibition by small-molecule compounds (York and Nunberg, 2006; York et al., 2008). The present study identifies the critical role of the first membrane-spanning domain of SSP in these events. By characterizing a series of SSP chimeras containing JUNV and LASV sequences, we demonstrate that a homotypic pairing between TM1 and G2 is required for GPC-mediated membrane fusion. We propose that multiple intersubunit contacts between these transmembrane helices serve to position the critical K33 side chain in the SSP ectodomain for pH-sensitive interactions with the G2 ectodomain. Small-molecule compounds that stabilize these interactions in the prefusion GPC complex have been shown to prevent pH-induced fusion activation in the endosome and thereby inhibit arenavirus entry. Detailed knowledge of the atomic interactions between SSP and G2 in the membrane-anchored GPC trimer will be important for understanding the mechanism of pH-dependent membrane fusion and guiding the design of potent and broadly active small-molecule fusion inhibitors.

Acknowledgements

We are grateful to Min Lu (Public Health Research Institute, University of Medicine and Dentistry, New Jersey) and Meg Trahey (The University of Montana) for their editorial comments and assistance. We are also grateful to Sean Amberg and Dongcheng Dai (SIGA Technologies, Inc., Corvallis, OR) for providing small-molecule fusion inhibitors and to Celestine Thomas (The University of Montana) for assistance in 3D modeling of SSP. We thank Connie Schmaljohn (USAMRIID) for providing the LASV G1-specific hybridoma L52 134-23, Klaus Conzelmann (Ludwig-Maximilians-University, Munich, Germany) for the BSR T7/5 cell line, and Yoshiharu Matsuura (Osaka University, Japan) and Juan Carlos de la Torre (The Scripps Research Institute, La Jolla, CA), respectively, for the pT7EMC-luc and pCAGGS-MCS expression

plasmids. JUNV G1-specific MAbs were provided by the CDC through the NIH Biodefense and Emerging Infections Research Resources Program.

This work was supported by U.S. Public Health Service grants R01 AI074818 and U54 AI065357 (Rocky Mountain Regional Center of Excellence for Biodefense and Emerging Infectious Diseases at Colorado State University) from the National Institutes of Health.

Chapter 4: Engineering of a Potential Model for Transmembrane Interactions within the Trimeric Arenaviral Glycoprotein Complex

A. Introduction

Mutational analysis and fusion inhibition studies have illustrated the dependence of pH-mediated fusion on the interaction between SSP and G2. While several key residues in the pH-sensitive interface are in the membrane proximal and extracellular domains, residues within the TM domains have also been shown to alter fusion activity (F427A, A435I, F438I, W428A in G2 and N20A in SSP) and drug sensitivity (F427A in G2 and P12A, T13A, and N20A in SSP) (Messina et al., 2012; York and Nunberg, 2009; York et al., 2008). In contrast to the second TM region of SSP (TM2), which has been shown to be resilient to alanine mutations and uniformly hydrophobic (Agnihothram et al., 2007), side-chain specific interactions within the N-terminal TM region of SSP (TM1) are important for fusion activity and both the TM domain in G2 and TM1 are predicted to be amphipathic helices. Therefore, we hypothesize that TM1 and the TM region of G2 interact with each other within the trimeric GPC. We propose that the polar faces of the TM domains will be buried, interacting with each other, and the hydrophobic faces will be presented outward to interact with the hydrophobic membrane.

To pursue this hypothesis, I engineered a novel TM construct, termed TMCON, which might serve as a model for the potential interactions between the TM domains. TMCON is comprised of the first 34 residues of SSP connected to a FLAG tag, which is flanked by short linker regions, and then connected to the terminal 70 residues of G2 (figure 18). I also created two more constructs, with the S-peptide tag (spep) on the N- or C-terminus, respectively. The objective of this work is to express, purify, and perform

preliminary biochemical and *in vitro* characterizations of the construct.

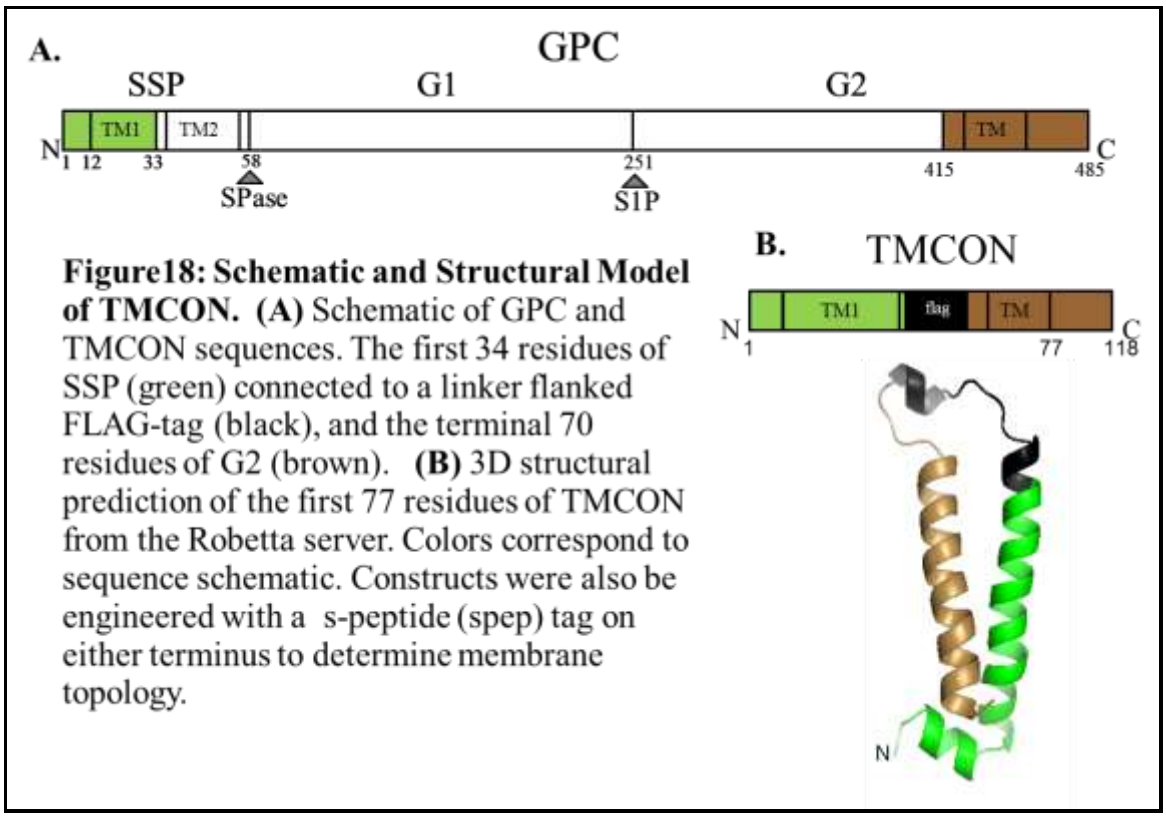

Figure18: Schematic and Structural Model of TMCON. (A) Schematic of GPC and TMCON sequences. The first 34 residues of SSP (green) connected to a linker flanked FLAG-tag (black), and the terminal 70 residues of G2 (brown). **(B)** 3D structural prediction of the first 77 residues of TMCON from the Robetta server. Colors correspond to sequence schematic. Constructs were also be engineered with a s-peptide (spep) tag on either terminus to determine membrane topology.

B. Methods

Cloning. pcDNA3.1 TMCON was created using the primers GC-SSPTM1-G2TM and SSPTM1-G2TM (table 3), with the Junin GPC-spep plasmid as a template, in the QuikChange II XL Site-Directed Mutagenesis (Agilent 200521). To express TMCON in insect cells, the TMCON open reading frame transferred into the pDEST8 plasmid using the Gateway System (Invitrogen) two-step protocol.

Membrane preparations. Hi5 cell pellets were thawed in cold TMNZ buffer (25mM Tris pH 7.6, 5mM $MgCl_2$, 250mM NaCl, 100 µM $ZnSO_4$, plus protease inhibitors (1 µg [each] of aprotinin, leupeptin, and pepstatin/ml). All subsequent steps are performed at 4^o. Nitrogen decompression (1000 PSI in a Parr Bomb for 60 min) was used to disrupt

cells, which were then spun at 3,000 RPM for 10 min to remove cellular debris. Membranes were then isolated from the supernatant by ultracentrifugation at 100,000 × *g* for 1 h. The pellet was resuspended by dounce homogenization in TMNZ buffer and the high speed spin was repeated. The pellet was then dounced again in TMNZ buffer with detergent (either 3% DDM or 10% sarkosyl) and then allowed to solubilize with mild agitation for either 2 hrs or overnight. A final 1hr 100,000 × *g* spin was performed and both the pellet and supernatant are saved to analyze the detergent insoluble (pellet) and soluble fractions (supernatant).

The lipids, palmitoyloleoyl phosphatidylcholine, palmitoyloleoyl phosphatidylethanol, and palmitoyloleoyl phosphatidylglycerol (POPC, POPE, and POPG, respectively) were used as a mixture at a ratio of 3:1:1 to improve purification efficiency from FLAG-resin (Sigma A2220).

Size Exclusion Chromatography (SEC). DDM soluble protein was allowed bind to FLAG-affinity resin for 2 or more hours. The resin was subsequently washed twice with TMNZ containing 1% DDM and 1 time with TMNZ buffer containing 0.1% DDM. TMCON was then eluted with 5 μM of 3×FLAG peptide in (Sigma F4799). The eluate was subjected to SEC using a Superdex-200/G-75 tandem column (GE) to purify TMCON and determine its oligomeric state. SEC buffer contained 0.05% DDM. Molecular weight sizes were determined by comparison to the elution profile of the Gel Filtration Standard (BioRad 151-1901).

Co-immunoprecipitation. BSR cells were transfected as described in chapter 3. Cells were harvested in cold PBS, and suspended in TX-100 lysis buffer (50 mM Tris-HCl (pH 7.5), 150 mM NaCl, 1% Triton X-100, and protease inhibitors). Lysates were cleared by centrifugation at 14,000RPM, 4^{o}, 15 min, and then supernatants were incubated for 2 hrs, with rocking, at 4^{o}, with 1µL BF11 (1mg/ml) and 50µL protein-A sepharose beads. After washing, samples were heated in 2X LDS (Invitrogen) with reducing agent at 70^{o}, run on pre-cast 4-12% Bis-Tris polyacrylamide gels (Invitrogen), and transferred to PVDF membranes. The blots were probed sequentially with the monoclonal anti-spep mouse IgG antibody (Pierce MA1-981) at a 1:1000 dilution for 60 min, and then the secondary horseradish peroxidase tagged goat anti-mouse.

Crosslinking. SEC purified TMCON was dialyzed into 10mM HEPES plus .05% DDM to remove the Tris. The Bis(sulfosuccinimidyl)suberate (BS^3, Pierce 21585) crosslinking agent is an amine-reactive crosslinker with an 8-carbon spacer arm. To crosslink TMCON, 2 µL of BS^3 was added to 32µL of dialyzed TMCON. The reaction was then vortexed and incubated on ice for 2 hrs. The reaction was quenched by adding 2µL 1M Tris pH 7.5. Samples were then run on reducing SDS-PAGE gels and analyzed by Western blotting as described above.

Confocal Microscopy. Transiently transfected BSR cells were re-seeded into 4-chamber glass bottom dishes (Greiner 627870), 80,000 cells per chamber, 16 hrs post-transfection. 12 hrs later, cells were washed 3 times with RT PBS and then fixed for 45 min at RT with ice-cold and freshly prepared 4% Paraformaldehyde (PFA). Next, cells were treated with

50mM Tris for 20 min then and permeabilized with 0.2% TX-100 in PBS for 10 min. Cells were blocked for 20 min and then probed for 90 min with primary antibody (Golgi specific α-GM130 (abcam at 1:250, TMCON-spep specific α-spep at 1:250, or α-G1 MAB BE08 at 1:500) in block solution (5% BSA in 0.1% TX-100 PBS). Chambers were washed 5 times with block solution and then cells were incubated with the secondary, GAM-568 or GAR- 488, at a 1:800 dilution for 90 min. After washing five times, cells were treated with SlowFade Gold with DAPI (Invitrogen S36938) and examined using an Olympus Fluoview 1000 laser scanning confocal microscope.

Flow cytometry. Cells were transfected with TMCON-spep plasmid alone or with wtJGPC plasmid, or salmon sperm DNA as a negative control, harvested 24hrs later, washed and resuspended in PBS, and stained with either anti-FLAG, anti-spep, or BE08 Ab (all used at 1:50) for 45 min on ice. Cells were then washed and probed with a secondary fluorescein isothiocyanate (FITC)-labeled anti-mouse antibody. The cell populations were then stained with propidium iodine to exclude dead cells, fixed with fresh 2% PFA, and immediately analyzed using a FACSCalibur flow cytometer (BD Biosciences).

C. Results

Develop a Purification Scheme for TMCON expressed in Insect Cells. Our laboratory has an established protocol for the purification of JGPC from Hi5 cells using DDM to solubilize JGPC as a soluble trimer (Thomas et al., 2011, 2012). My initial attempts to purify TMCON using this protocol resulted in a large portion of the protein in a

remaining in the detergent-insoluble pellet (figure 19). I examined several conditions to solubilize the peptide. TMCON is not readily soluble in acetic acid, methanol, DDM, or TX-100. TMCON can be solubilized in GnHCl, Urea, SDS, and sarkosyl. Sarkosyl has been used to efficiently solubilize proteins in a native form from inclusion bodies in *E. coli* (Francis et al., 2012; Tao et al., 2010). Following the strategy from Tao *et al*, I solubilized the isolated membrane fraction in 10% sarkosyl overnight. To affinity purify TMCON using FLAG-affinity beads, I diluted the sarkosyl solution with TX-100 and CHAPS to a final concentration 1% sarkosyl, 2% TX-100 and 20mM CHAPS. This creates mixed micelles which prevents the sarkosyl from interfering with the interaction between the anti-FLAG MAB and the FLAG tag. The diluted protein was applied to a FLAG-affinity column, washed once with 1% sarkosyl, 2% TX-100, and 20mM CHAPS, washed a second time with 1% sarkosyl, and then eluted with 3X-FLAG peptide. With this protocol, I was able to purify TMCON, but I required excessively high concentrations of the 3X-FLAG peptide to elute the construct (up to four times the recommended 100 µg/ml recommended by Sigma). To improve solubility and elution efficiency, I added a 0.1mg/ml mixture of lipids to all detergent containing buffers, which allowed efficient elution from the FLAG-resin with 100 µg/ml 3X-FLAG peptide (figure 19). Purified TMCON remained soluble in sarkosyl + lipid solutions with as little as 0.1% sarkosyl, which may aid downstream applications.

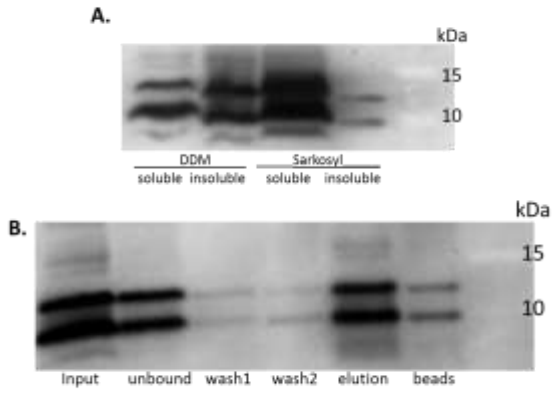

Figure 19: Purification of TMCON. **(A)** Membrane preparations solubilized using 3% DDM or 10% sarkosyl. More than half of TMCON remains is in the DDM - insoluble pellet. Almost all of TMCON is solubilized using sarkosyl. **(B)** Purification of sarkosyl solubilized TMCON using FLAG-resin. TMCON extracted from membranes solubilized in 10% sarkosyl + 0.1mg/ml lipid was diluted to 1% sarkosyl, 2% TX-100 and 20mM CHAPS + 0.1mg/ml lipid (input). The diluted protein was incubated with FLAG-beads for 2 hrs at 4°. The beads were then spun down, the supernatant was saved (unbound), the beads were washed once with 1% sarkosyl, 2% TX-100, and 20mM CHAPS + 0.1mg/ml lipid(wash1), then washed a second time with 1% sarkosyl + 0.1mg/ml lipid (wash2), and then eluted with 3X-FLAG peptide (100 µg/ml) in wash2 buffer at RT for 1hr. Equal percentages of sample were resolved under reducing conditions on an SDS-PAGE gel and analyzed by Western blot probed with α-spep.

TMCON can form trimers. To determine the oligomeric state TMCON, we analyzed the DDM-soluble fraction of the membrane prep by SEC. Most of TMCON elutes as aggregates. However, some TMCON elutes in a minor peak consistent in size with a dimer or trimer (figure 20). To further study this fraction, we treated it the crosslinker, BS^3. Significantly, when incubated with increasing amounts of BS^3, TMCON from this peak undergoes specific crosslinking, as shown in figure 20. In a dose dependent fashion, TMCON forms specific crosslinked species consistent in size with a timer and a hexamer.

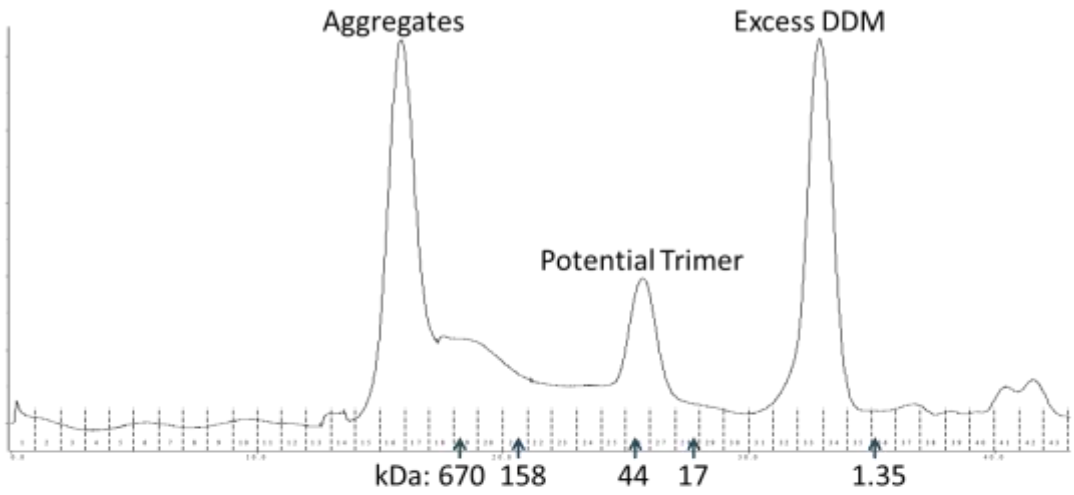

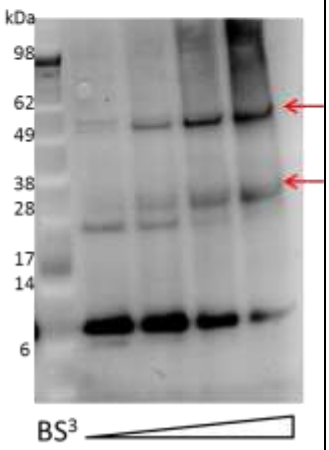

Figure 20: Oligomeric State of TMCON. (A) SEC elution profile of DDM soluble FLAG purified TMCON. Peak intensity is measured in A280. Estimated molecular weights (blue arrows) are based on the elution profile of a size standard (BioRad). TMCON has a predicted molecular weight of 13kDa. Most of TMCON elutes as higer order aggregates, however a small fraction elutes at a size consistent with a trimer. **(B)** Specific crosslinking of TMCON. SEC separated TMCON from potential trimer fraction was incubated with increasing concentrations of BS^3, resolved on a reducing SDS-PAGE, and analyzed by Western blot probed with α-FLAG. Red arrows indicate specific crosslinking products.

TMCON associates weakly with JGPC. We next asked if TMCON can associate with Junín GPC (JGPC) *in vitro.* If TMCON is well-folded, we reasoned it may form mixed trimers with JGPC and perhaps traffic through the cell in a similar fashion to JGPC. To determine if TMCON can associate with JGPC, I expressed TMCON alone or with JGPC in mammalian BSRT7/5 cells and then performed a co-immunoprecipitation with the G1 specific MAB, BF11, to pull-down JGPC and any associated TMCON. I was able to reproducibly detect a faint TMCON-spep band that co-precipitated with GPC (figure 21E). To determine if TMCON could traffic properly through the cell, I

performed confocal microscopy experiments to determine the intracellular localization of TMCON with and without co-expression of JGPC. Previous work in our laboratory has demonstrated that wt-JGPC traffics through the cell from the ER to the Golgi, and then to the cell surface. The cytosolic region of G2 contains two dibasic sequences which serve as ER-retention/retrieval signals. Co-expression of SSP with G1/G2 is essential to masking these dibasic ER-retention sequences for transport. However, removal of these sequences relieves G2 of its dependence on SSP for proper trafficking (Agnihothram et al., 2006). Expressed alone, TMCON aggregated as large puncta in the cell. When co-expressed with JGPC, TMCON was found more diffusely in the cell and in the Golgi apparatus. We next asked if mutating the ER-retention signals in TMCON would affect its intracellular localization. When I expressed the mutant TMCON KK/RR, which contains alanine substitutions in place of the dibasic sequences, this construct was found throughout the cytosol and in the Golgi. However, expressed alone or with wtJGPC, neither TMCON nor TMCON KK/RR was detectable on the surface of healthy cells by surface staining and confocal microscopy. This result was confirmed by flow cytometry. Because TMCON could insert into the membrane in a variety of orientations with one or both of the TM domains crossing the membrane, we used both α-spep and α-FLAG to detect possible cell surface expression, but we saw no significant population of cells positive for surface expression of TMCON with either antibody (figure 21A-D,F,G).

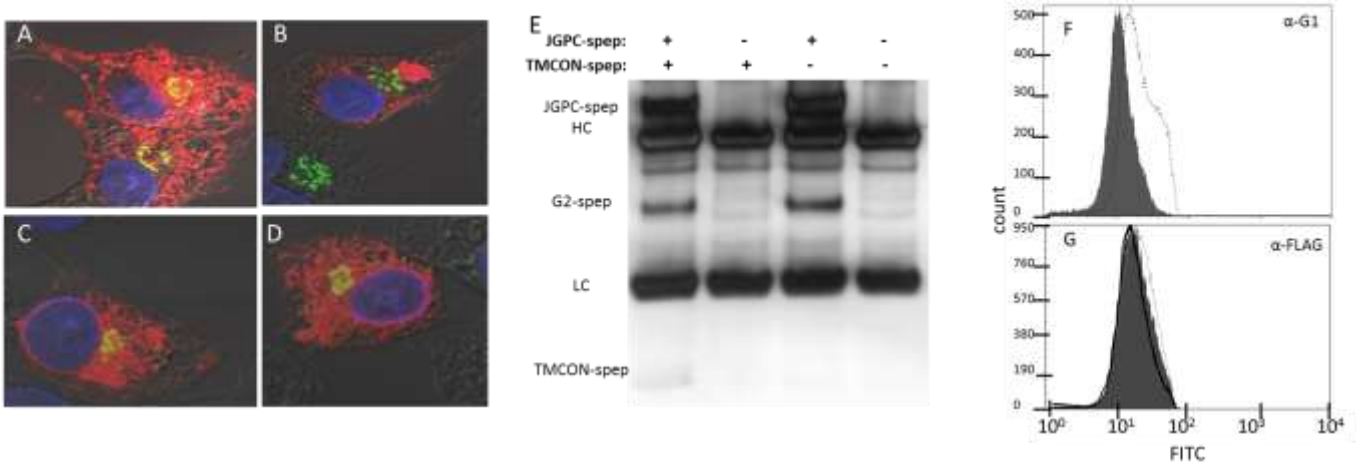

Figure 21. TMCON associates weakly with GPC. (A-D) Confocal Microscopy: Transfected BSR cells with **(A)** wtJGPC only, **(B)** TMCON-spep only, **(C)** TMCON-spep and wtJGPC, or **(D)** TMCON KK/RR-spep only, were fixed, permeabilized, and then co-stained with Golgi specific α-GM130 (green) and appropriate primary **(A)** α-G1 MAB BE08 (red) or **(B-D)** α-spep (red). Cells were then incubated with secondaries GAM-568 and GAR- 488, washed and treated with treated with SlowFade Gold with DAPI (nucleus –blue). **(E)** Co-immunoprecipitation. Cells were transfected with JGPC-spep, TMCON-spep or both, harvested, and immuno-precipitated with α-G1 MAB BF11. Samples were run on a reducing gel and the Western was probed with anti-spep.HC-heavy chain, LC-light chain. **(F & G)** Flow Cytometry to detect cell surface expression. BSR cells transfected with TMCON alone, or with wtJGPC, or salmon sperm DNA (negative control) were stained with **(F)** α-G1 MAB BE08 or **(G)** α-FLAG, and GAM-FITC. Cells were then stained with propidium iodine, fixed with fresh 2% PFA, and immediately analyzed. Shaded histogram represents the salmon sperm control. The dashed gray line represents cells transfected with (F) wtJGPC or (G) wtJGPC and TMCON. The solid black line **(G)** represents cells transfected with TMCON only.

D. Discussion

TMCON contains the first TM region of SSP and the C-terminal 70 residues of G2, which includes both the TM region and cytosolic region. Expressed alone, TMCON appears to be excluded from the Golgi and remains in the cytosol as large puncta, suggesting misfolding and aggregation of the construct. Notably, removing the ER-retention signals does alter its intracellular localization, indicating that the G2 region within TMCON does behave in a similar fashion to wtJGPC. Pulldown experiments further demonstrate that TMCON can interact with JGPC. Though this interaction may not be robust, the fact that co-expression of the two proteins changes the trafficking of TMCON indicates the interaction is functional. These data, combined with the observation that TMCON can form trimers, suggest that the construct might capture

elements of the inter-helical interactions within the trimer.

With a purification protocol in place, TMCON can be produced and purified in large quantities, which will ease future biochemical studies. Further characterization to determine if it is a suitable model for studying the interactions between the TM domains will be required. Limited proteolysis experiments may be performed to identify a stable protease resistant core (Blacklow et al., 1995; Lu et al., 1995). To determine the structure and orientation of TMCON in a membrane, protease protection assays in the presence and absence of liposomes can be done to determine which residues are protected and which are accessible to proteolysis. The resulting peptide fragments could be analyzed using silver-stained gels, mass spectrometry, and protein sequencing. If TMCON is well folded, it may be a suitable candidate for future structural studies such as electron paramagnetic resonance (EPR) (Mchaourab et al., 2011) or X-ray crystallization.

Chapter 5: Cysteine Scanning Mutagenesis and Crosslinking within the G2 Transmembrane Domain

A. Introduction

GPC, like other class-I fusion proteins, takes the form of a trimeric spike on the viral envelope. The "head" of the spike is comprised of the receptor binding subunit (in our case, G1) and the subunit that contains the fusion peptide and spans the membrane (in GPC, this is G2) forms the "stalk" (figure 2 and figure 5). Studies detailing the arrangement of other class-I fusion proteins reveal that the "stalk" forms a tightly associated trimer and that the TM domain is important to fusion (Bissonnette et al., 2009a; Chang et al., 2008; Kemble et al., 1994; Lamb and Jardetzky, 2007; Smith et al., 2012; Weissenhorn et al., 2007). Because site-directed mutagenesis has indicated that that specific residues within the TM domain of G2 and TM1 are important to fusion and drug sensitivity (Messina et al., 2012; York and Nunberg, 2009; York et al., 2008), we reasoned that the specific packing interactions between these TM domains are important to the overall geometry and function of GPC. We hypothesized that the first TM region of SSP and the TM region of G2 interact with each other within the trimeric complex. We predict the G2 forms a tight trimer through the TM domain which is surrounded by the SSP TM domains (figure 22). However, GPC is unique in its retention of SSP in the mature complex and other arrangements are possible. To determine the orientation of these TM domains to each other, I used a cysteine-scanning mutagenesis and disulfide crosslinking approach as described below. This strategy has proven very useful in probing the structures of several other membrane proteins and the class-I paramyxovirus F protein (Amin et al., 2006; Bissonnette et al., 2009a; Hamdan et al., 2002; Lee et al.,

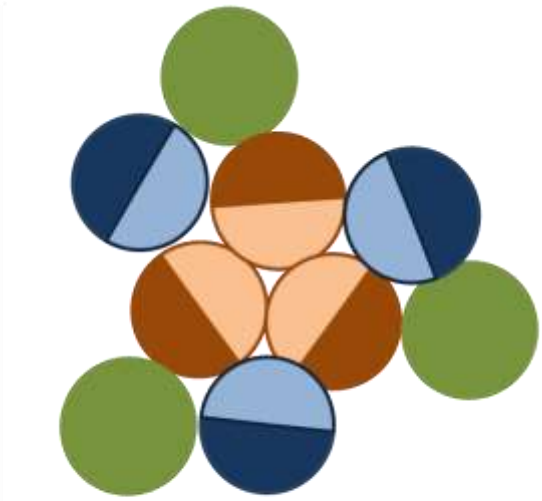

Figure 22: Possible arrangement of TM domains in GPC (top-down view). G2-orange; N-terminal SSP TM domain – blue; C-terminal TM domain – green; Dark colors represent hydrophobic faces and lighter colors represent hydrophilic faces. A tightly associated trimer of G2 helices would be consistent with other class-I fusion proteins.

2006; Loo et al., 2004; Schwem and Fillingame, 2006; Winston et al., 2005).

I created a library of single cysteine mutations spanning the entire TM of G2 (between residues proline-419 and proline-445). The wt-G2 contains one cysteine within its TM, so I used the TM cys-less background mutant C426S (which mediates wt-level fusion) for this mutational analysis. In each mutant GPC trimer, there will be three cysteines in the TM available for crosslinking. We predicted that if they are oriented towards each other, and are within bonding distance, two will form a disulfide bond (and one will remain unbound) when exposed to a membrane soluble oxidant, such as I_2 (Bass et al., 2007) or Cu(II)(1,10-phenanthroline)$_3$ (Bissonnette et al., 2009). If, on the other hand, they are not facing each other, they will not readily form a disulfide bond. Thus, under non-reducing conditions on a SDS-PAGE gel, we should be able to readily distinguish a significant shift in the population of G2 monomers to dimers. In this fashion, we hoped to map which face(s) of the G2 TM region may be interacting with each other and which may be free to interact with SSP.

I first characterized this library of mutants by examining fusion activity. I then

attempted to crosslink G2:G2 and G2:SSP cysteine pairs using multiple crosslinking agents under a variety of conditions. Unfortunately, I was unable to detect any specific crosslinking under the conditions tested.

B. Methods

Cysteine mutants. Individual cysteine substitutions were made in G2 residues from P419 to P445 in the pcDNA3.1 CD4-Adapt C426S-spep plasmid. In other work, cysteine substitutions were also made in the pcDNA3.1 SSP plasmid to change residues T13, E17, and N20. All substitutions were made using the QuikChange Lightning Multi Site-Directed Mutagenesis Kit (Agilent 210516). Primers used are listed in table 3. Cycling conditions were as follows: 95^{o} for 2 min, 30 cycles (95^{o} for 20 sec, 55^{o} for 30 sec, 65^{o} for 4 min), 65^{o} for 5 min, hold at 4^{o}. Cysteine mutants within the TM region of the fusion subunit (F) of the Paramyxovirus glycoprotein were kindly provided by Dr. Robert Lamb at Northwestern University (Bissonnette et al., 2009a) and used as positive controls.

Protein expression, processing and detection. Junin proteins were expressed in BSRT7/5 cells (described in chapter 3) and the paramyxovirus F proteins were expressed in 293 cells by transient transfection. 6µg of G1G2 and 2µg of SSP plasmid were transfected into a 6well cluster plate seeded with 450,000 cells using 25µL lipofectamine2000 (Invitrogen). Starting at 6 hrs post-transfection, cells were metabolically labeled using ^{35}S-labeled amino acids (GE) overnight. 293 cells were transfected using the manufacturer recommend amounts of DNA and lipofectamine2000. 18hrs post transfection, 293 cells were metabolically starved for 1 hour and then ^{35}S-labeled for 2 hours per the Lamb's laboratory protocol (Bissonnette et al., 2009a).

For oxidative crosslinking in membranes, cells were dounce homogenized (50 strokes) in RSB buffer (10mM Tris pH 7.5, 10mM KCl, 15mM $MgCl_2$ plus protease inhibitors). Homogenates were then treated with CuP, I_2, or mock treated with equal volumes 50mM Tris pH7.5 or ethanol, respectively. Specific crosslinking conditions are discussed in the Results and Discussion section below. Reactions were quenched with 10mM EDTA alone or with an additional 10mM NEM and 100mM IAM for 10 min at RT. Samples were then solubilized with an equal volume 2X lysis buffer. Bissonette et al utilize 2X RIPA buffer (50mM Tris pH 7.5, 1mM EDTA, 150mM NaCl, 2% NP40, 0.2% sodium deoxycholate, 0.2% SDS plus protease inhibitors) (Bissonnette et al., 2009a) whereas our established IP protocol uses a TX-100 lysis buffer described above (1% TX-100 final). Solubilized samples were then spun at maximum speed in a microcentrifuge for 15 min. Cleared supernatants were then immuno-precipitated with 1µL of the anti-G1 MAB BF11 or 10µL of the paramyxovirus F protein specific polycolonal α-F2 (kindly provided by Robert Lamb). For the crosslinking of solubilized protein, cells were harvested in cold PBS, spun at 1500 RPM for 10 min, and then resuspended in 1ml TX-100 lysis buffer. Lysates were cleared, treated with crosslinker (I_2 or CuP), and then quenched and immunoprecipitated as described above. Buffers used during oxidative crosslinking of GPC samples also contained 50µM zinc to maintain the intersubunit zinc-binding domain (Briknarová et al., 2011).

For non-oxidative crosslinking experiments in membranes with bis(maleimido)ethane (BMOE, Pierce 22323), a bifunctional maleimide crosslinker with an 8Å linker arm, cells were dounce homogenized (50 strokes) in hypotonic lysis buffer (0.1X PBS) with protease inhibitors. Homogenates were then spun at maximum speed in

the microcentrifuge for 15 min at 4°. Pelleted membranes were then resuspended in 1X PBS plus protease inhibitors and either treated with BMOE or mock-treated with an equal volume of DMSO. Crosslinking conditions are discussed in the following section. After crosslinking, reactions were quenched with DTT (10mM final) for 15min at RT. Samples were then diluted 5 fold in 1.2X TX-100 lysis buffer (final 1% TX100) and immunoprecipitated with the α-G1 antibody, BF11.

After immunoprecipitation, samples are heated to 90° for 20 min in 4X LDS buffer (Invitrogen) with or without reducing agent and subsequently resolved on 4-12% Bis-Tris pre-cast polyacrylamide gels (Invitrogen), which were subsequently fixed, dried, and proteins were visualized by phosphorimaging with a Fuji FLA-3000G instrument.

Fusion assays were performed as described in chapter 3.

Table 3: List of Primers Used

Primer	Sequence
SSPTM1-G2TM	GCTCTTGTTGCAGTCAGTCTCATTGCCATCATTAAGGGTCGCCGGCAGGACTACAAGGACGATGAT GACAAGGGATCCGCCGGCAAAACTCCCTTGACTTTAGTTGACATCTGTTTTTGGAGC
GC-SSPTM1-G2TM	GCTCCAAAAACAGATGTCAACTAAAGTCAAGGGAGTTTTGCCGGCGGATCCCTTGTCATCATCGTC CTTGTAGTCCTGCCGGCGACCCTTAATGATGGCAATGAGACTGACTGCAACAAGAGC
P419C	CGGACAGGCAGGGCAAAACTTGCTTGACTTTAGTTGACATCAGTTTC
L420C	CAGGCAGGGCAAAACTCCCTGTACTTTAGTTGACATCAGTTTCTGG
T421C	GGCAGGGCAAAACTCCCTTGTGTTTAGTTGACATCAGTTTCTGGAG
L422C	GCAGGGCAAAACTCCCTTGACTTGTGTTGACATCAGTTTCTGGAG
V423C	GCAGGGCAAAACTCCCTTGACTTTATGTGACATCAGTTTCTGGAGC
D424C	GCAGGGCAAAACTCCCTTGACTTTAGTTTGCATCAGTTTCTGGAGC
I425C	CTCCCTTGACTTTAGTTGACTGCAGTTTCTGGAGCACAGTATTCTTCAC
F427C	CTCCCTTGACTTTAGTTGACATCAGTTGTTGGAGCACAGTATTC
W428C	CTCCCTTGACTTTAGTTGACATCAGTTTCTGTAGCACAGTATTCTTC
S429C	GACTTTAGTTGACATCAGTTTCTGGTGCACAGTATTCTTCACAGCG
T430C	CCCTTGACTTTAGTTGACATCAGTTTCTGGAGCTGTGTATTCTTCACAGCGTCC
V431C	GTTGACATCAGTTTCTGGAGCACATGTTTCTTCACAGCGTCCCTCTTCC
F432C	CAGTTTCTGGAGCACAGTATGCTTCACAGCGTCCC
F433C	GGAGCACAGTATTCTGCACAGCGTCCCTCTTCC
T434C	GGAGCACAGTATTCTTCTGTGCGTCCCTCTTCCTTCACTTGGTGG
A435C	GGAGCACAGTATTCTTCACATGTTCCCTCTTCCTTCACTTGGTGGGC
S436C	GGAGCACAGTATTCTTCACAGCGTGCCTCTTCCTTC
L437C	CAGTATTCTTCACAGCGTCCTGCTTCCTTCACTTGGTGGGC
F438C	GTATTCTTCACAGCGTCCCTCTGCCTTCACTTGGTGG
L439C	GCGTCCCTCTTCTGTCACTTGGTGGGCATACCCACC
H440C	CAGCGTCCCTCTTCCTTTGCTTGGTGGGCATACCCAC
L441C	GCGTCCCTCTTCCTTCACTGTGTGGGCATACCCACC
V442C	CGTCCCTCTTCCTTCACTTGTGTGGCATACCCACCCATAGGC
G443C	CTTCCTTCACTTGGTGTGCATACCCACCCATAGGC
I444C	CTTCCTTCACTTGGTGGGCTGTCCCACCCATAGGCACATCAG
P445C	CCTCTTCCTTCACTTGGTGGGCATATGCACCCATAGGCAC

C. Results and Discussion

TM Cysteine Substitutions are well tolerated. The nominal N-terminal junction of the G2 TM is at the charged D424. Structural prediction programs (Roy et al., 2010) suggest the TM of G2 extends from L420 to L441 or I444. I extended our cysteine-scanning analysis from P419 to P445 to ensure complete coverage of the G2 TM. We also created three cysteine substitutions in SSP: T13C, E17C, and N20C. These residues are all predicted to be on the same helical face of the first TM domain and alanine substitutions at these residues were shown to alter drug sensitivity (Messina et al., 2012). Each of the G2 mutants was assessed biochemically for association between G2 and SSP

by radio-IP and for cell-cell fusion activity. SSP association and cleavage of G1-G2 was observed in all cases. Figure 23C,D shows an example of these data. A subset of the mutation panel biochemical data is shown in figure 23C. All of the mutants displayed greater fusion activity than the negative (no SSP) control and, with few exceptions (P419C, L420C, L422C), all demonstrated greater than 25% activity (figure 23A, B).

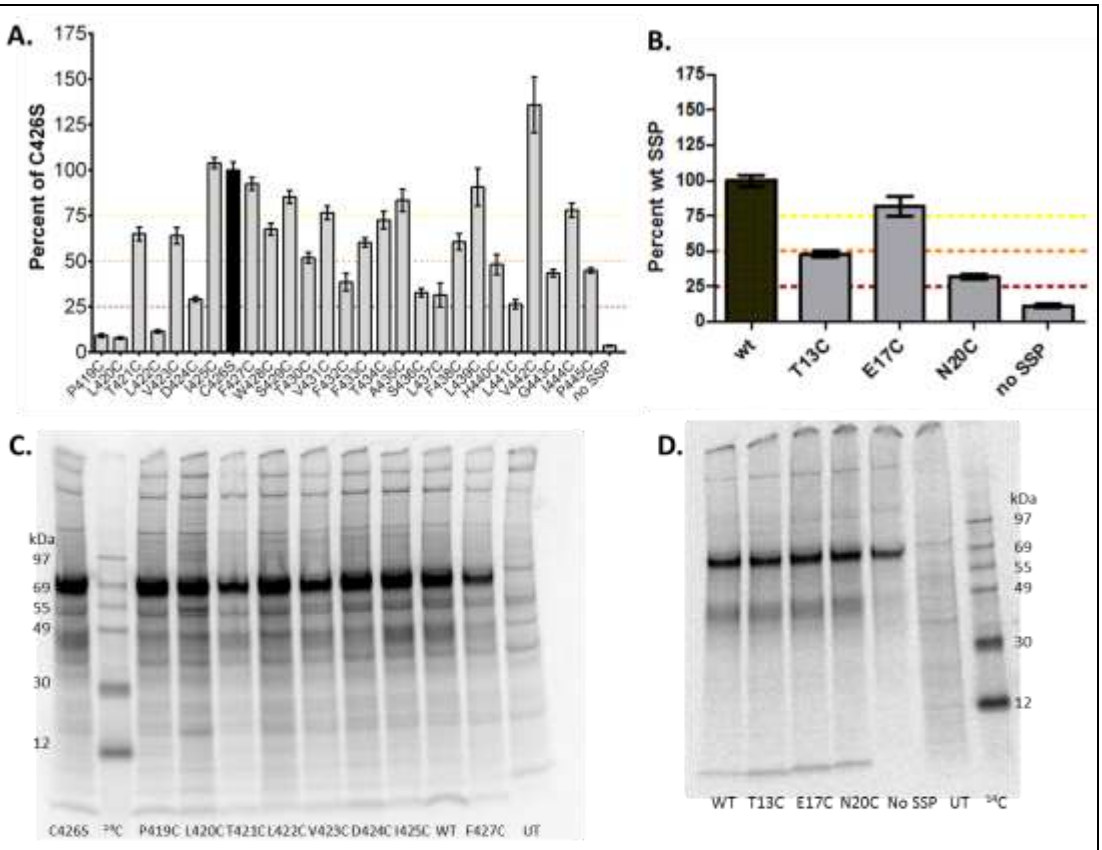

Figure 23: Cysteine mutations are well tolerated. (A) Fusion activity of G2 cysteine mutants expressed as a percentage of the parent mutant C426S. Results are representative of 3 separate assays. Bars are average of 6 replicates and error bars indicate SEM. **(B)** Fusion assay results of SSP cysteine mutations expressed as a percentage of wtSSP representative of two assays. Bars are average of at least 4 replicates and error bars indicate SEM. **(C)** Biochemical analysis of a subset of the G2 and **(D)** SSP cysteine mutants. Proteins were expressed in BSR cells, metabolically labeled, solubilized in TX-100, immuno-precipitated with BF11, and resolved on a reducing gel. Uncleaved G1G2 is observed as a strong band of near the 69 kDa marker. Cleaved G1 and G2 are observed as a smear between 49 and 30 kDa. SSP is associated and seen at the bottom of the gel (6kDa).

Looking at the fusion assay data we observed some degree of periodicity, particularly between residues V431 and P445 (figure 23A). The rise and fall of fusion activity about every 4 residues may be consistent with an important α-helical interface. These data also indicate that the cysteine mutations were not disruptive to the structure of GPC, and thus we hypothesized that a specific pattern of crosslinking would reveal the G2 TM domain to have a G2:G2 interacting face and a G2:SSP face.

Crosslinking Conditions. I attempted to oxidatively crosslink G2 in dounced homogenates using CuP and I_2. I searched the literature to define the ranges of conditions used for oxidative crosslinking within membrane proteins (Hamdan et al., 2002; Loo et al., 2004; Ma et al., 2004; Miller et al., 2003). I then proceeded to test a range of crosslinker concentrations (25 – 3000 μM CuP and 20 – 500 μM I_2), temperatures (4^o, RT, 37^o), and reaction times (5 min to 1hr for CuP and 30 sec to 5m for I_2) with my samples. The primary stumbling block was in finding a set of conditions which did not result in a loss of GPC protein. At high concentrations of crosslinking agent, GPC precipitated out of solution and I saw a significant loss in signal. Longer reaction times and crosslinking at 37^o caused excessive background crosslinking and higher order aggregates such that proteins did not enter the gel. After lengthy troubleshooting, the conditions which worked best for preserving signal and reducing background were to treat dounced homogenized cells with 25μM CuP for 20m at RT. However, under these conditions, I detected no specific crosslinking between G2 or SSP mutants.

As crosslinking maybe inefficient in the membrane and given that our laboratory

has an established protocol for immunoprecipitating solubilized GPC (Agnihothram et al., 2006; York et al., 2004, 2005), I also attempted crosslinking in TX-100 solubilized samples over a similar range of conditions listed above. However, excessive background crosslinking and protein precipitation (figure 24C) again proved to be problematic. After examining the same range in crosslinker concentration, temperature, and timing as described above, I established a protocol of crosslinking for 10m at RT using 25μM CuP (figure 24D). To verify this protocol with a positive control, we obtained paramyxovirus F protein samples from Dr. Robert Lamb's laboratory (Bissonnette et al., 2009). Using both their published protocol (3mM CuP) and the one described above (25μM CuP), I was able to demonstrate strong and specific crosslinking at residue 506, but not 505, replicating their published results (figure 24 B,A respectively). In this figure, one can observe a clear increase in the ratio of F dimers (about 55kDa) to monomers (about 100 kDa) using both protocols. However, I was not able to demonstrate any specific crosslinking with my G2 or SSP mutants using either protocol (figure 24 C, D). Under low CuP concentrations (25 μM), I do observe a band consistent in size (about 120 kDa) with an uncleaved G1G2 dimer (figure 24D). However, I also see this band in untreated controls resolved under non-reducing conditions (data not shown) and this band is seen consistently in all the G2 mutants without variation in the ratio of this potential dimer to the monomer. Therefore, we have concluded this band is most likely background dimer formation. A similar background level of dimer formation may be seen in the paramyxovirus F mutants (figure 24 A,B).

To address the possibility that the G2 domains are not oriented symmetrically, I also tried crosslinking each G2 cysteine mutant with each of its four upstream and four

downstream neighboring residues. This set of experiments also failed to yield any specific crosslinking.

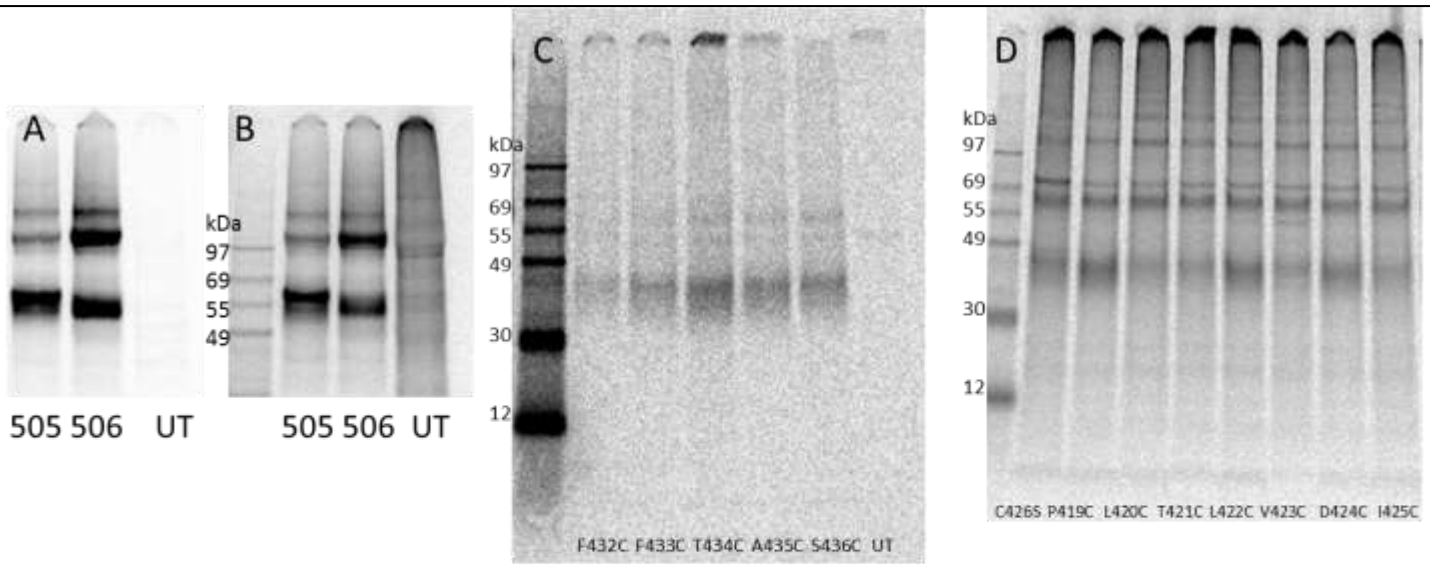

Figure 24: Oxidative Crosslinking. **(A)** Paramyxovirus F protein samples subjected to dounce homogenization, 3mM CuP 10m, solubilized in RIPA, IP with α-F2, run under non-reducing conditions. **(B)** Paramyxovirus F protein samples solubilized in TX-100 and then crosslinked with 25 μM CuP. **(C)** G1G2 cysteine mutants processed as in **(A)**. **(D)** G1G2 cysteine mutants processed as in **(B)**.

To address the possibility that the G2 helices maybe not be packed tightly enough for cysteine pairs to form a disulfide bond (2 Å), I used a bifunctional maleimide crosslinker with an 8Å linker arm, BMOE (Hamdan et al., 2002). This non-oxidative crosslinker will form a covalent bond between two cysteine residues. I tried BMOE (0.02 mM to 2.0mM) using both solubilized and dounce-homogenized samples at 4^{o}, RT, and 37^{o}, over a range of reaction times (20 min to 120 min) without a positive result.

We expected these crosslinking studies to show that the G2 TM domains associate with each other and with the TM1 (figure 22). As the G2 TM is thought to be α-helical, we predicted a periodicity in disulfide bond forming which would allow us to determine

the inner and outer faces of the G2 TM domain (Bissonnette et al., 2009). By extending our cysteine substitution library past the nominal borders of the TM domain and using a longer crosslinker, we hoped to account for the possibility that the TM domains may curve or tilt away from each other in such a way that only residues within a certain region of the helix are close enough form disulfide bonds (Alisio and Mueckler, 2004). However, as I was unable to demonstrate any specific G2:G2 or G2: SSP crosslinking similar to what we observed with the paramyxovirus controls, we were unable to elucidate the arrangement of the TM domains using this approach.

Potential reasons for my negative results are manifold. Despite the exhaustive search for appropriate crosslinking conditions, it is possible that I was unable to identify the specific reaction conditions necessary to induce crosslinking within GPC. This hurdle may be related to the intersubunit zinc-binding domain (ZBD). The zinc-interacting cysteines may not be protected from crosslinking agents, even in the presence of excess zinc. It is possible that at the concentrations of crosslinker needed to induce G2:G2 or G2:SSP dimers, the crosslinker is disrupting the ZBD, causing non-specific crosslinking or a collapse of the GPC trimer. It could also be that the helices are arranged in novel way so that the G2 domains are not facing each other or that the TM helices are spaced further apart and a crosslinker with a longer (than 8Å) arm is required.

Chapter 6: Conclusions and Future Directions

Arenaviruses continue to be a significant public health threat due to severity of illness caused and the lack of suitable treatments. Therefore, the search continues for improved antiviral strategies and better understanding of arenavirus biology. My dissertation research has centered on two important topics. The first project, as detailed in chapter 2, addresses the question of how T-705 inhibits highly pathogenic arenaviruses. Chapters 3-5 discuss the second thrust of my research that focuses on defining the inter-subunit interactions within GPC and how these interactions may affect fusion and drug sensitivity.

Options for treating severe arenaviral hemorrhagic fever cases are limited to the off-label use of ribavirin, which is known for its negative side effects, and transfer of immune plasma for JUNV patients (Borio et al., 2002; Chapman et al., 1999; Rusnak et al., 2009). Thus, the development of alternative antivirals for use in arenaviral infection is critical. T-705 has been shown to be an effective inhibitor of RNA viruses, but it had not been previously evaluated against highly pathogenic arenaviruses. Studies in chapter two demonstrate for the first time that T-705 is effective at inhibiting the replication of highly pathogenic viruses *in vitro*. Further, we show that T-705 works against these viruses in the middle of the viral life cycle and specifically inhibits viral transcription at concentrations similar to ribavirin. In contrast to ribavirin, T-705 showed very little reduction in cellular transcription activity, even at the highest doses tested. These data indicate T-705 may have fewer off-target cellular effects and be a safe alternative to ribavirin for treatment of arenaviral infection. This study is an important step in the process of understanding how T-705 inhibits arenaviral replication and in the

development of T-705 for use as a treatment for arenaviral HF. Our data are consistent with studies that show T-705 does not significantly inhibit IMPDH (Furuta et al., 2005) while ribavirin does (Graci and Cameron, 2006). It is known that T-705 RTP, likely acts as a purine analog against the influenza polymerase (Furuta et al., 2005). Our data demonstrating that nearly all purine-based compounds showed a significant effect on T-705 activity are consistent with this observation and suggest a conserved mechanism of action against viral RNA polymerases. A recent publication has shown that T-705 can be mutagenic in H1N1 influenza (Baranovich et al., 2013) serially passaged in tissue culture. Interestingly, another very recent report demonstrates that T-705RTP can block nascent RNA chain elongation in crude RdRp preparations (Sangawa et al., 2013). Further studies will be needed to determine which of these mechanisms may be at play during arenavirus infection and to study the safety and efficacy of using T-705 to treat arenaviral infection *in vivo*. Importantly, T-705 has completed phase 3 clinical trials in Japan and phase 2 clinical trials in the U.S. for the treatment of influenza infection. T-705 was demonstrated to significantly reduce the symptoms of influenza infection and shorten the time to clear virus with an excellent safety record (DOD, 2013; in Furuta et al, 2013). Our studies and those done by others demonstrate that T-705 is effective against arenaviruses in tissue culture and in animal models (reviewed in Furuta et al, 2013). Taken together, T-705 is a very good candidate for further study in the treatment of arenaviral HF.

Elucidating the detailed structure and function of GPC is critical to understanding and inhibiting membrane fusion. Previous studies in our laboratory have shown that the interactions between the membrane proximal region of G2 and the extracellular loop of

SSP are key to the pH-sensitive triggering of fusion (York and Nunberg, 2009). In chapter 3, I demonstrated a homotypic match between G2 and the ectodomain loop of SSP enhanced, but was not required, for fusion activity. Instead, a match between G2 and TM1 was shown to be necessary and sufficient for fusion competency. My work defined an essential sub-domain within SSP from residues P12-K33 and suggests that the TM domain begins at P12, not E17 as previously thought (Eichler et al., 2004). I also show that this TM region is more sensitive to mutation than the second SSP TM domain (Agnihothram et al., 2007). We further demonstrate that residues within this TM domain are key to drug sensitivity (T13, E17, N20). These data reveal an important role for the first SSP TM region and indicate that sequence specific interactions with the G2 TM region are necessary for the proper geometry of GPC.

This and previous work (York and Nunberg, 2009; York et al., 2008) demonstrating that some residues within the G2 TM domain are important for mediating fusion and drug sensitivity is consistent with the knowledge that the TM domains of class-I fusion proteins are more than simple membrane anchors (Kemble et al., 1994; Smith et al., 2012). Studies show that in many of these TM domains, a degree of sequence specificity is required for fusion activity, that these domains are closely associated with each other (Bissonnette et al., 2009a; Chang et al., 2008; Smith et al., 2012) and are important to protein folding and trimer formation (Smith et al., 2012).

As GPC is unique among class-I fusion proteins in its retention of SSP, and given that the trimer has nine TM domains instead of three, it will have a unique arrangement of helices in the membrane. By analogy to other class-I fusion proteins, we hypothesize that the G2 helices form a tight core that is closely associated with the SSP TM domains

(figure 22). This arrangement seems likely because the G2 TM domain has clear hydrophilic and hydrophobic faces, as does SSP TM1. Additionally, side chain-specific interactions between the helices appear to be important for fusion and drug sensitivity. Further, we know that residues at the periphery of the membrane regions must be in close proximity to interact with each other (K33 in SSP with membrane proximal residues in G2) (Messina et al., 2012; York and Nunberg, 2009; York et al., 2008). Given the difficulties inherent in crystallizing glycoproteins (Chasman, 2003; Forster et al., 2005; Shimizu et al., 2008), other approaches to elucidating the interactions within GPC should be explored. I created a novel truncated construct, TMCON, to serve as a potential model for these TM interactions (chapter 4) and I attempted to map the arrangement of the TM domains within the GPC trimer using cysteine-scanning mutagenesis and crosslinking assays (chapter 5).

Until the structure of the intact GPC complex can be determined, deciphering the structure of specific subdomains within GPC remains a valid approach. I cloned and characterized the model construct, TMCON, to serve as a potential tool in this divide-and-conquer approach to elucidating the relationship between the TM domains within GPC. TMCON does not perform like wtJGPC, but it does retain some important functional properties, such as its ER-retention pattern and the abilities to form trimers and associate with wtJGPC. Thus, this novel construct has the potential to be an informative model of the interactions between TM1 and the TM domain of G2. However, additional questions regarding its structure and its interactions with membranes remain. For instance, I have shown that TMCON and wtJGPC can associated with each other, but the nature of this interaction is unclear. We could examine the ability of wtJGPC to traffic

and mediate fusion when co-expressed with TMCON to determine if the interaction between these two proteins is detrimental to the functioning of wtJGPC. Additionally, while I have demonstrated that TMCON is purified in membrane preps from insect cells, we may address the possibility that the construct maybe pelleted as aggregates by performing floatation assays. We expect that these assays would show a significant portion of TMCON is membrane associated, as others have shown that insertion of Lassa GPC into the ER-membrane requires only one of the two SSP TM domains (Eichler et al, 2004). Further, assuming that TMCON is a bona-fide membrane-associated protein, it is essential to determine its topology in the membrane. To characterize the structure and orientation of TMCON in a membrane, protease protection assays in the presence and absence of liposomes can be done to determine which residues are protected and which are accessible to proteolysis. The resulting peptide fragments could be analyzed using silver-stained gels, mass spectrometry, and protein sequencing.

In chapter 5, I used a cysteine-scanning mutagenesis approach that has proven useful in mapping TM domains in other proteins (Amin et al., 2006; Bissonnette et al., 2009a; Hamdan et al., 2002; Lee et al., 2006; Loo et al., 2004; Schwem and Fillingame, 2006; Winston et al., 2005). However, as I was unable to achieve specific crosslinked products despite an exhaustive search of reaction conditions, we cannot make any definitive statements about the arrangement of the GPC TM domains. It is possible that the G2 TM arrangement varies from the typical coiled central core, as has been suggested for Moloney murine leukemia virus (MoMuLV). If the G2 TM domains are arranged in a similar fashion to the TM domains of the MoMuLV glycoprotein, splayed like a tripod (Forster et al., 2005; Löving et al., 2012), or are in a novel configuration in which the

TM domains are not tightly packed, they will not be amenable to crosslinking. It is also possible that I was unable to find the reaction conditions that induce specific crosslinking and maintain the structural integrity of the GPC trimer. Other crosslinking conditions, such as lysis buffer used, crosslinking *in vivo*, or using a longer crosslinker could be explored. Theoretically, if cysteine substitutions were made throughout all the TM domains in GPC, we could ascertain the TM organization of GPC even if the TM domains were not symmetrically arranged. However, this would be logistically unfeasible. Others in our laboratory are currently working to establish protocols for mass-spectrometry (MS) analysis of GPC TM peptides. If these studies are successful, another approach of using a heterobifunctional (sulfhydryl to non-specific) crosslinker may be informative. Using a G2 cysteine mutant, we could perform a crosslinking reaction which would link the free cysteine nonspecifically to whichever TM domain(s) are nearby. After isolating crosslinked products on a gel, they could be analyzed using MS to narrow down the interacting domains within the TM region of GPC. Other approaches to studying the structure of the TM region within GPC could include cryo-EM of viruses or virus-like particles (Forster et al., 2005; Zhang, et al, 2013) and EPR (Mchaourab et al., 2011).

Taken together, the works presented in this dissertation provide new insights into the action of T-705 arenaviral inhibition and the interactions within GPC, though much work remains to be done. Absent any structural data of the TM domains, several important questions remain. We do not know how the TM domains physically interact with each other nor do we know at which step(s) of the fusion process these interactions occur. Understanding the geometry within the TM region of GPC would be a great boon

to our knowledge of how SSP and G2 function together during fusion and may lead to novel improvements in fusion inhibitors.

Works Cited

Agnihothram, S.S., York, J., and Nunberg, J.H. (2006). Role of the stable signal peptide and cytoplasmic domain of G2 in regulating intracellular transport of the Junín virus envelope glycoprotein complex. J. Virol. *80*, 5189–5198.

Agnihothram, S.S., York, J., Trahey, M., and Nunberg, J.H. (2007). Bitopic membrane topology of the stable signal peptide in the tripartite Junín virus GP-C envelope glycoprotein complex. J. Virol. *81*, 4331–4337.

Albariño, C.G., Bird, B.H., Chakrabarti, A.K., Dodd, K.A., White, D.M., Bergeron, E., Shrivastava-Ranjan, P., and Nichol, S.T. (2011). Reverse genetics generation of chimeric infectious Junin/Lassa virus is dependent on interaction of homologous glycoprotein stable signal peptide and G2 cytoplasmic domains. J. Virol. *85*, 112–122.

Alisio, A., and Mueckler, M. (2004). Relative proximity and orientation of helices 4 and 8 of the GLUT1 glucose transporter. J. Biol. Chem. *279*, 26540–26545.

Ambrosio, A., Saavedra, M., Mariani, M., Gamboa, G., and Maiza, A. (2011). Argentine hemorrhagic fever vaccines. Hum Vaccin *7*, 694–700.

Amin, D.N., Taylor, B.L., and Johnson, M.S. (2006). Topology and boundaries of the aerotaxis receptor Aer in the membrane of Escherichia coli. J. Bacteriol. *188*, 894–901.

Baranovich, T., Wong, S.-S., Armstrong, J., Marjuki, H., Webby, R.J., Webster, R.G., and Govorkova, E.A. (2013). T-705 (favipiravir) induces lethal mutagenesis in influenza A H1N1 viruses in vitro. J. Virol. *87*, 3741–3751.

Barton, L.L., Mets, M.B., and Beauchamp, C.L. (2002). Lymphocytic choriomeningitis virus: Emerging fetal teratogen. American Journal of Obstetrics and Gynecology *187*, 1715–1716.

Bass, R.B., Butler, S.L., Chervitz, S.A., Gloor, S.L., and Falke, J.J. (2007). Use of site-directed cysteine and disulfide chemistry to probe protein structure and dynamics: applications to soluble and transmembrane receptors of bacterial chemotaxis. Meth. Enzymol. *423*, 25–51.

Bissonnette, M.L.Z., Donald, J.E., DeGrado, W.F., Jardetzky, T.S., and Lamb, R.A. (2009). Functional analysis of the transmembrane domain in paramyxovirus F protein-mediated membrane fusion. J. Mol. Biol. *386*, 14–36.

Blacklow, S.C., Lu, M., and Kim, P.S. (1995). A trimeric subdomain of the simian immunodeficiency virus envelope glycoprotein. Biochemistry *34*, 14955–14962.

Bloom, J.D., Gong, L.I., and Baltimore, D. (2010). Permissive secondary mutations enable the evolution of influenza oseltamivir resistance. Science *328*, 1272–1275.

Bolken, T.C., Laquerre, S., Zhang, Y., Bailey, T.R., Pevear, D.C., Kickner, S.S., Sperzel, L.E., Jones, K.F., Warren, T.K., Amanda Lund, S., et al. (2006). Identification and characterization of potent small molecule inhibitor of hemorrhagic fever New World arenaviruses. Antiviral Res. *69*, 86–97.

Borio, L., Inglesby, T., Peters, C.J., Schmaljohn, A.L., Hughes, J.M., Jahrling, P.B., Ksiazek, T., Johnson, K.M., Meyerhoff, A., O'Toole, T., et al. (2002). Hemorrhagic fever viruses as biological weapons: medical and public health management. JAMA *287*, 2391–2405.

Briese, T., Paweska, J.T., McMullan, L.K., Hutchison, S.K., Street, C., Palacios, G., Khristova, M.L., Weyer, J., Swanepoel, R., Egholm, M., et al. (2009). Genetic detection and characterization of Lujo virus, a new hemorrhagic fever-associated arenavirus from southern Africa. PLoS Pathog. *5*, e1000455.

Briknarová, K., Thomas, C.J., York, J., and Nunberg, J.H. (2011). Structure of a zinc-binding domain in the Junin virus envelope glycoprotein. J. Biol. Chem. *286*, 1528–1536.

Buchholz, U.J., Finke, S., and Conzelmann, K.K. (1999). Generation of bovine respiratory syncytial virus (BRSV) from cDNA: BRSV NS2 is not essential for virus replication in tissue culture, and the human RSV leader region acts as a functional BRSV genome promoter. J. Virol. *73*, 251–259.

Cao, W., Henry, M.D., Borrow, P., Yamada, H., Elder, J.H., Ravkov, E.V., Nichol, S.T., Compans, R.W., Campbell, K.P., and Oldstone, M.B. (1998). Identification of alpha-dystroglycan as a receptor for lymphocytic choriomeningitis virus and Lassa fever virus. Science *282*, 2079–2081.

Cashman, K.A., Smith, M.A., Twenhafel, N.A., Larson, R.A., Jones, K.F., Allen, R.D., 3rd, Dai, D., Chinsangaram, J., Bolken, T.C., Hruby, D.E., et al. (2011). Evaluation of Lassa antiviral compound ST-193 in a guinea pig model. Antiviral Res. *90*, 70–79.
Centers for Disease Control and Prevention (CDC) (2000). Fatal illnesses associated with a new world arenavirus--California, 1999-2000. MMWR Morb. Mortal. Wkly. Rep. *49*, 709–711.

Chang, D.-K., Cheng, S.-F., Kantchev, E.A., Lin, C.-H., and Liu, Y.-T. (2008). Membrane interaction and structure of the transmembrane domain of influenza hemagglutinin and its fusion peptide complex. BMC Biology *6*, 2.

Chapman, L.E., Mertz, G.J., Peters, C.J., Jolson, H.M., Khan, A.S., Ksiazek, T.G., Koster, F.T., Baum, K.F., Rollin, P.E., Pavia, A.T., et al. (1999). Intravenous ribavirin for hantavirus pulmonary syndrome: safety and tolerance during 1 year of open-label experience. Ribavirin Study Group. Antivir. Ther. (Lond.) *4*, 211–219.

Charrel, R.N., and de Lamballerie, X. (2010). Zoonotic aspects of arenavirus infections. Veterinary Microbiology *140*, 213–220.

Charrel, R.N., de Lamballerie, X., and Emonet, S. (2008). Phylogeny of the genus Arenavirus. Curr. Opin. Microbiol. *11*, 362–368.

Charrel, R.N., Coutard, B., Baronti, C., Canard, B., Nougairede, A., Frangeul, A., Morin, B., Jamal, S., Schmidt, C.L., Hilgenfeld, R., et al. (2011). Arenaviruses and hantaviruses: from epidemiology and genomics to antivirals. Antiviral Res. *90*, 102–114.

Chasman, D. (2003). Protein Structure: Determination, Analysis, and Applications for Drug Discovery (CRC Press).

Choe, H., Jemielity, S., Abraham, J., Radoshitzky, S.R., and Farzan, M. (2011). Transferrin receptor 1 in the zoonosis and pathogenesis of New World hemorrhagic fever arenaviruses. Curr. Opin. Microbiol. *14*, 476–482.

Clercq, E.D. (2006). Antiviral agents active against influenza A viruses. Nature Reviews Drug Discovery *5*, 1015–1025.

Clercq, E.D. (2012). Highlights in Antiviral Drug Research: Antivirals at the Horizon. Medicinal Research Reviews n/a–n/a.

Colebunders, R., Van Esbroeck, M., Moreau, M., and Borchert, M. (2002). Imported viral haemorrhagic fever with a potential for person-to-person transmission: review and recommendations for initial management of a suspected case in Belgium. Acta Clin Belg *57*, 233–240.

Conzelmann, K.K. (1996). Genetic manipulation of non-segmented negative-strand RNA viruses. J. Gen. Virol. *77 (Pt 3)*, 381–389.

Crotty, S., Maag, D., Arnold, J.J., Zhong, W., Lau, J.Y., Hong, Z., Andino, R., and Cameron, C.E. (2000). The broad-spectrum antiviral ribonucleoside ribavirin is an RNA virus mutagen. Nat. Med. *6*, 1375–1379.

Cummins, D. (1991). Arenaviral haemorrhagic fevers. Blood Rev. *5*, 129–137.

Cummins D, McCormick JB, Bennett D, and et al (1990). ACute sensorineural deafness in lassa fever. JAMA *264*, 2093–2096.

Damonte, E.B., and Coto, C.E. (2002). Treatment of arenavirus infections: from basic studies to the challenge of antiviral therapy. Adv. Virus Res. *58*, 125–155.

DOD. Flu Drug Under DOD Development Completes Second Clinical Trial [(accessed on 08 December 2013)]. Available online: http://www.defense.gov/news/newsarticle.aspx?id=121023

Eichler, R., Lenz, O., Strecker, T., Eickmann, M., Klenk, H.-D., and Garten, W. (2003).

Identification of Lassa virus glycoprotein signal peptide as a trans-acting maturation factor. EMBO Rep. *4*, 1084–1088.

Eichler, R., Lenz, O., Strecker, T., Eickmann, M., Klenk, H.-D., and Garten, W. (2004). Lassa virus glycoprotein signal peptide displays a novel topology with an extended endoplasmic reticulum luminal region. J. Biol. Chem. *279*, 12293–12299.

Emonet, S.F., de la Torre, J.C., Domingo, E., and Sevilla, N. (2009). Arenavirus genetic diversity and its biological implications. Infection, Genetics and Evolution *9*, 417–429.

Enria, D.A., Briggiler, A.M., and Sánchez, Z. (2008). Treatment of Argentine hemorrhagic fever. Antiviral Res. *78*, 132–139.

Eschli, B., Quirin, K., Wepf, A., Weber, J., Zinkernagel, R., and Hengartner, H. (2006). Identification of an N-terminal trimeric coiled-coil core within arenavirus glycoprotein 2 permits assignment to class I viral fusion proteins. J. Virol. *80*, 5897–5907.

Flatz, L., Bergthaler, A., de la Torre, J.C., and Pinschewer, D.D. (2006). Recovery of an arenavirus entirely from RNA polymerase I/II-driven cDNA. Proc. Natl. Acad. Sci. U.S.A. *103*, 4663–4668.

Forster, F., Medalia, O., Zauberman, N., Baumeister, W., and Fass, D. (2005). Retrovirus envelope protein complex structure in situ studied by cryo-electron tomography. Proc Natl Acad Sci U S A *102*, 4729–4734.

Francis, V.G., Majeed, M.A., and Gummadi, S.N. (2012). Recovery of functionally active recombinant human phospholipid scramblase 1 from inclusion bodies using N-lauroyl sarcosine. J. Ind. Microbiol. Biotechnol. *39*, 1041–1048.

Froeschke, M., Basler, M., Groettrup, M., and Dobberstein, B. (2003). Long-lived signal peptide of lymphocytic choriomeningitis virus glycoprotein pGP-C. J. Biol. Chem. *278*, 41914–41920.

Ftika, L., and Maltezou, H.C. (2013). Viral haemorrhagic fevers in healthcare settings. Journal of Hospital Infection *83*, 185–192.

Fuerst, T.R., Niles, E.G., Studier, F.W., and Moss, B. (1986). Eukaryotic transient-expression system based on recombinant vaccinia virus that synthesizes bacteriophage T7 RNA polymerase. Proc. Natl. Acad. Sci. U.S.A. *83*, 8122–8126.

Fuller-Pace, F.V., and Southern, P.J. (1988). Temporal analysis of transcription and replication during acute infection with lymphocytic choriomeningitis virus. Virology *162*, 260–263.

Furuta, Y., Takahashi, K., Fukuda, Y., Kuno, M., Kamiyama, T., Kozaki, K., Nomura, N., Egawa, H., Minami, S., Watanabe, Y., et al. (2002). In vitro and in vivo activities of

anti-influenza virus compound T-705. Antimicrob. Agents Chemother. *46*, 977–981.

Furuta, Y., Takahashi, K., Kuno-Maekawa, M., Sangawa, H., Uehara, S., Kozaki, K., Nomura, N., Egawa, H., and Shiraki, K. (2005). Mechanism of Action of T-705 against Influenza Virus. Antimicrob Agents Chemother *49*, 981–986.
Furuta, Y., Takahashi, K., Shiraki, K., Sakamoto, K., Smee, D.F., Barnard, D.L., Gowen, B.B., Julander, J.G., and Morrey, J.D. (2009). T-705 (favipiravir) and related compounds: Novel broad-spectrum inhibitors of RNA viral infections. Antiviral Res. *82*, 95–102.

Furuta Y, Gowen BB, Takahashi K, Shiraki K, Smee DF, Barnard DL. (2013). Favipiravir (T-705), a novel viral RNA polymerase inhibitor. Antiviral Res. *100*, 446-54.

Gallaher, W.R., DiSimone, C., and Buchmeier, M.J. (2001). The viral transmembrane superfamily: possible divergence of Arenavirus and Filovirus glycoproteins from a common RNA virus ancestor. BMC Microbiol. *1*, 1.

Geisbert, T.W., and Jahrling, P.B. (2004). Exotic emerging viral diseases: progress and challenges. Nat. Med. *10*, S110–121.

Ghiringhelli, P.D., Rivera-Pomar, R.V., Lozano, M.E., Grau, O., and Romanowski, V. (1991). Molecular organization of Junin virus S RNA: complete nucleotide sequence, relationship with other members of the Arenaviridae and unusual secondary structures. J. Gen. Virol. *72 (Pt 9)*, 2129–2141.

Gowen, B.B., Wong, M.-H., Jung, K.-H., Sanders, A.B., Mendenhall, M., Bailey, K.W., Furuta, Y., and Sidwell, R.W. (2007). In Vitro and In Vivo Activities of T-705 against Arenavirus and Bunyavirus Infections. Antimicrob. Agents Chemother. *51*, 3168–3176.

Gowen, B.B., Smee, D.F., Wong, M.-H., Hall, J.O., Jung, K.-H., Bailey, K.W., Stevens, J.R., Furuta, Y., and Morrey, J.D. (2008). Treatment of late stage disease in a model of arenaviral hemorrhagic fever: T-705 efficacy and reduced toxicity suggests an alternative to ribavirin. PLoS ONE *3*, e3725.

Gowen, B.B., Wong, M.-H., Jung, K.-H., Smee, D.F., Morrey, J.D., and Furuta, Y. (2010). Efficacy of favipiravir (T-705) and T-1106 pyrazine derivatives in phlebovirus disease models. Antiviral Res. *86*, 121–127.

Graci, J.D., and Cameron, C.E. (2006). Mechanisms of action of ribavirin against distinct viruses. Reviews in Medical Virology *16*, 37–48.

Günther, S., and Lenz, O. (2004). Lassa virus. Crit Rev Clin Lab Sci *41*, 339–390.

Hamdan, F.F., Ward, S.D.C., Siddiqui, N.A., Bloodworth, L.M., and Wess, J. (2002). Use of an in Situ Disulfide Cross-Linking Strategy To Map Proximities between Amino Acid Residues in Transmembrane Domains I and VII of the M3 Muscarinic Acetylcholine Receptor. Biochemistry *41*, 7647–7658.

Harrison, S.C. (2008). Viral membrane fusion. Nat. Struct. Mol. Biol. *15*, 690–698.

Harrison, L.H., Halsey, N.A., McKee, K.T., Peters, C.J., Oro, J.G.B., Briggiler, A.M., Feuillade, M.R., and Maiztegui, J.I. (1999). Clinical Case Definitions for Argentine Hemorrhagic Fever. Clin Infect Dis. *28*, 1091–1094.

Igonet, S., Vaney, M.-C., Vonrhein, C., Vonhrein, C., Bricogne, G., Stura, E.A., Hengartner, H., Eschli, B., and Rey, F.A. (2011). X-ray structure of the arenavirus glycoprotein GP2 in its postfusion hairpin conformation. Proc. Natl. Acad. Sci. U.S.A. *108*, 19967–19972.

Julander, J.G., Shafer, K., Smee, D.F., Morrey, J.D., and Furuta, Y. (2009). Activity of T-705 in a hamster model of yellow fever virus infection in comparison with that of a chemically related compound, T-1106. Antimicrob. Agents Chemother. *53*, 202–209.

Kemble, G.W., Danieli, T., and White, J.M. (1994). Lipid-anchored influenza hemagglutinin promotes hemifusion, not complete fusion. Cell *76*, 383–391.

Khan, S.H., Goba, A., Chu, M., Roth, C., Healing, T., Marx, A., Fair, J., Guttieri, M.C., Ferro, P., Imes, T., et al. (2008). New opportunities for field research on the pathogenesis and treatment of Lassa fever. Antiviral Research *78*, 103–115.

Kim, Y., and Lee, C. (2013). Ribavirin efficiently suppresses porcine nidovirus replication. Virus Res. *171*, 44–53.

Kim, D.E., Chivian, D., and Baker, D. (2004). Protein structure prediction and analysis using the Robetta server. Nucleic Acids Res *32*, W526–W531.

Kim, Y.H., Donald, J.E., Grigoryan, G., Leser, G.P., Fadeev, A.Y., Lamb, R.A., and DeGrado, W.F. (2011). Capture and imaging of a prehairpin fusion intermediate of the paramyxovirus PIV5. Proc Natl Acad Sci U S A *108*, 20992–20997.

Kiso, M., Takahashi, K., Sakai-Tagawa, Y., Shinya, K., Sakabe, S., Le, Q.M., Ozawa, M., Furuta, Y., and Kawaoka, Y. (2010). T-705 (favipiravir) activity against lethal H5N1 influenza A viruses. Proc. Natl. Acad. Sci. U.S.A. *107*, 882–887.

Kunz, S. (2009). Receptor binding and cell entry of Old World arenaviruses reveal novel aspects of virus-host interaction. Virology *387*, 245–249.

Kunz, S., Edelmann, K.H., de la Torre, J.-C., Gorney, R., and Oldstone, M.B.A. (2003). Mechanisms for lymphocytic choriomeningitis virus glycoprotein cleavage, transport, and incorporation into virions. Virology *314*, 168–178.

Lamb, R.A., and Jardetzky, T.S. (2007). Structural basis of viral invasion: lessons from paramyxovirus F. Curr. Opin. Struct. Biol. *17*, 427–436.

Larson, R.A., Dai, D., Hosack, V.T., Tan, Y., Bolken, T.C., Hruby, D.E., and Amberg, S.M. (2008). Identification of a broad-spectrum arenavirus entry inhibitor. J. Virol. *82*, 10768–10775.

Lee, A.M., Rojek, J.M., Spiropoulou, C.F., Gundersen, A.T., Jin, W., Shaginian, A., York, J., Nunberg, J.H., Boger, D.L., Oldstone, M.B.A., et al. (2008). Unique small molecule entry inhibitors of hemorrhagic fever arenaviruses. J. Biol. Chem. *283*, 18734–18742.

Lee, K.J., Novella, I.S., Teng, M.N., Oldstone, M.B.A., and Torre, J.C. de la (2000). NP and L Proteins of Lymphocytic Choriomeningitis Virus (LCMV) Are Sufficient for Efficient Transcription and Replication of LCMV Genomic RNA Analogs. J. Virol. *74*, 3470–3477.

Lee, K.J., Perez, M., Pinschewer, D.D., and de la Torre, J.C. (2002). Identification of the lymphocytic choriomeningitis virus (LCMV) proteins required to rescue LCMV RNA analogs into LCMV-like particles. J. Virol. *76*, 6393–6397.

Lee, P.A., Orriss, G.L., Buchanan, G., Greene, N.P., Bond, P.J., Punginelli, C., Jack, R.L., Sansom, M.S.P., Berks, B.C., and Palmer, T. (2006). Cysteine-scanning mutagenesis and disulfide mapping studies of the conserved domain of the twin-arginine translocase TatB component. J. Biol. Chem. *281*, 34072–34085.

Lenz, O., ter Meulen, J., Klenk, H.D., Seidah, N.G., and Garten, W. (2001). The Lassa virus glycoprotein precursor GP-C is proteolytically processed by subtilase SKI-1/S1P. Proc. Natl. Acad. Sci. U.S.A. *98*, 12701–12705.

Leyssen, P., Balzarini, J., Clercq, E.D., and Neyts, J. (2005). The Predominant Mechanism by Which Ribavirin Exerts Its Antiviral Activity In Vitro against Flaviviruses and Paramyxoviruses Is Mediated by Inhibition of IMP Dehydrogenase. J. Virol. *79*, 1943–1947.

Loo, T.W., Bartlett, M.C., and Clarke, D.M. (2004). Disulfide cross-linking analysis shows that transmembrane segments 5 and 8 of human P-glycoprotein are close together on the cytoplasmic side of the membrane. J. Biol. Chem. *279*, 7692–7697.

Löving, R., Wu, S.-R., Sjöberg, M., Lindqvist, B., and Garoff, H. (2012). Maturation cleavage of the murine leukemia virus Env precursor separates the transmembrane subunits to prime it for receptor triggering. Proc. Natl. Acad. Sci. U.S.A. *109*, 7735–7740.

Lu, M., Blacklow, S.C., and Kim, P.S. (1995). A trimeric structural domain of the HIV-1 transmembrane glycoprotein. Nat. Struct. Biol. *2*, 1075–1082.

Ma, Q., Roy, F., Herrmann, S., Taylor, B.L., and Johnson, M.S. (2004). The Aer protein

of Escherichia coli forms a homodimer independent of the signaling domain and flavin adenine dinucleotide binding. J. Bacteriol. *186*, 7456–7459.

Maag, D., Castro, C., Hong, Z., and Cameron, C.E. (2001). Hepatitis C Virus RNA-dependent RNA Polymerase (NS5B) as a Mediator of the Antiviral Activity of Ribavirin. J. Biol. Chem. *276*, 46094–46098.

Macher, A.M., and Wolfe, M.S. (2006). Historical Lassa fever reports and 30-year clinical update. Emerging Infect. Dis. *12*, 835–837.
McCormick, J.B., Webb, P.A., Krebs, J.W., Johnson, K.M., and Smith, E.S. (1987). A prospective study of the epidemiology and ecology of Lassa fever. J. Infect. Dis. *155*, 437–444.

Mchaourab, H.S., Steed, P.R., and Kazmier, K. (2011). Toward the Fourth Dimension of Membrane Protein Structure: Insight into Dynamics from Spin-labeling EPR Spectroscopy. Structure *19*, 1549–1561.

McLay, L., Ansari, A., Liang, Y., and Ly, H. (2013). Targeting virulence mechanisms for the prevention and therapy of arenaviral hemorrhagic fever. Antiviral Research *97*, 81–92.

Mendenhall, M., Russell, A., Juelich, T., Messina, E.L., Smee, D.F., Freiberg, A.N., Holbrook, M.R., Furuta, Y., de la Torre, J.-C., Nunberg, J.H., et al. (2011). T-705 (favipiravir) inhibition of arenavirus replication in cell culture. Antimicrob. Agents Chemother. *55*, 782–787.

Messina, E.L., York, J., and Nunberg, J.H. (2012). Dissection of the role of the stable signal peptide of the arenavirus envelope glycoprotein in membrane fusion. J. Virol. *86*, 6138–6145.

Meyer, B.J., de la Torre, J.C., and Southern, P.J. (2002). Arenaviruses: genomic RNAs, transcription, and replication. Curr. Top. Microbiol. Immunol. *262*, 139–157.

Miller, S., Edwards, M.D., Ozdemir, C., and Booth, I.R. (2003). The closed structure of the MscS mechanosensitive channel. Cross-linking of single cysteine mutants. J. Biol. Chem. *278*, 32246–32250.

Moreno, H., Gallego, I., Sevilla, N., de la Torre, J.C., Domingo, E., and Martín, V. (2011). Ribavirin can be mutagenic for arenaviruses. J. Virol. *85*, 7246–7255.
Morrey, J.D., Taro, B.S., Siddharthan, V., Wang, H., Smee, D.F., Christensen, A.J., and

Furuta, Y. (2008). Efficacy of orally administered T-705 pyrazine analog on lethal West Nile virus infection in rodents. Antiviral Res. *80*, 377–379.

NIAID. NIAID Category A, B, and C Priority Pathogens. [(accessed on 31 October 2011)]. Available online:

http://www.niaid.nih.gov/topics/BiodefenseRelated/Biodefense/research/Pages/CatA.aspx.

Niwa, H., Yamamura, K., and Miyazaki, J. (1991). Efficient selection for high-expression transfectants with a novel eukaryotic vector. Gene *108*, 193–199.

Nussbaum, O., Broder, C.C., and Berger, E.A. (1994). Fusogenic mechanisms of enveloped-virus glycoproteins analyzed by a novel recombinant vaccinia virus-based assay quantitating cell fusion-dependent reporter gene activation. J. Virol. *68*, 5411–5422.

Ogbu, O., Ajuluchukwu, E., and Uneke, C.J. (2007). Lassa fever in West African sub-region: an overview. J Vector Borne Dis *44*, 1–11.

Parodi, A.S., GREENWAY, D.J., RUGIERO, H.R., FRIGERIO, M., DE LA BARRERA, J.M., METTLER, N., GARZON, F., BOXACA, M., GUERRERO, L., and NOTA, N. (1958). [Concerning the epidemic outbreak in Junin]. Dia Med *30*, 2300–2301.

Pasqual, G., Rojek, J.M., Masin, M., Chatton, J.-Y., and Kunz, S. (2011). Old World Arenaviruses Enter the Host Cell via the Multivesicular Body and Depend on the Endosomal Sorting Complex Required for Transport. PLoS Pathog *7*, e1002232.

Pasquato, A., Burri, D.J., Traba, E.G.-I., Hanna-El-Daher, L., Seidah, N.G., and Kunz, S. (2011). Arenavirus envelope glycoproteins mimic autoprocessing sites of the cellular proprotein convertase subtilisin kexin isozyme-1/site-1 protease. Virology *417*, 18–26.

Perez, M., and de la Torre, J.C. (2003). Characterization of the genomic promoter of the prototypic arenavirus lymphocytic choriomeningitis virus. J. Virol. *77*, 1184–1194.

Peters, C.J. (2006). Lymphocytic Choriomeningitis Virus — An Old Enemy up to New Tricks. New England Journal of Medicine *354*, 2208–2211.

Radoshitzky, S.R., Abraham, J., Spiropoulou, C.F., Kuhn, J.H., Nguyen, D., Li, W., Nagel, J., Schmidt, P.J., Nunberg, J.H., Andrews, N.C., et al. (2007). Transferrin receptor 1 is a cellular receptor for New World haemorrhagic fever arenaviruses. Nature *446*, 92–96.

Radoshitzky, S.R., Kuhn, J.H., de Kok-Mercado, F., Jahrling, P.B., and Bavari, S. (2012). Drug discovery technologies and strategies for Machupo virus and other New World arenaviruses. Expert Opin Drug Discov *7*, 613–632.

Reed, L.J., and Muench, H. (1938). A Simple Method of Estimating Fifty Per Cent Endpoints,. Am. J. Epidemiol. *27*, 493–497.

Rojek, J.M., and Kunz, S. (2008). Cell entry by human pathogenic arenaviruses. Cellular Microbiology *10*, 828–835.

Rojek, J.M., Sanchez, A.B., Nguyen, N.T., Torre, J.-C.D.L., and Kunz, S. (2008). Different Mechanisms of Cell Entry by Human-Pathogenic Old World and New World Arenaviruses. J. Virol. *82*, 7677–7687.

Rost, B., and Sander, C. (1993). Prediction of protein secondary structure at better than 70% accuracy. J. Mol. Biol. *232*, 584–599.

Roy, A., Kucukural, A., and Zhang, Y. (2010). I-TASSER: a unified platform for automated protein structure and function prediction. Nat Protoc *5*, 725–738.

Ruo, S.L., Mitchell, S.W., Kiley, M.P., Roumillat, L.F., Fisher-Hoch, S.P., and McCormick, J.B. (1991). Antigenic relatedness between arenaviruses defined at the epitope level by monoclonal antibodies. J. Gen. Virol. *72 (Pt 3)*, 549–555.

Rusnak, J.M., Byrne, W.R., Chung, K.N., Gibbs, P.H., Kim, T.T., Boudreau, E.F., Cosgriff, T., Pittman, P., Kim, K.Y., Erlichman, M.S., et al. (2009). Experience with intravenous ribavirin in the treatment of hemorrhagic fever with renal syndrome in Korea. Antiviral Res. *81*, 68–76.

Russier, M., Pannetier, D., and Baize, S. (2012). Immune Responses and Lassa Virus Infection. Viruses *4*, 2766–2785.

Safronetz, D., Lopez, J.E., Sogoba, N., Traore', S.F., Raffel, S.J., Fischer, E.R., Ebihara, H., Branco, L., Garry, R.F., Schwan, T.G., et al. (2010). Detection of Lassa virus, Mali. Emerging Infect. Dis. *16*, 1123–1126.

Salazar-Bravo, J., Ruedas, L.A., and Yates, T.L. (2002). Mammalian reservoirs of arenaviruses. Curr. Top. Microbiol. Immunol. *262*, 25–63.

Sanchez, A., Pifat, D.Y., Kenyon, R.H., Peters, C.J., McCormick, J.B., and Kiley, M.P. (1989). Junin virus monoclonal antibodies: characterization and cross-reactivity with other arenaviruses. J. Gen. Virol. *70 (Pt 5)*, 1125–1132.

Sangawa, H., Komeno, T., Nishikawa, H., Yoshida, A., Takahashi, K., Nomura, N., and Furuta, Y. (2013). Mechanism of action of T-705 ribosyl triphosphate against influenza virus RNA polymerase. Antimicrob. Agents Chemother. AAC.00649–13.

Satoh, T., Arii, J., Suenaga, T., Wang, J., Kogure, A., Uehori, J., Arase, N., Shiratori, I., Tanaka, S., Kawaguchi, Y., et al. (2008). PILRalpha is a herpes simplex virus-1 entry coreceptor that associates with glycoprotein B. Cell *132*, 935–944.

Saunders, A.A., Ting, J.P.C., Meisner, J., Neuman, B.W., Perez, M., de la Torre, J.C., and Buchmeier, M.J. (2007). Mapping the landscape of the lymphocytic choriomeningitis virus stable signal peptide reveals novel functional domains. J. Virol. *81*, 5649–5657.

Schibli, D.J., and Weissenhorn, W. (2004). Class I and class II viral fusion protein structures reveal similar principles in membrane fusion. Mol. Membr. Biol. *21*, 361–371.

Schwem, B.E., and Fillingame, R.H. (2006). Cross-linking between helices within subunit a of Escherichia coli ATP synthase defines the transmembrane packing of a four-helix bundle. J. Biol. Chem. *281*, 37861–37867.

Shimizu, H., Nihei, C., Inaoka, D.K., Mogi, T., Kita, K., and Harada, S. (2008). Screening of detergents for solubilization, purification and crystallization of membrane proteins: a case study on succinate:ubiquinone oxidoreductase from Escherichia coli. Acta Crystallogr. Sect. F Struct. Biol. Cryst. Commun. *64*, 858–862.

Sidwell, R.W., Barnard, D.L., Day, C.W., Smee, D.F., Bailey, K.W., Wong, M.-H., Morrey, J.D., and Furuta, Y. (2007). Efficacy of Orally Administered T-705 on Lethal Avian Influenza A (H5N1) Virus Infections in Mice. Antimicrob Agents Chemother *51*, 845–851.

Sleeman, K., Mishin, V.P., Deyde, V.M., Furuta, Y., Klimov, A.I., and Gubareva, L.V. (2010). In vitro antiviral activity of favipiravir (T-705) against drug-resistant influenza and 2009 A(H1N1) viruses. Antimicrob. Agents Chemother. *54*, 2517–2524.

Smee, D.F., Hurst, B.L., Egawa, H., Takahashi, K., Kadota, T., and Furuta, Y. (2009). Intracellular metabolism of favipiravir (T-705) in uninfected and influenza A (H5N1) virus-infected cells. J. Antimicrob. Chemother. *64*, 741–746.

Smith, E.C., Culler, M.R., Hellman, L.M., Fried, M.G., Creamer, T.P., and Dutch, R.E. (2012). Beyond anchoring: the expanding role of the hendra virus fusion protein transmembrane domain in protein folding, stability, and function. J. Virol. *86*, 3003–3013.

Snell, N.J.C. (2001). Ribavirin - current status of a broad spectrum antiviral agent. Expert Opinion on Pharmacotherapy *2*, 1317–1324.

Streeter, D.G., Witkowski, J.T., Khare, G.P., Sidwell, R.W., Bauer, R.J., Robins, R.K., and Simon, L.N. (1973). Mechanism of action of 1- -D-ribofuranosyl-1,2,4-triazole-3-carboxamide (Virazole), a new broad-spectrum antiviral agent. Proc. Natl. Acad. Sci. U.S.A. *70*, 1174–1178.

Tao, H., Liu, W., Simmons, B.N., Harris, H.K., Cox, T.C., and Massiah, M.A. (2010). Purifying natively folded proteins from inclusion bodies using sarkosyl, Triton X-100, and CHAPS. BioTechniques *48*, 61–64.

Thomas, C.J., Casquilho-Gray, H.E., York, J., DeCamp, D.L., Dai, D., Petrilli, E.B., Boger, D.L., Slayden, R.A., Amberg, S.M., Sprang, S.R., et al. (2011). A specific interaction of small molecule entry inhibitors with the envelope glycoprotein complex of the Junín hemorrhagic fever arenavirus. J. Biol. Chem. *286*, 6192–6200.

Thomas, C.J., Shankar, S., Casquilho-Gray, H.E., York, J., Sprang, S.R., and Nunberg, J.H. (2012). Biochemical reconstitution of hemorrhagic-fever arenavirus envelope glycoprotein-mediated membrane fusion. PLoS ONE *7*, e51114.

Urata, S., Yun, N., Pasquato, A., Paessler, S., Kunz, S., and de la Torre, J.C. (2011). Antiviral activity of a small-molecule inhibitor of arenavirus glycoprotein processing by the cellular site 1 protease. J. Virol. *85*, 795–803.

Vela, E.M., Zhang, L., Colpitts, T.M., Davey, R.A., and Aronson, J.F. (2007). Arenavirus entry occurs through a cholesterol-dependent, non-caveolar, clathrin-mediated endocytic mechanism. Virology *369*, 1–11.

Weber, G., Nakamura, H., Natsumeda, Y., Szekeres, T., and Nagai, M. (1992). Regulation of GTP biosynthesis. Advances in Enzyme Regulation *32*, 57–69.

Weissenhorn, W., Hinz, A., and Gaudin, Y. (2007). Virus membrane fusion. FEBS Letters *581*, 2150–2155.

White, J.M., Delos, S.E., Brecher, M., and Schornberg, K. (2008). Structures and Mechanisms of Viral Membrane Fusion Proteins. Crit Rev Biochem Mol Biol *43*, 189–219.

Winston, S.E., Mehan, R., and Falke, J.J. (2005). Evidence that the adaptation region of the aspartate receptor is a dynamic four-helix bundle: cysteine and disulfide scanning studies. Biochemistry *44*, 12655–12666.

York, J., and Nunberg, J.H. (2006). Role of the stable signal peptide of Junín arenavirus envelope glycoprotein in pH-dependent membrane fusion. J. Virol. *80*, 7775–7780.

York, J., and Nunberg, J.H. (2007a). A novel zinc-binding domain is essential for formation of the functional Junín virus envelope glycoprotein complex. J. Virol. *81*, 13385–13391.

York, J., and Nunberg, J.H. (2007b). Distinct requirements for signal peptidase processing and function in the stable signal peptide subunit of the Junín virus envelope glycoprotein. Virology *359*, 72–81.

York, J., and Nunberg, J.H. (2009). Intersubunit interactions modulate pH-induced activation of membrane fusion by the Junin virus envelope glycoprotein GPC. J. Virol. *83*, 4121–4126.

York, J., Romanowski, V., Lu, M., and Nunberg, J.H. (2004). The signal peptide of the Junín arenavirus envelope glycoprotein is myristoylated and forms an essential subunit of the mature G1-G2 complex. J. Virol. *78*, 10783–10792.

York, J., Agnihothram, S.S., Romanowski, V., and Nunberg, J.H. (2005). Genetic analysis of heptad-repeat regions in the G2 fusion subunit of the Junín arenavirus envelope glycoprotein. Virology *343*, 267–274.

York, J., Dai, D., Amberg, S.M., and Nunberg, J.H. (2008). pH-induced activation of arenavirus membrane fusion is antagonized by small-molecule inhibitors. J. Virol. *82*, 10932–10939.

York, J., Berry, J.D., Ströher, U., Li, Q., Feldmann, H., Lu, M., Trahey, M., and Nunberg, J.H. (2010). An antibody directed against the fusion peptide of Junin virus envelope glycoprotein GPC inhibits pH-induced membrane fusion. J. Virol. *84*, 6119–6129.

Zhang X, Ge P, Yu X, Brannan JM, Bi G, Zhang Q, Schein S, Zhou ZH. (2013). Cryo-EM structure of the mature dengue virus at 3.5-Å resolution. Nat Struct Mol Biol. 20(1): 105–110